Petrology of Greisenized Granites from the Eibenstock Region, Saxony, Germany



T.P. van der Ven

TU Delft HiF

1 Abstract

Greisen deposits can host significant amounts of economic elements such as Sn, W, and Li. A good understanding how these deposits form is important for effective mineral exploration. This formation process is currently not fully understood, as theories of metal transportation and deposition in greisen deposits, and the mechanics of greisenization, are incomplete. This thesis tried to address a number of these unknowns by analysing samples from the Eibenstock-Nejdek granite, a large granite body on the border of Germany and the Czech Republic that has seen few dedicated studies as of recently. Samples were analysed using μXRF-spectrometry, optical microscopy, and cathodoluminescence microscopy in order to deepen understanding of greisen formation and to provide practical workflows for mineral exploration.

μXRF maps were converted to two sets of mineral maps, one set created using unsupervised gaussian-mixture model (GMM) clustering, and the other created using empirically defined phase rules. These maps proved to be a fast way of obtaining automated mineralogy data from μXRF maps. The results imply that residual melt enriched in volatiles may precede the magmatic-hydrothermal transition, as pegmatite or aplite facies granites show fewer signs of greisenization. Tourmaline appears to record the magmatic-hydrothermal transition at one of the locations studied, and is highly correlated with these pegmatite and aplite facies granites.

Furthermore, the textures in thin sections or hand samples can be used to infer information about greisen systems. These textures include amoeboid or irregular grain boundaries, greisen veins crosscutting granite, and the presence of multiple pegmatite shells (stockscheider) which all indicate multiple intrusion episodes. These textures may be used in mineral exploration to increase geological knowledge of specific deposits. XRF-based mineralogy data may be viable for some exploration ventures, though access to the required equipment may be a limiting factor.

Cover image:	Eibenstock.de, retrieved 06-07-2026
Author:	T.P. van der Ven
Supervisors:	Dr. Tobias Schmiedel (TU Delft)
	Dr. Auke Barnhoorn (TU Delft)
	Dr. Axel Renno (HIF)
	Dr. Robert Möckel (HIF)
Program	MSc Applied Earth Sciences - Geo-resource Engineering
Course:	AESM7000: Master thesis
Faculty:	Civil Engineering and Geosciences
Date:	July 7, 2026

Contents

1 Abstract **1**

2 Introduction **3**
2.1 Problem definition . . . 3
2.2 Objectives . . . 3
2.3 Research questions . . . 3

3 Background **4**
3.1 Geological Setting . . . 4
3.1.1 Variscan History of the Erzgebirge . . . 4
3.1.2 Formation of the Eibenstock granite . . . 5
3.1.3 Greisen formation models . . . 6
3.1.4 Greisen deposits of the Eibenstock granite . . . 8
3.1.5 Eibenstock granite and greisen petrology . . . 9

4 X-ray Fluorescence **11**
4.1 Micro-XRF spectrometry . . . 11

5 Samples **12**

6 Methodology **15**
6.1 Micro-XRF . . . 15
6.1.1 Processing of XRF data . . . 16
6.1.2 XRF-based Automated Mineralogy . . . 16
6.2 Thin section microscopy . . . 18

7 Results **18**
7.1 Micro-XRF spectrometry . . . 19
7.1.1 Unsupervised Clustering and Manual Clustering . . . 20
7.2 Global textures . . . 23
7.3 Mineralogy . . . 24
7.4 Detailed textural and compositional descriptions per mineral . . . 25
7.4.1 Quartz . . . 32
7.4.2 Feldspars . . . 33
7.4.3 Biotite . . . 37
7.4.4 White mica and alteration-related micas . . . 38
7.4.5 Accessory minerals . . . 38

8 Discussion **39**
8.1 Additions to the Genetic Model of Greisen Formation . . . 39
8.2 Location markers in a greisen system . . . 41
8.3 Clustering of μXRF data . . . 44
8.4 Practical Implications for Mineral Exploration . . . 44
8.5 Petrogenesis of the Eibenstock granite . . . 45

9 Conclusions **46**

10 Recommendations **47**

References **47**

11 Appendix **53**

12 μXRF Element maps **54**

2 Introduction

2.1 Problem definition

Greisen deposits are significant sources of important metals such as tin, tungsten and lithium, which are used in everyday technologies such as electronics, alloys, and batteries. Locating and mining such deposits provides economic benefits and aids in resource independence. In order to find new greisen deposits, a good understanding of their formation is an important asset. Greisen deposits are a feature of highly-evolved granites, typically constrained to the upper reaches of the intrusion. Greisen deposits commonly form in a cupola, which is a dome-like shape at the very top of a granitic intrusion. The greisen itself forms when a hydrothermal fluid exsolves from the magma, which alters the granite, the surrounding rock, or both, depositing economic metals in the process. However, this formation model is currently incomplete, as it is not well understood how and where these metals are deposited and what controls this depostion. The most well-studied greisen systems in Germany are the lithium greisens of the Altenberg-Teplice caldera in the eastern Erzgebirge, but little dedicated studies of greisens in the western Erzgebirge have been done recently. The largest outcrop of granite in the Western Erzgebirge is the Eibenstock granite, which host many, although mostly small, greisen deposits. The mechanism of greisenization in the Eibenstock granite is not fully understood, and dating has shown that greisen deposits in the Eibenstock granite are younger than the granite itself. Furthermore, the Eibenstock granite has seen few dedicated studies in recent years. These problems make the Eibenstock granite a promising research target and are the starting point for this thesis.

2.2 Objectives

The objective of this thesis is to gain more understanding into the formation of greisen systems for the benefit of mining exploration. To fulfill this objective, greisenized granites from the Eibenstock region will be studied using μXRF spectrometry, optical microscopy, and cathodoluminescence microscopy.

This main objective can be split into three smaller objectives. The first objective is to study the macroscopic and microscopic textures in the samples and link these to specific parts of the greisen system. The second objective is to automatically characterize samples based on measurements from microscopy and XRF spectrometry. The final objective is to translate the findings from the first two objectives into practical methodologies for mineral exploration.

2.3 Research questions

To fullfill the objectives introduced in the section above, a number of research questions were devised:

1. Which textures present in the samples could be used as location markers in greisen systems, and what do these textures reveal about the greisen system at hand?
    - Do these textures indicate metal-rich and metal-poor regions?
    - Are such markers feasible for use in mineral exploration?
2. Can μXRF data be used to automatically classify minerals in rock samples?
    - Can such a method be used in mineral exploration?
    - What are the benefits of a machine-learning based approach to a manual approach?

3 Background

3.1 Geological Setting

The Eibenstock granite is one of several granitic intrusions in the Erzgebirge (ore mountains). The Erzgebirge is a low mountain range along the north-western edge of the Bohemian massif, on the border of Germany and the Czech republic. On the german side it is located in Saxony, and in the Czech Republic it covers parts of Karlovy Vary and Ústí nad Labem. The geology of the Erzgebirge mainly comprises of rocks deformed and metamorphosed during the Variscan orogeny, a continental collision between the paleocontinents Laurussia and Gondwana. The collision of these two continents resulted in the formation of Pangaea, producing a mountain range that stretched thousands of kilometers in the process. ((Rast, 1988), (Franke, 1989)). The Variscan orogeny lasted from the early Devonian to the early Permian (400 Ma-290 Ma) and remnants of the Variscan orogenic belt (variscides) crop out in various massifs in Europe. The Iberian massif, the Ardennes and the Bohemian massif are examples of Variscides in Europe. (Matte, 1986). The Variscan origin of basement rocks is clear in the Erzgebirge, as it comprises mostly of metamorphic rocks such as phyllites, schists and gneisses, in addition to a number of late-collisional intrusions. (Rötzler, 2025).

3.1.1 Variscan History of the Erzgebirge

The Variscan orogeny occurred in the late Paleozoic when the paleocontinents Laurussia and Gondwana collided to form Pangaea, producing a massive orogenic belt that stretched for thousands of kilometers. Prior to the Variscan orogeny the Rheic ocean was located in between these continents, which closed completely over the course of the orogeny. The line along which Laurussia and Gondwana met after closure of the Rheic ocean is an important tectonic boundary called the Rheic suture. Because of the large scale of this orogeny, rocks dating back to the Variscan orogeny (variscides) can be found throughout Europe. Among others, the Armorican massif, Bohemian massif, Ardennes, and Iberian massif all formed during the Variscan orogeny (Kroner & Romer, 2013). The central-European variscides are often classified into zones, originally developed by (Franke, 1989). From north to south, this zonation divides the variscides into the Rheno-Hercynian zone, the mid-German crystalline high, the Saxo-Thuringian zone, and the Moldanubian zone (Franke & Żelaźniewicz, 2023).

The Erzgebirge is located in the Saxo-Thuringian zone (Förster, 1998). This zone mainly comprises of metamorphosed Cadomian basement and metamorphosed paleozoic sediments. These metamorphic rocks range from low grade to very high pressure, high temperature metamorphics, in some places even reaching diamond-forming conditions, as is evident from micro-diamonds found in garnets from ultra-high pressure (UHP) metamorphic zones in the central Erzgebirge (Schönig et al., 2019). The peak intensity of metamorphism in the Variscan orogeny occurred at 340 ± 1 Ma, after which the thickened orogenic crust spread out laterally due to gravitational effects. This post-orogenic collapse caused the orogenic wedge to thin (Kröner & Willner, 1998). This gravitational thinning and paired erosion of the orogenic wedge was accompanied by a period of magmatic activity that formed most of the granites in the Erzgebirge, including the Eibenstock granite. Two theories exist for the connection between post-orogenic collapse and this late-collisional magmatism: One is the sinking of the lithosphere into the asthenosphere causing it to heat up and melt (Houseman et al., 1981) and the other is a rising of the astenosphere melting the bottom part of the lithosphere (C. Wang et al., 2021). Regardless of which theory is true, this crustal thinning gave rise to the magmatic activity that emplaced numerous igneous bodies across the Variscan orogenic belt, including the Erzgebirge intrusions (e.g. Finger et al., 2022, Weil et al., 2019, Buzzi & Gaggero, 2008, Boscaini et al., 2025).

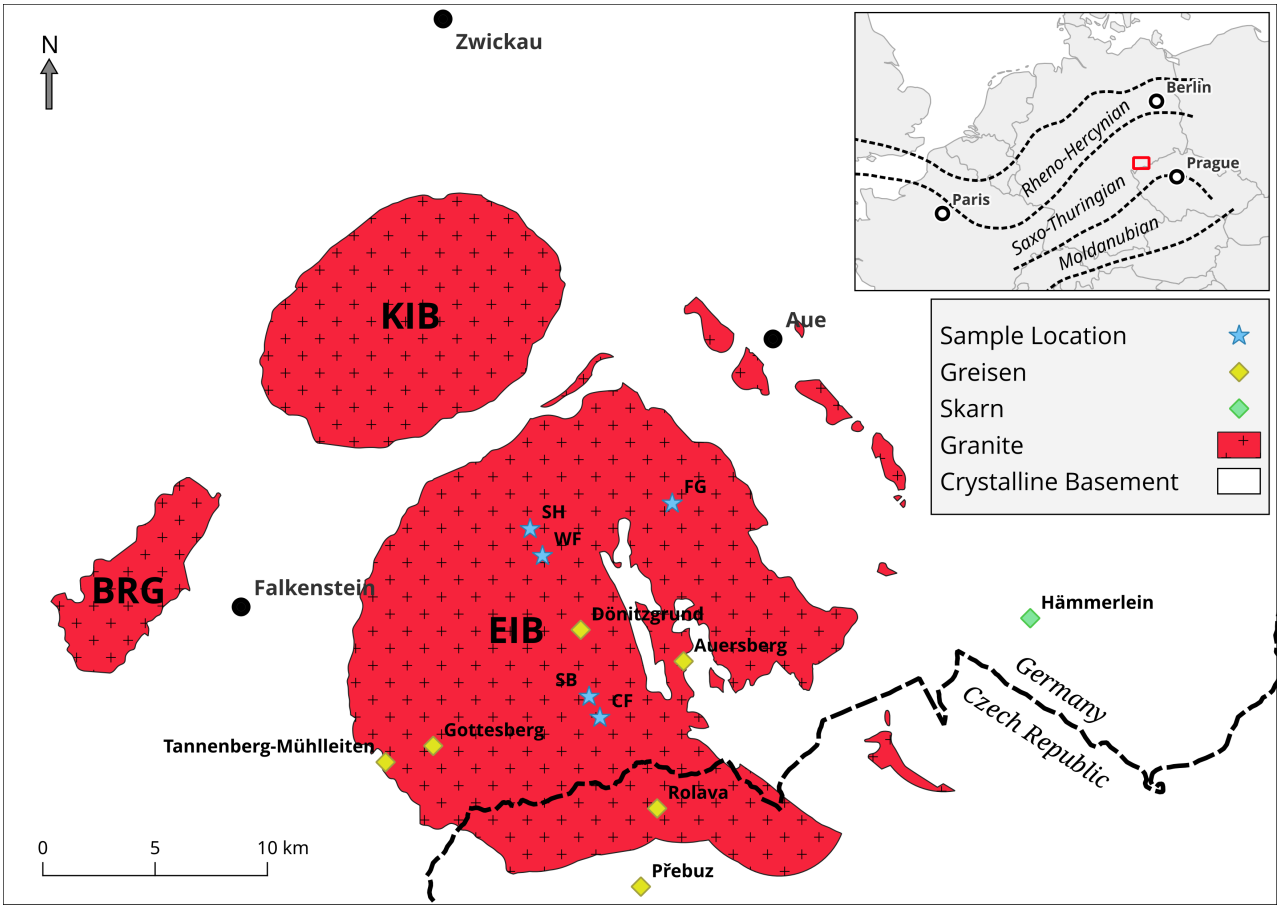


Figure 1: *Geological map of the western Erzgebirge Showing the Bergen, Kirchberg, Eibenstock granites, as well as smaller granite bodies to the northeast towards Aue. KIB: Kirchberg, BRG: Bergen, EIB: Eibenstock. For a detailed breakdown of sample locations, see Table 2. After Förster et al., 1999.*

3.1.2 Formation of the Eibenstock granite

The late- to post-collisional intrusions of the Erzgebirge include the Bergen, Kirchberg, and Eibenstock granites in the western Erzgebirge, the Ehrenfriedersdorf, Pobershau and Satzung granites in the central Erzgebirge, and finally the Niederbobritzsch granite and the Altenberg-Tepliče caldera complex in the eastern Erzgebirge (Förster et al., 1999). In the eastern Erzgebirge volcanics are far more common than the western Erzgebirge. A geological map including the intrusions of the western Erzgebirge can bee seen in Figure 1. In the past it was believed that there was a single large intrusion connecting all intrusions of the Erzgebirge at depth, similar to the Cornubian batholith. However, geophysical studies investigating this have shown that every intrusion is independent (Förster et al., 1998).

Historically, these intrusive bodies have been classified into two groups, the pre-Westphalian (>315 Ma) older intrusive complex (OIC), and the post-Westphalian (<307 Ma) younger intrusive complex (YIC) (Tischendorf & Förster, 1994). In this classification, the Eibenstock belongs to the YIC. However, later dating of the Erzgebirge granites showed the limitations of this classification scheme, as several YIC granites were found to be older and vice versa (Förster et al., 1998). This can be seen by recent dating of the Eibenstock, which dated the emplacement of the granite to between 315 and 314 Ma using U-Pb dating. This age places the granite on the boundary between between OIC and YIC, which highlights the shortcomings of this classification scheme (Tichomirowa, Käßner, et al., 2019).

The currently used classification scheme is more elaborate and is based on geochemistry rather than age. It categorizes the granites into five groups: **1)** Low-F biotite granites, **2)** low-F two-mica granites, **3)** high-F, high-P_2O_5 Li-mica granites, **4)** High-F, low-P_2O_5 Li-mica granites, and **5)** medium-F, low-P_2O_5 biotite granites (Förster et al., 1999). The Eibenstock granite falls into the third category, and is a high-F, high-P_2O_5 Li-mica granite. Examples

of low-F biotite granites in the Erzgebirge are the Kirchberg and Niederbobritzsch granites, and the Bergen granite belongs to the low-F two-mica granite group. The precise protolith that formed the melt that crystallized as the Eibenstock granite is still debated. Most authors propose a mix of sedimentary and metamorphic rocks, but the addition of volcanic rocks or oceanic crust has also been proposed (Tichomirowa, Gerdes, et al., 2019). For an overview of the classifications used for the Eibenstock granite, see Table 1

The Eibenstock granite crops out in a 25x22km area around the German town of Eibenstock and continues across the Czech border towards the town of Nejdek. Accordingly, the intrusion is often called the Eibenstock-Nejdek pluton (Korges et al., 2020). The emplacement depth of the granite was shallow, at a depth of 3-6.5 km, with a solidification temperature of 600-700 ^oC. (Thomas & Klemm, 1997) The dating of the granite between 315 and 314 Ma means it formed around the late stages of the Variscan orogeny, after peak metamorphism. For this reason the granite is linked to orogenic collapse (Förster et al., 1999). The granite is peraluminous with an A/CNK value of 1.17-1/36 (Förster et al., 1999) and is enriched in incompatible elements such as Li, Rb and Y (Förster, 2018). Numerous ore deposits are linked to the Eibenstock granite, such as skarns, greisens and hydrothermal veins (Korges et al., 2020) (Lefebvre et al., 2019).

The Eibenstock intrusion is surrounded by a contact metamorphic aureole of around 200 to 300m wide. This aureole consists of metamorphic rocks from the Variscan orogeny further metamorphosed to hornfels by the heat of the intrusion (Achtziger-Zupančič et al., 2017). In several places, mainly around Schneckenstein/Tannenberg, younger intrusions have intruded the Eibenstock granite and surrounding contact metamorphic aureole. These include subvolcanic felsic intrusions, breccia pipes and lamprophyre dikes (Seifert, 2017). These younger intrusions have been dated to 290$\pm$5 Ma, which corresponds to the ages found by (Lefebvre et al., 2019) for greisens near the Hämmerlein skarn deposit, thereby providing a strong link between these younger intrusions and the greisen mineralization.

In the present day the Eibenstock granite crops out at the surface, yet it was emplaced at a depth of around 3-6.5 km as mentioned previously. After the Variscan orogeny, much of the Variscan mountain range was eroded during the early Permian, and subsequently buried underneath Jurassic to Cretaceous sediments. This sedimentary cover was slowly exhumed and eroded starting from the late cretaceous until the present, with some small periods of sedimentation in between (Wolff et al., 2015). In the late Jurassic to early Cretaceous, activity along a transfer fault around modern-day Dresden resulted in a local area of extension, which caused subsidence in the area and provided accommodation space for Cretaceous sediments. This localized subsidence in the eastern Erzgebirge is the reason why there are more exposed volcanics in the eastern Erzgebirge, which have been eroded in the western Erzgebirge. The Eger rift opened in the Oligocene, practically parallel to the present-day border between Germany and the Czech Republic. This rift resulted in the uplift of the Erzgebirge, creating the topography that is seen in the area today.

3.1.3 Greisen formation models

Greisenization is a specific type of hydrothermal alteration caused by fluids originating from granite intrusions (Štemprok, 1987). During crystallization of granitic magmas with high water contents a hydrothermal phase separates from the magma in a process known as the magmatic-hydrothermal transition. The subsequent hydrothermal alteration of the intrusion and host rock due to this phase is known as greisenization (Breiter et al., 2019).

Greisenization transforms biotite and feldspars into quartz and muscovite assemblages (feldspar hydrolysis). Different types of greisens exist, including but not limited to: quartz-topaz, quartz-mica, topaz-mica and quartz-tourmaline greisens (Štemprok, 1987). These greisens often contain economically interesting minerals such as wolframite, cassiterite and zinnwaldite (Halter et al., 1998). There are various mechanisms that lead to enrichment of elements like Sn and W and their subsequent deposition. These elements are preferentially partitioned in the hydrothermal fluid during the magmatic-hydrothermal transition. The exact fluid/melt partitioning coefficients, which controls the enrichment in the hydrothermal fluid, depend on many factors, such as the salinity of the hydrous phase, melt composition, and oxygen fugacity. For example, fluid/melt partitioning coefficients of Ag, Zn, and Pb show a positive correlation with increasing salinity, while relationships for elements like Sn, W, and Mo are

Table 1: *Overview of the Eibenstock granite, mineralogy, classifications*

Sub-type	Texture	Main minerals	Accessory minerals
Förster et. al:			
EIB 1	mostly porphyritic; m.g. to c.g. matrix; coarse Kfs, Pl, and Qz phenocrysts; pink	Qz, Kfs, Pl, Bt, Msc	Top, Ap, Zir, Mon, Op, Xen, Tur, Rut, Cst, Ura, Fl
EIB 2	m.g. mostly equigranular; local Kfs and Qz phenocrysts; pink	Qz, Kfs, Pl, Bt, Msc	Top, Ap, Zir, Mon, Op, Xen, Crd, Fl, Tur, Ura, Cst, Rut
EIB 3	f.g. equigranular; very light color, locally pink	Qz, Kfs, Pl, Bt, Msc	Top, Ap, Zir, Mon, Xen, Op, Crd, Rut, Fl, Ura, Cst
Schust & Wasternack:			
EI 1	porphyritic type with abundant phenocrysts	-	-
EI 2	m.g. mostly equigranular, local phenocrysts	-	-
EI 3	f.g. equigranular granite, no phenocrysts	-	-

Abbreviations: f.g.: fine grained, m.g.: medium-grained, c.g.: coarse grained, Qz: quartz, Kfs: K-feldspar, Pl: plagioclase, Bt: biotite, Msc: muscovite, Top: topaz, Ap: apatite, Zir: zircon, Mon: monazite, Xen: xenotime, Op: opaques, Crd: cordierite, Rut: rutile, Fl: fluorite, Ura: uraninite, Cst: cassiterite, Tur: tourmaline, After (Förster et al., 1999) and (Schust & Wasternack, 2002).

more complicated (Zajacz et al., 2008). Intrusions that host greisen deposits are often pre-enriched in rare metals like Li, Sn and W by magmatic fractionation, pre-enrichment of the protolith, or both (e.g. (Romer et al., 2010), (Förster et al., 1999)). Furthermore, hydrothermal solutions may become enriched in certain elements by the preferential dissolution of certain minerals. For example, in the case of the consumption of feldspars and biotite in greisen reactions, these minerals can be enriched in trace elements compared to the bulk geochemistry of the rock. Examples are the incorporation of Pb in feldspars, or Sn in biotite. In some deposits the Sn content in biotites can reach up to 500 ppm (Pirajno, 2009) and recent research shows that micas in the non-greisenized granite at the Zinnwald deposit contain up to 800 ppm Sn, which drastically decreases in micas of the greisens, indicating that these hydrothermal fluids remobilize elements like Sn (Breiter et al., 2019). If these minerals are dissolved by a fluid the concentrations of these trace elements in the hydrothermal fluid will rise accordingly. In short, the combination of magma pre-enrichment, fluid/melt partitioning, and preferential dissolution of pre-enriched minerals results in high concentrations of elements like Sn and W in the greisenizing fluid (Burisch et al., 2025). To what degree each of these mechanisms play a role appears to vary per deposit (e.g. (Lefebvre et al., 2019)).

A distinction is often made between endogreisens and exogreisens. An endogreisen is a greisen that formed within the source intrusion, whereas an exogreisen is a greisen that formed outside the intrusion, such as in the contact-metamorphic aureole surrounding most plutons and beyond. Texturally, endogreisens are often pervasively altered host granites, whereas exogreisens often occur as stockwork, vein, or breccia zones (Burisch et al., 2025).

Although no widely-accepted model that explains all different types of greisenization exists, many recent publications report a similar vertical evolution from the upper part of the granite cupola upwards: 1) Sodic±potassic alteration of the upper granite stock, gradually transitioning to 2) Mostly barren pervasively greisenized endogranites with local Sn-W mineralization 3) Stockscheider pegmatite separating the granite stock from the host rock 4) Increasing Sn-W mineralization in breccia or vein-like exogreisens with increasing distance from the cupola 5) Decreasing Sn-W mineralization and increasing sulfide mineral deposition 6) Increasingly barren greisen-associated hydrothermal veins (e.g. (Markovic et al., 2025) (Burisch et al., 2025), (Štemprok, 1987), (Varga et al., 2023), (Peterková & Dolejš, 2019), (Lefebvre et al., 2019)) Figure 2 provides a visual representation of this idealized greisen formation model.

Reasons for these different zones are most likely effects of changing fluid properties such as pressure and temperature leading to changing thermodynamic equilibria (Launay et al., 2021). Additionally, mixing of magmatic-

hydrothermal fluids with meteoric water from overlying rocks may also play a key role in the shallower parts of greisen-related mineralization (Krejčí Kotlánová et al., 2024). Greisenization is associated with a wide range of hydrothermal fluid conditions, ranging from low temperatures (200 ^{o}C) and low salinities (10 wt% eq.) to high temperatures (600 ^{o}C) and high salinities (40 wt% eq.).

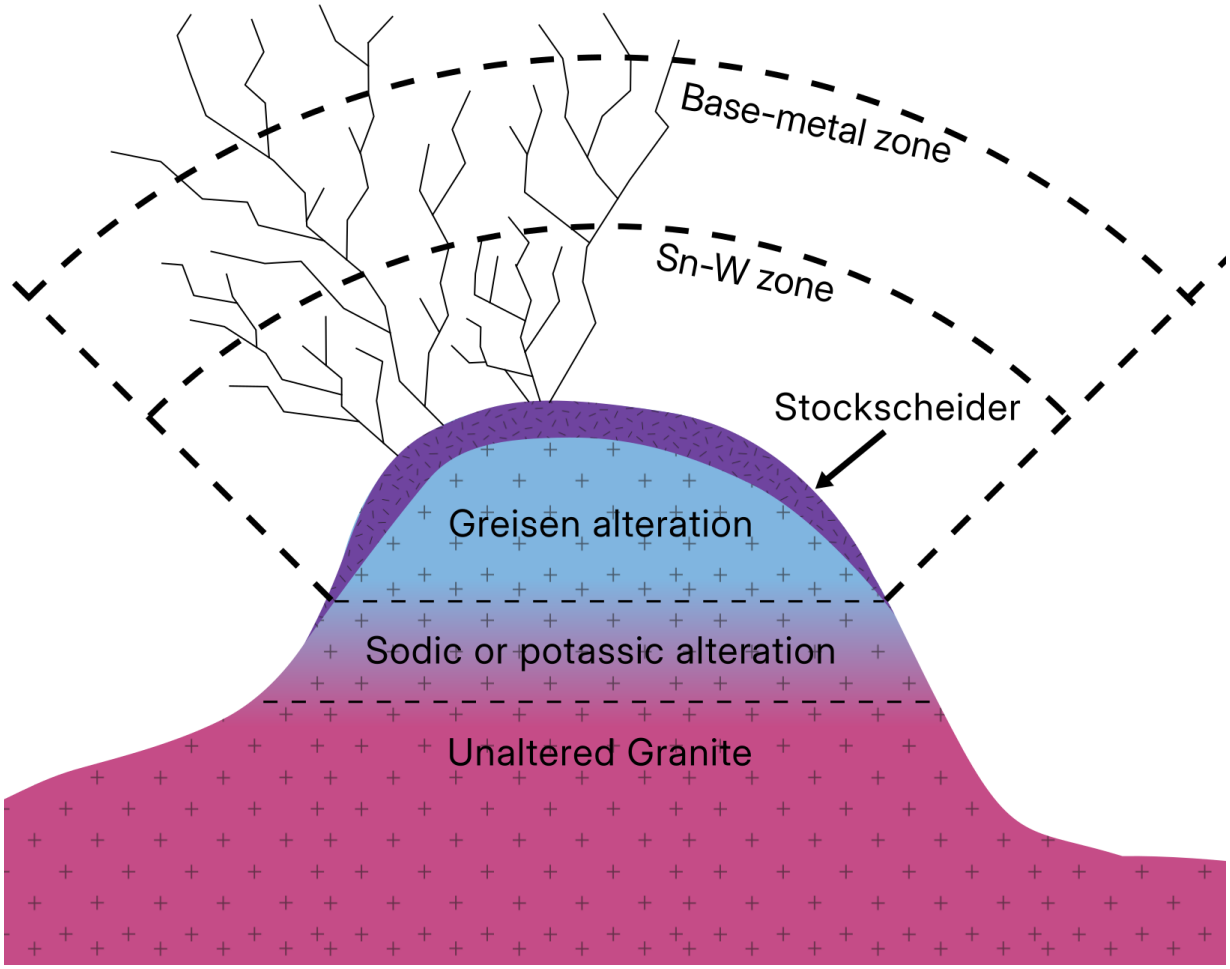


Figure 2: *Sketch of a model greisen system. Granitic stock is shown in purple.* ***1)*** *Self-altered sodic±potassic altered zone* ***2)*** *Mostly barren greisen endogreisen of the upper stock* ***3)*** *Stockscheider pegmatite separating intrusion and host rock* ***4)*** *Sn-W exogreisen zone, hosted by breccia and veins* ***5)*** *Veins with decreasing Sn-W mineralization and increasing sulfide mineralization.*

3.1.4 Greisen deposits of the Eibenstock granite

The Eibenstock granite hosts several greisen deposits and many more small-scale occurrrences of greisens (see Figure 1). Many of the greisen deposits, both small and large scale, have been mined at some point throughout history. Greisen deposits in the Eibenstock include Gottesberg (Sn-W), Tannenberg-Mühlleiten (Sn), Dönitzgrund (Sn), Přebuz (Sn), Rolava (Sn) and Auersberg (Sn) where Gottesberg is the only large deposit. Furthermore, the Hämmerlein Sn-In skarn deposit is linked to magmatic-hydrothermal fluids originating from the Eibenstock granite. All of these deposits are endogreisens except for Auersberg (Štemprok & Blecha, 2015). This can be explained by the fact that the top part of the Eibenstock granite is heavily eroded, which resulted in the removal of the main greisens and exogreisens over geologic time.

Currently, exploration is happening in the Eibenstock granite for Sn near Gottesberg, by the Australian company First Tin PLC. The company reports 6.1 Mt of indicated ore at 0.23% Sn, in total good for 14200 t of Sn, with an additional inferred 31.1 Mt at 0.25% Sn, which amounts to 77100 t of Sn (First Tin PLC, 2025).

3.1.5 Eibenstock granite and greisen petrology

Macroscopic textures Granites with similar bulk geochemistries can still vary significantly in texture, both at the macroscopic and microscopic level. The macroscopic texture describes the overall grain size and grain size distribution of a rock. Grain sizes in granites can range from very fine-grained (aplitic) to very coarse grained (pegmatitic), and the grain size distribution can be equigranular, where all crystals are of similar size, or porphyritic, where larger crystals sit in a fine-grained ground mass. Furthermore, the granite can contain megacrysts, which are crystals that are significantly larger than the average grain size. Megacrysts in granites are usually all the same mineral, i.e. a granite with quartz megacrysts or K-feldspar megacrysts. For a good overview of different macroscopic textures in granites, see (Breiter et al., 2022).

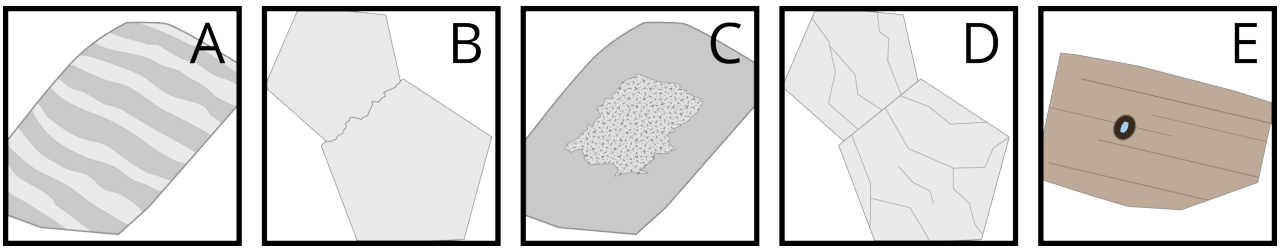


Figure 3: *Illustration of microscopic textures commonly encountered in granites.* ***A)*** *Exsolution lamellae of Na-feldspar and K-feldspar in a feldspar that crystallized as a solid solution.* ***B)*** *Recrystallization of quartz along a grain boundary due to interfacial energy minimization.* ***C)*** *Alteration of a feldspar core by white mica.* ***D)*** *Fractured quartz crystal.* ***E)*** *Pleochroic radiation halo surrounding a radioactive zircon in a biotite crystal.*

Microscopic textures **A) Exsolution textures** are often found in feldspars. Feldspars form a solid solution at higher temperatures, but when a granite starts to cool this solution becomes unstable. This is when unmixing starts. During unmixing the feldspars dissociates into an amalgamation of potassium feldspar and sodium feldspar (Abart et al., 2009). This unmixing is called perthite and it can occur at different scales, from microscopic perthite only visible with electron microscopy to perthite visible in light microscopy or even with the naked eye (Yund & Ackermand, 1979). A distinction must be made between two different types of perthite, ”regular perthite” and antiperthite. ”Regular” perthite occurs when a potassium feldspar shows an exsolution texture that consists of sodium feldspar. Antiperthite on the other hand is when a plagioclase feldspar shows an exsolution texture consisting of potassium feldspar (Song et al., 2025).

B) Recrystallization is a broad term that covers a range of phenomena. The term recrystallization generally means: The growth of a new crystal within another crystal (Poirier & Guillopé, 1979). The new crystal can be of the same phase or a different phase. An example of same phase recrystallization is recrystallized calcite in marble that formed from limestone. Here the chemical formula of the crystal stays the same, while the orientation or size of the new crystal is different.

One phenomenon that falls under the umbrella of recrystallization is subgrain rotation recrystallization (SRR), where a part of the grain breaks off and rotates, thereby essentially nucleating a new crystal with a different orientation. This is a mechanism for the rock to accommodate stress, and the rotated subgrain can often accommodate more strain (Pongrac et al., 2022). Another mechanism of stress relief is grain boundary migration recrystallization, which occurs when two grains of the same mineral meet that have different crystallographic orientations. Because of this difference one of these orientations will be able to accommodate slightly more strain, creating a pressure gradient. Under the right conditions the strained crystal can recrystallize into the orientation of the less-strained crystal at their interface to reduce this gradient (Rohrer et al., 2023).

C) Alteration in granites can occur in several forms. A common alteration pattern is the alteration by hydrothermal fluids. There are many different types of hydrothermal alteration such as sericitization, silicification and chloritization (Mathieu, 2018). Sericitization is an acidic alteration process that produces white micas like muscovite. It mostly affects feldspars. Silicification occurs when a silica-rich fluid alters a rock, depositing quartz and transforming minerals into more silica-rich minerals (e.g. Magnetite into Grunerite) ((H. Wang et al., 2023),

(Mathieu, 2018)). Chloritization is most easily recognized by the transformation of micas to chlorite and is a common alteration pattern in many rocks (Beaufort et al., 2015). Chlorite is often green in plane polarized light and is thus not difficult to locate.

D) Deformation, either brittle or ductile, can show itself in many ways in thin sections and actually resembles macroscopic deformation features quite well. At the microscopic scale brittle deformation causes fractures and displacement in and around mineral grains. Here, small fractures in a grain can cause deformation twinning, where a fracture allows part of the mineral to rotate slightly, giving it a different extinction angle. This gives the false impression that the mineral is twinned when it is actually deformed (Mirijam et al., 2018). Another characteristic of brittle deformation is the presence of fractures, these may be limited to single grains or stretch across multiple grains. Both brittle and ductile deformation can produce undulose extinction in minerals, where the mineral is bent to accommodate strain. This bending means that the crystal axes rotate slightly, which manifests itself as a slight difference in extinction angle throughout the grain. This can be recognized as a ”patchy” or ”wavy” extinction pattern (Phillips, 1965).

Ductile deformation can be very clear, e.g. when observing kink banding, mica fish or foliation. It can also be more subtle, like seeing fringed minerals or symplectites. Kink banding is the bending or ”kinking” of a mineral to accommodate deformation. This can be seen in minerals with otherwise straight features, like biotite or twinned plagioclase (Cummings, 1965). Mica fish are shear-deformed mica crystals that have a very characteristic fish-like shape. These crystals align themselves and deform corresponding to the shear direction (Ribeiro et al., 2023). Foliation can be recognized in thin section by a lineation, e.g. minerals dominantly present along a line or crystal sizes following a lineation (e.g. (Kästner et al., 2021). Fringed minerals occur when mineral grains are stronger or more rigid than the surrounding grains. This causes a change in the stresses around the mineral and can cause ”fringes” that form through various different mechanisms. (e.g. (Passchier & Trouw, 1998),(Sherlock et al., 2003)). Symplecites are intergrowths of minerals that grow after an initial mineral often formed during metamorphism becomes unstable. They are thus useful to determine P-T trajectories of a rock (Dharmapriya et al., 2020). It is easy to mistake a symplectite for myrmekite and vice versa, however myrmekite is the intergrowth of quartz and alkali feldspar, formed during the initial cooling of a plutonic rock (Song et al., 2025).

E) Pleochroic radiation haloes are dark, sometimes pleochroic rings around a mineral, usually seen when the mineral is an inclusion in another mineral like biotite. These haloes are caused by radiation damage to the enclosing mineral caused by the emission of alpha particles from the included mineral. In some cases, several concentric rings are present, where each ring reflects a different energy alpha particle (Nasdala et al., 2006). Measuring these radii makes it possible to determine the range of energy of the alpha particles, as particles with higher energies will travel further. This phenomenon has been studied well, and equations exist for calculating the penetration depth of an alpha particle of different energies, which allows determination of the radioactive isotopes in an inclusion, see (Pattrick et al., 2013). If two similarly sized minerals with radiation haloes can be found where one has a larger radius than the other, then the mineral with the bigger halo most likely contains an isotope that has a higher maximum alpha particle energy in its decay chain, for example thorium (Henderson, 1939).

In some cases the radiation a mineral emits is so strong that it completely destroys its own crystal structure. When this occurs the mineral turns into an amorphous state, with no crystal structure and litte to no birefringence. In this state of destruction the mineral is called metamict (Yu et al., 2021). This can occur in minerals that have a high concentration of radioactive elements, for example allanite or thorite, but also zircon if the concentration of radioactive minerals is high enough (e.g. (Chen et al., 2025), (Zamiatina et al., 2025)). There are many more textures in thin sections. However, these are the most common in granites. A visual illustration of the textures described above can be seen in Figure 3. For a more complete description of textures in plutonic rocks, see (Philpotts & Ague, 2021).

Mineralogy The mineralogy of the Eibenstock granite can be split up into two categories: Granite-related minerals and greisen-related minerals. There is some overlap between these two categories, indicating that some minerals form in both granites and greisens. The main granite-related minerals found in the Eibenstock granite are quartz, K-feldspar, plagioclase, biotite, muscovite, topaz, apatite and zircon (Förster et al., 1999). Alongside

these minerals, monazite, xenotime, cordierite, rutile, fluorite, uraninite, tourmaline, and cassiterite can also be found (Förster, 2018). Greisen-related minerals found in the Eibenstock granite include tourmaline, white mica, quartz, cassiterite, apatite, topaz, and wolframite (Lefebvre et al., 2019).

Texturally, the Eibenstock granite generally appears medium to coarse grained with common K-feldspar megacrysts. Additionally, quartz megacrysts are common, albeit less common than K-feldspar megacrysts (Kempe et al., 2004). Less commonly, a medium to fine grained equigranular variant occurs, which forms small stocks and dykes with sharp contacts against the regular granite variant (Förster et al., 1999). The most common variants were classified EIB1 and EIB2 by (Förster et al., 1999), and the less common fine-grained variant is EIB3.

4 X-ray Fluorescence

X-ray Fluorescence (XRF) is the excitation of a material by powerful X-rays, resulting in a secondary emission of X-rays by the excited material. X-rays with a high enough energy can ionize atoms, causing them to lose an electron. This destabilizes the atom, which causes an electron from a different electron shell to fill the electron vacancy. This movement of electrons between shells results in emission of electromagnetic energy proportional to the difference in energy between the two electron shells. X-ray emission from electrons moving from the L to K shell are known as Kαemissions, while emissions from movement from the M to K shell are known as Kβemissions. Similarly, M to L movement results in an Lαemission, and N to L movement is an Lβemission (Mantler et al., 2006). Each element contains electron shells at specific energies, which makes it possible to determine the elements present in a sample from the fluorescent X-rays emitted, as the energy difference between shells is proportional to the X-ray wavelength through Planck's law:

$$E = hf = \frac{hc}{\lambda} \tag{1}$$

The intensity and wavelength of these secondary X-rays can be measured using a spectrometer, and identifying peaks in this spectrum allows the determination of the elements present in the sample.

The high-energy, primary X-rays needed for XRF are often generated using vacuum tubes. These are glass tubes held under vacuum that contain an anode of a heavy metal, such as tungsten or rhodium. The potential across these vacuum tube is very high, on the order of several thousands of volts, which causes electrons to mvoe from cathode to anode at a very high speed. At the anode these high-speed electrons are slowed down due to interaction with the nuclei of the anode material. This speed decrease causes the electrons to emit X-rays. This process of emission of X-rays by slowing down electrons is known as "Bremsstrahlung", i.e. "Braking radiation" (Langhoff et al., 2006).

4.1 Micro-XRF spectrometry

Micro-XRF (μXRF) spectrometry is similar to regular XRF spectrometry, however with the difference that much smaller spot sizes can be measured. μXRF spectrometers are often used to measure large areas of a sample at a high resolution, thereby obtaining a two-dimensional map of the samples surface. This 2-D mapping is done by either moving the X-ray source and detector across the sample, or by moving the sample relative to the source and detector. Spot sizes of regular XRF spectrometers are generally on the order of millimeters or even centimeters for handheld devices (Young et al., 2016), while μXRF spot sizes can be as small as a several micrometers (Komatani et al., 2013). This is achieved by X-ray focusing optics that narrow the X-ray beam to a very small size, while retaining most of the energy flux from the vacuum tube X-ray beam. A good overview of X-ray optics is seen in (Erko et al., 2006).

5 Samples

The sample material used in this study consists of granite and greisen samples from the Eibenstock granite. This material was collected from five locations during a sampling campaign in the western Eibenstock area. Locations where samples were taken are Fahsel quarry, Carlsfeld, Schönheide, Wallfischkopf and Steinberg. Sampling was hindered by bad weather and snow cover, which explains the lack of samples for some of the sites.

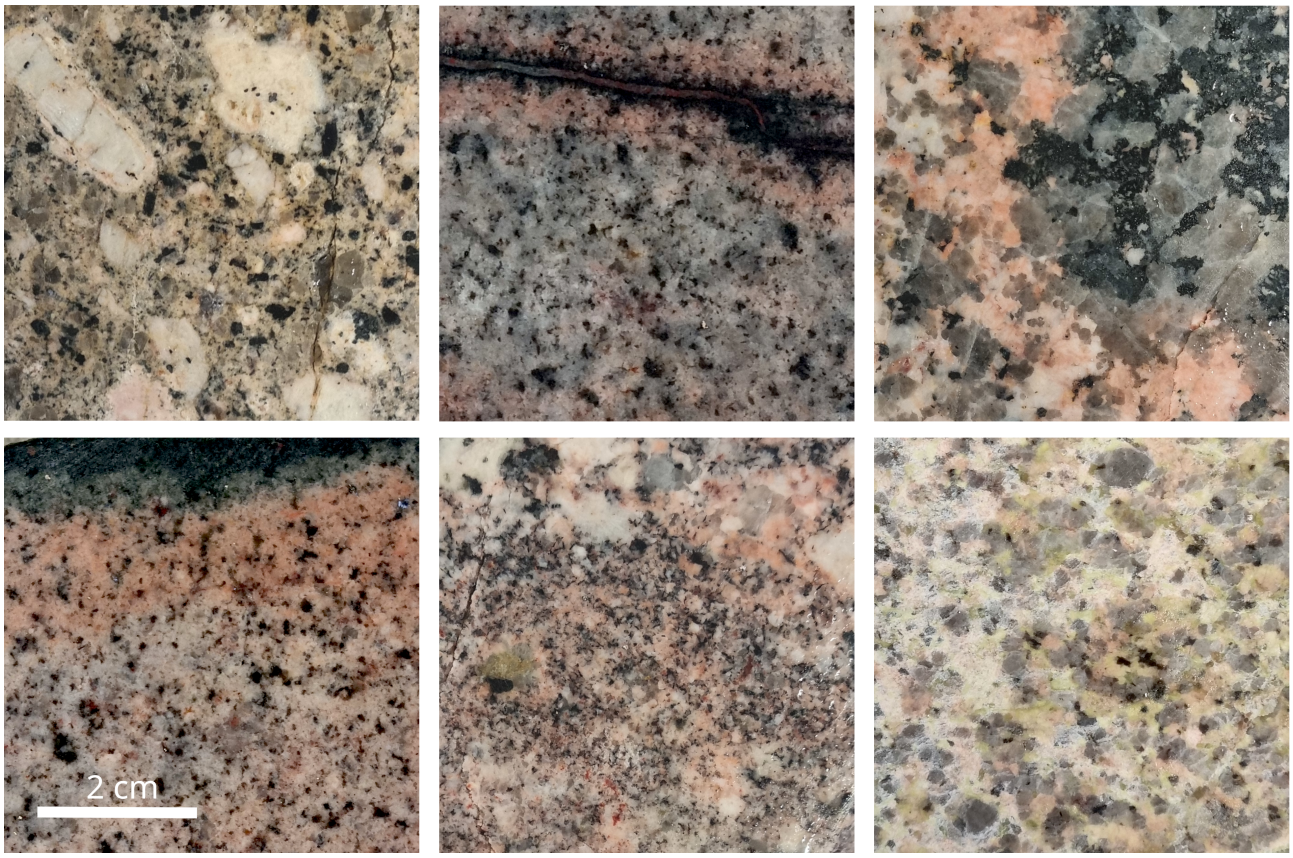


Figure 4: *Overview of the variety of textures and grain sizes between the different samples. From left to right, top to bottom: WF1, FG1, FG7, FG4, FG13, FG11*

Fahsel quarry is an active quarry where granite is mined for the production of gravel. Of all locations this is the location where the most fresh rock was available, which is a large number of samples were collected here. Field photos from this location are shown in Figure 5a,b. The granite at Fahsel is mostly equigranular, fine-grained to medium-grained. However, small lenses or veins of coarse-grained or pegmatitic granite are not uncommon. In some places K-feldspar megacrysts and more rarely quartz megacrysts can be found, though they are much rarer than in the more porphyritic variants of the Eibenstock granite. Tourmaline is rather common at this location and often forms spherical aggregates together with quartz, so-called tourmaline suns. These tourmaline suns are commonly surrounded by a ring of K-feldspars and range in size from a centimeter to around ten centimeters. Small greisen veinlets were found in the granite at this location, however these are often narrow and none wider than half a centimeter have been found. The granite at Fahsel is cut by a large fault that is accompanied by Fe-Mn mineralization and alteration of the granite, and hematite-colored alteration of the granite is very common around the fault zone. A green chloritic or epidote alteration is found in some areas of the quarry that could be related to greisenization or to the fault.

Walfischkopf Is a granite outcrop on top of a hill near Schönheide. Here the Eibenstock is porphyritic with a medium-grained ground mass. It has a pale color and the megacrysts are mostly feldspar and more rarely quartz. A field photo showing this texture is shown in Figure 5d. In the town of **Schönheide** there is a small hill where waste dumps and remnants of historical small-scale mining operations are common. One small sample of medium-grained quartz greisen was taken at this location. **Steinberg** is a small hill near the town of Carlsfeld.

One sample of unaltered, coarse-grained, equigranular granite was taken here. In **Carlsfeld**, an old quarry hosts a small outcrop of heavily greisenized granite. This granite has a very clear banding due to the greisenization (Figure 5a). This is the largest greisen occurrence that was visited, which is reflected in the samples that were taken here. The samples CF1 and CF2 are very heavily greisenized, containing only small bands of less altered granite in between. The greisen is relatively fine-grained and the granite is medium-grained and equigranular.

A map view of these locations is seen in Figure 1, and a detailed description of the samples and how they were analyzed can be seen in Table 2. The samples are granites and greisens belonging to the Eibenstock pluton, with variation in their mineralogy and modal composition. The samples were selected to show maximal diversity, and special care was taken to select samples that showed a transition from clean granite to greisen. An visual overview of selected samples is seen in Figure 4. In this overview, samples FG1 and FG4 show clear greisenization with the veins running through them. Samples FG11, FG13 and FG7 show alteration textures, with FG7 hosting a spherical assemblage of tourmaline, which is the dark area in the picture. It is not possible to determine from these pictures if these samples are greisenized or not. WF1 is the only relatively fresh sample in this overview, showing only minor signs of alteration along the edges of the large feldspar in the bottom right. The overview also shows the variation of grain sizes in the samples, with fine grained samples like FG13 along with coarse medium-grained to coarse-grained samples such as FG7 and FG11.

After collection the samples were cleaned, labeled and selected samples were cut into slabs for scanning using μXRF. The element maps measured using μXRF were used to decide where to take thin sections, which were cut from the same slabs that were measured. This method additionally allows plotting of the thin sections directly on the element maps.

Table 2: *Sample locations, rock descriptions and applied geochronological methods.*

Sample	Location	Lat (N)	Long (E)	Rock description	μXRF	No. of thin sections	CL	Optical Microscopy
Granite samples								
FG1	Fahsel Quarry	50.5196039	12.6403136	f.g. m.g. equigranular with greisen veinlet surrounded by potassic alteration	x	0		
FG2	Fahsel Quarry	50.5196039	12.6403136	m.g. equigranular, some Fe-Mn alteration	x	1	x	x
FG3	Fahsel Quarry	50.5196039	12.6403136	c.g. equigranular, trend from tourmaline sun to regular granite with Tur+Qz -> K-fsp+Qz -> Plg+Qz	x	2	x	x
FG4	Fahsel Quarry	50.5196039	12.6403136	c.g. equigranular + greisen vein	x	1	x	x
FG5	Fahsel Quarry	50.5196039	12.6403136	f.g. to aplitic + greisen veinlet	x	1	x	x
FG6	Fahsel Quarry	50.5196039	12.6403136	f.g. m.g. equigranular, pale	x	0		
FG7	Fahsel Quarry	50.5196039	12.6403136	m.g. c.g. equigranular, tourmaline sun surrounded by K-fsp	x	1	x	x
FG8	Fahsel Quarry	50.5196039	12.6403136	f.g. equigranular + greisen vein	x	1	x	x
FG9	Fahsel Quarry	50.5196039	12.6403136	m.g. c.g. equigranular, transition to tourmaline sun	x	1		x
FG10	Fahsel Quarry	50.5196039	12.6403136	m.g. equigranular heavily altered green fsp + vein	x	1	x	x
FG11	Fahsel Quarry	50.5196039	12.6403136	m.g. equigranular heavily altered green fsp	x	1	x	x
FG12	Fahsel Quarry	50.5196039	12.6403136	altered granite from fault zone with hematite and chalcedony	x	1		x
FG13	Fahsel Quarry	50.5196039	12.6403136	f.g. m.g. c.g. equigranular granite showing all textures from FG samples + pegmatite	x	3	x	x
WF1	Walfischkopf	50.4981844	12.5583078	f.g. m.g. porphyritic, Or-rimmed Ab megacrysts	x	1		x
SH1	Schönheide	50.5090719	12.5506500	m.g. c.g. equigranular, little to no fsp, greisen, heavily weathered	x	1	x	x
SB1	Steinberg	50.4419297	12.5881044	c.g. equigranular "typical" granite	x	1		x
Greisen samples								
CF1	Carlsfeld	50.4336617	12.5943919	Quartz-White mica greisen	x	2		x
CF2	Carlsfeld	50.4336617	12.5943919	Quartz-White mica greisen	x	2	x	x

Methods: μXRF = Micro X-ray Diffraction; CL = Cathodoluminescence microscopy; **Abbreviations**: f.g. = Fine-grained; m.g. = Medium-grained; c.g. = Coarse-grained; fsp = Feldspar; ab = Albite; or = Orthoclase; qz = Quartz; tur = Tourmaline. An 'x' means that a method was applied to the sample or its thin sections.



Figure 5: ***a)*** *Greisenized granite showing vertical banding, Carlsfeld;* ***b)*** *Quarry face at Fahsel, trees in background for scale;* ***c)*** *Pegmatite lens at Fahsel with fine-grained equigranular granite on the left of the lens;* ***d)*** *Porphyritic medium-grained granite at Walfischkopf.*

6 Methodology

6.1 Micro-XRF

Micro X-ray fluorescence spectrometry (μXRF) is a non-destructive method of elemental analysis. In this thesis μXRF spectrometry was used to get a qualitative estimate of the geochemistry of the sample material. This was done by scanning a large area of each sample at a relatively coarse resolution to get adequate sample coverage while keeping the total measurement time reasonable. For this analysis a Bruker M4 Tornado PLUS μXRF spectrometer was used, which is fitted with rhodium and tungsten tubes. Bruker Nano GmbH, 2026 X-rays were generated using the rhodium tube at an accelerating voltage of 50 kV and a current of 300 μA. Samples were measured at a spatial resolution of 150 μm with a measurement time of 100ms per pixel over one cycle. The X-ray chamber was held under a vacuum of 2 mbar residual pressure, which provides increased detection of lighter elements by reducing the attenuation of lower-energy X-rays due to air. This setup technically allows for the detection of elements down to C. In practice however, the measurement time of only 100ms does not allow accurate measurements of the lightest elements, and the lightest element which can be measured with an acceptable signal-to-noise ratio is sodium. Elements were selected from the raw spectral data using the Bruker M4 Tornado software and were exported as raw intensity maps for further analysis. The element maps produced after measurement were used to select areas of interest for polished thin sections. These could then be used to further analyse the samples with

CL and optical microscopy. The elements that were able to be measured using this experimental setup were Si, Al, Fe, K, Na, Ca, Rb, P, Mg, Mn, and Ti. These elements were present in measurable amounts in all samples. Additionally, elements with less pronounced peaks (i.e. with a low signal-to-noise ratio) were selected to provide some additional information for machine learning purposes. These elements were S, O, Zr, Zn, and Ga. Sn was also measurable, with a good signal-to-noise ratio, but only in samples SH1, CF1, and CF2.

Bulk measurements were obtained from micro-XRF maps by averaging the spectra for selected pixels prior to running the quantification method in the M4 Tornado software. This allows multiple bulk measurements for a single sample by selectively including or excluding parts of the map. This was done for samples that contain greisen veins, such as FG5 and FG8. For these samples two bulk measurements were made, one for the granite without the greisen vein, and one for the greisen vein itself.

6.1.1 Processing of XRF data

The elemental maps were produced by selecting peaks corresponding to each element in the M4 TORNADO software and exporting these as raw text files for each element, with each file containing the intensity per pixel for that element. For ease of use and further analysis these text files were combined into a single file using a simple python script. This resulted in a three-dimensional $.npz$ datacube $X_{i,j,k}$ for each sample that contains pixels in the first two dimension i, j, and elemental intensities in the third dimension k for each pixel. The file also contains a list of elements in the same order as the element maps in the datacube.

6.1.2 XRF-based Automated Mineralogy

Manual Phase Identification Alongside identifying the phases using machine learning methods, a manual mineral phase attribution was made. This was done to compare to the clustering model and to check its performance. In this manual phase attribution, minerals are classified by applying different rules to the elemental maps. The most confident rules come first, such as the rule for apatite, which states that any high-Ca, high-P, and low-Si mineral should be classified as apatite. This is the clearest mineral to identify which is why it comes first in the rule set. Secondly, the rule for quartz is applied, which is any pixel that has an Al/Si ratio close to zero. Afterwards comes the rules for feldspar, which is then split into albite and K-feldspar, then the rule for tourmaline, and lastly the rule for micas, which are subsequently split into biotite and muscovite. A graphical overview of the set of rules can be seen in Figure 6.

Tuning of the rules to the dataset was greatly aided by the thin sections and the photographs of the slabs, as these gave a rough idea of what minerals should be present in which samples. An example is tourmaline, which is only present in large quantities in samples FG3, FG9, and FG7. The rule sets were adjusted so the classification fit this observation. In this sense the classification is biased, unlike the clustering algorithm, which is unbiased and purely works on the relationships in the data. The set of rules that was used is as follows, where percentages are in weight percent: **Apatite** is classified by any pixel with a $P_2O_5 > 10\%$ and $CaO > 10\%$ and $SiO_2 < 20\%$. **Quartz** is classified by any pixel with $Al_2O_3/SiO_2 < 0.2$. **Feldspar** is classified by $Al_2O_3/SiO_2 >= 0.2$ and $FeO < 5\%$ and $P_2O_5, CaO < 10\%$, which is then split into **Plagioclase** which is a feldspar pixel with $K_2O/(K_2O+CaO+Na_2O) <= 0.8$, and **K-Feldspar** is any feldspar pixel with $K_2O/(K_2O+CaO+Na_2O) > 0.8$. Then, the remaining pixels with $FeO > 5\%$ are classified into **Tourmaline** with $MnO/(FeO + MnO) < 0.01$ and **Mica** with $MnO/(FeO + MnO) >= 0.01$. This group is then split into **Biotite** with $K_2O/(K_2O + FeO) < 0.5$ and **White mica** with $K_2O/(K_2O + FeO) >= 0.5$.

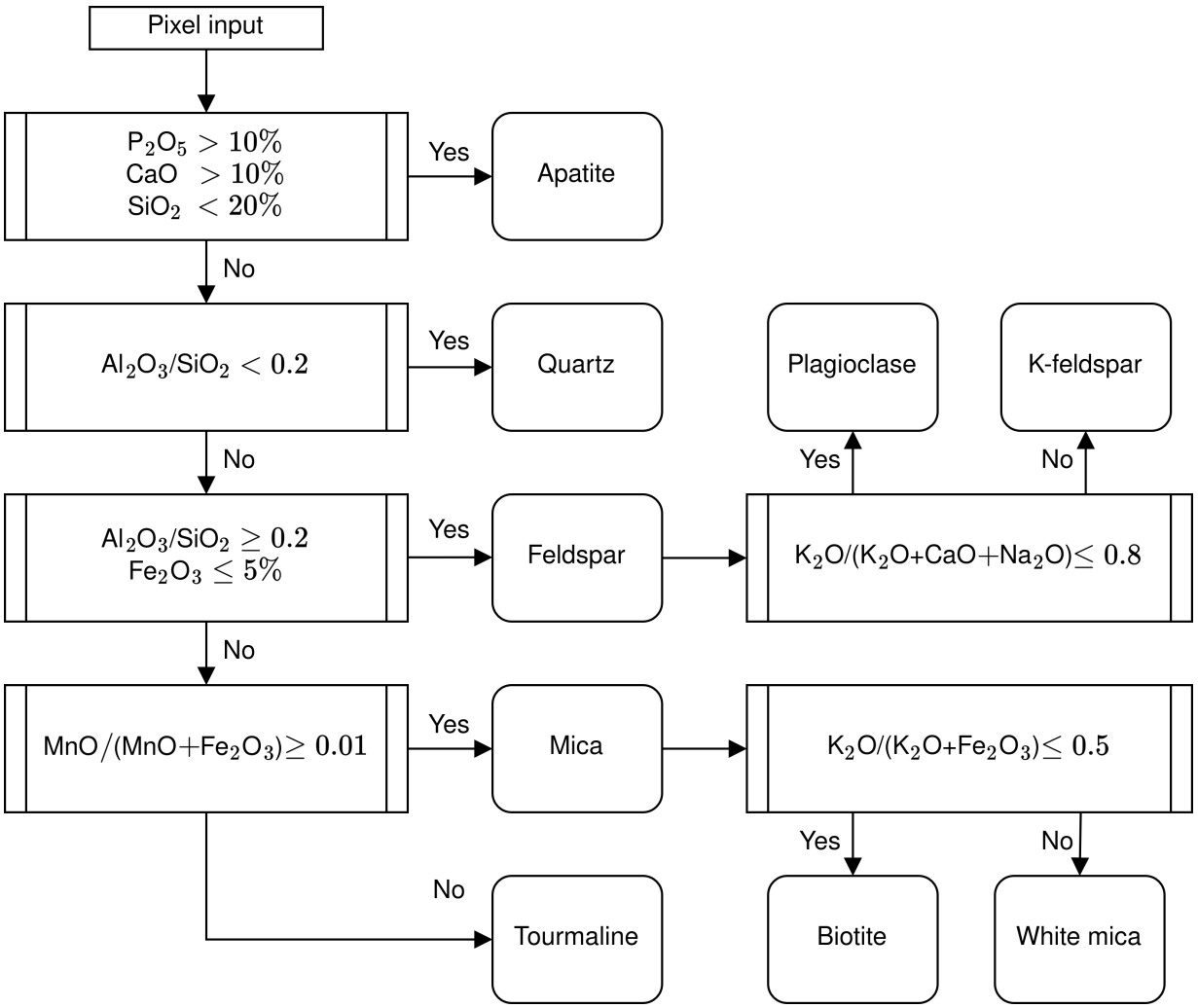


Figure 6: *Flowchart for determining the mineralogy for a given XRF map pixel corresponding to the rules specified above. Every pixel is assigned a single mineralogy corresponding to the rules. Minerals such as mica are also grouped for further analysis.*

Unsupervised Learning In addition to selecting areas for thin sections, the elemental maps were also used for unsupervised machine learning. This allowed for the automatic identification of different mineral phases across all samples. The model used to cluster the data is a Gaussian mixture model. This model was chosen because it outputs probability maps in addition to simply labelling the data, which can be used to evaluate the confidence of the classification per cluster or pixel. This also aids in finding mixed pixels, where a mixed signal from two mineral phases was measured. Another reason why this model was chosen is because it takes into account the covariance between features, which is useful when working with XRF data, as many elements are correlated because of the mineral compositions.

All measurements were combined into one big dataset prior to clustering. The clustering algorithm was thus fitted on all samples at once, instead of being re-fitted for each sample.

Before clustering the data was processed to provide the best results. First each pixel was normalized by the sum of all element intensities for that pixel according to the formula

$$X_{i,j,k} = X_{i,j,k} / \sum_{k=0}^{K} X_{i,j,k} \qquad \forall i, j \tag{2}$$

This results in an XRF map where all pixels sum to one when summing along the element dimension. The total intensity

$$X_{i,j}^{tot} = \sum_{k=0}^{K} X_{i,j,k} \tag{3}$$

was also stored as a separate variable, as it provides additional information that could be relevant for clustering. Specifically, this allows the clustering algorithm to identify noise more easily, as non-sample pixels have a lower total intensity. After normalization, a centered-log-ratio transform was applied to transform the data:

$$\mu_k^{geom} = exp(\frac{1}{n}\sum_{i=1}^{n} ln(X_{i,k})) \tag{4}$$

$$X_{i,k}^{CLR} = ln(X_{i,k}/\mu_k^{geom}) \tag{5}$$

because many of the individual element distributions have medians close to zero but long tails with outliers. The CLR transform transforms these distributions to near gaussian distributions, which allows the clustering algorithm to perform better. The total intensity map was not incorporated in this transform as it is not a compositional variable. Instead it was transformed logarithmically:

$$X_{i,j}^{tot} = ln(X_{i,j}^{tot} + 10^{-9}) \tag{6}$$

To bring it to the same statistical scale as the element maps. A small constant 10^{-9} was added to prevent zeroes from blowing up to $-\infty$ The CLR-transformed element maps and the log-transformed intensity map were combined and used as input data for a principal-component analysis (PCA). The first 8 components explain 95% of the variance in the dataset and were thus used for clustering while the other components were dropped. A gaussian mixture model was used for clustering the dataset as it allows probabilistic output of the confidence of clusters. This can be used to identify cluster boundaries or mixed pixels, where two or more minerals contribute to the signal.

6.2 Thin section microscopy

Both transmitted-light microscopy and cathodoluminescence microscopy were used to study the samples. the CL system used is optical instead of SEM-based, which allows full colour images of the CL to be captured.

Transmitted-light Microscopy Transmitted-light microscopy was carried out on the thin sections for textural and mineralogical analysis. For this, a Zeiss Axio Imager.M2 fitted with a Zeiss Axio Cam MRc5 camera for taking photomicrographs. Both plane-polarized light (PPL) and cross-polarized light (XPL) were used, as well as reflected light microscopy to gain insight into the opaque minerals present in a number of the thin sections.

Cathodoluminescence Microscopy The cathodoluminescence (CL) microscope used in this thesis is a Lumic HC1-LM ”hot cathode” cathodo-luminescence microscope fitted with an OLYMPUS DP72 digital video camera Neuser et al., 1995. CL measurements were taken at an accelerating voltage of 13 kV with a current of approximately 0.2 mA. The CL setup is fitted with an additional Acton SpectraPro 2300i spectrometer that allows the user to record the spectrum of CL emissions in a 10 µm spot. The spectrometer used is a Princeton Instruments Spectrapro

7 Results

In this chapter the results of CL, optical microscopy and XRF are presented. The aim of this chapter is to provide the reader with a clear overview of the mineralogy of the samples, the textures present both microscopically and macroscopically, and the chemical composition of the samples.

Sample / Oxide [Wt%]	Na_2O	MgO	Al_2O_3	SiO_2	K_2O	CaO	TiO_2	MnO	Fe_2O_3	P_2O_5	Total
Granite samples											
FG1	3.37	0.00	9.60	59.20	4.77	0.34	0.03	0.04	0.89	0.14	78.51
FG2	2.36	0.08	11.03	67.31	5.70	0.30	0.03	0.02	1.05	0.06	88.09
FG3	3.76	0.00	11.59	61.08	5.10	0.33	0.10	0.02	2.29	0.07	84.43
FG4	3.43	0.00	11.40	63.28	5.34	0.42	0.08	0.03	1.18	0.15	85.40
FG5	3.25	0.00	9.94	65.16	4.85	0.22	0.03	0.06	1.48	0.03	85.15
FG6	3.51	0.00	10.06	61.09	5.19	0.28	0.03	0.03	0.82	0.09	81.24
FG7	2.04	0.00	7.93	74.02	4.03	0.41	0.11	0.03	2.22	0.09	90.96
FG8	3.58	0.00	10.52	65.48	5.06	0.28	0.03	0.04	1.14	0.07	86.34
FG9	3.54	0.00	12.35	55.50	5.39	0.35	0.06	0.03	2.09	0.13	79.58
FG13	3.68	0.02	9.38	57.57	3.93	0.37	0.06	0.02	1.02	0.07	76.22
SB1	3.12	0.03	11.03	65.61	6.25	0.10	0.10	0.02	1.09	0.00	87.47
WF1	2.82	0.10	10.03	56.95	5.54	0.40	0.17	0.03	1.41	0.02	77.63
Altered samples											
FG10	0.01	0.02	10.17	66.52	5.38	0.01	0.04	0.10	1.16	0.00	83.56
FG11	0.00	0.01	9.67	64.89	5.69	0.11	0.04	0.07	0.96	0.00	81.58
Fault quartz											
FG12	0.00	0.00	1.04	69.87	0.27	1.00	0.01	0.04	3.53	0.83	76.62
Greisen samples											
FG5 (Greisen vein)	1.44	0.00	9.12	67.06	4.13	0.11	0.02	0.12	3.63	0.00	85.83
FG8 (Greisen vein)	1.59	0.00	11.86	66.89	5.12	0.57	0.03	0.14	3.36	0.24	90.00
CF1	0.07	0.00	8.66	62.76	4.91	0.12	0.06	0.10	3.91	0.00	80.77
CF2	0.09	0.01	10.00	66.91	5.56	0.20	0.06	0.07	3.17	0.05	86.30
SH1	0.05	0.07	9.80	66.49	4.73	0.17	0.12	0.06	2.60	0.03	84.26

Table 3: *Bulk measurements of samples calculated using XRF maps. MgO values are very close to zero, and CaO values are very low. In greisenized samples, the Fe_2O_3 content and MnO content are higher, whereas Na_2O contents are lower. Altered samples are different from greisen samples because of lower Fe_2O_3 values.*

7.1 Micro-XRF spectrometry

Bulk measurements shown in Table 3 show clearly that greisenization results in depletion of Na_2O, CaO, P_2O_5, (0.40x-0.15x, 0.40x-0.17x, 3.0x-0.0x) and enrichment of MnO and Fe_2O_3 (2x-3x, 2x-3x). This depletion is strongest in K_2O and CaO, and less strong in P_2O_5. Altered samples have a similar geochemical signature to greisen samples, but a lower iron content paired with a near-total depletion of Na_2O. This is illustrated in Figure 7, where greisen samples as well as altered samples, shown in blue and orange respectively, show very low concentrations of Na, as opposed to regular granite samples.

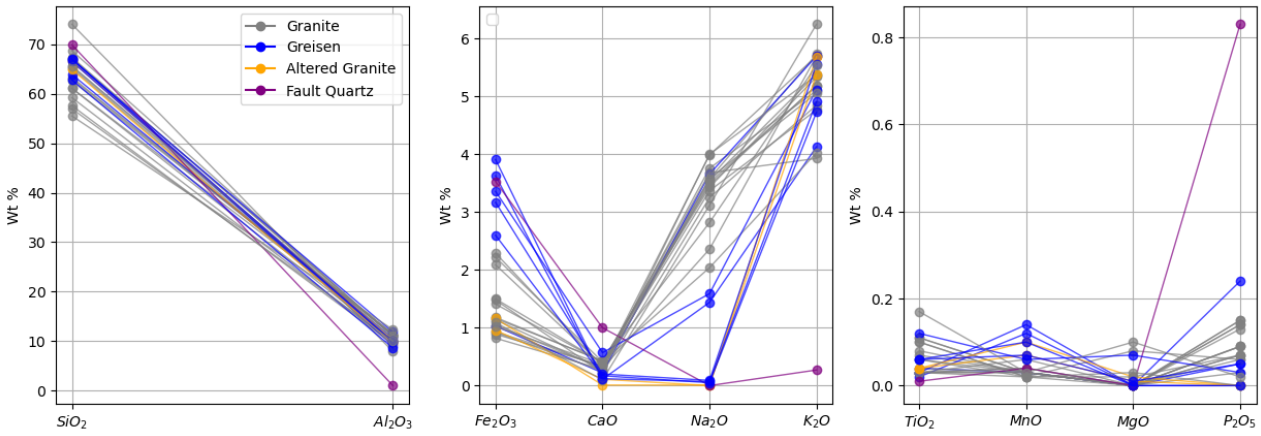


Figure 7: *Visual representation of change in oxide content throughout the samples. Greisen and altered granite samples are all depleted in Na_2O, but greisens are distinguished from altered granites by higher Fe_2O_3 and MnO content.*

7.1.1 Unsupervised Clustering and Manual Clustering

Manual clustering and unsupervised clustering of the XRF maps help understand both the nature of the samples and the XRF data itself. Figure 8 shows results of the unsupervised clustering for all samples except CF2. This figure shows that there appear to be four dominant clusters, clusters 2, 3, 4, and 5. The other clusters are much less common. Clusters 3 and 4 are very prominent in the greisenized and altered samples, whereas clusters 2 and 5 appear only sparsely in these samples. The unsupervised clustering, even though it is set to 8 phases, recognizes less phases than the manual clustering, which contains 7 phases, shown in Figure 9. The non-dominant clusters 1, 6, 7, and 8 in the unsupervised clusters contain mostly noise, and as a result mineral phases that are separate in the manual clustering are grouped together in the automated clustering.

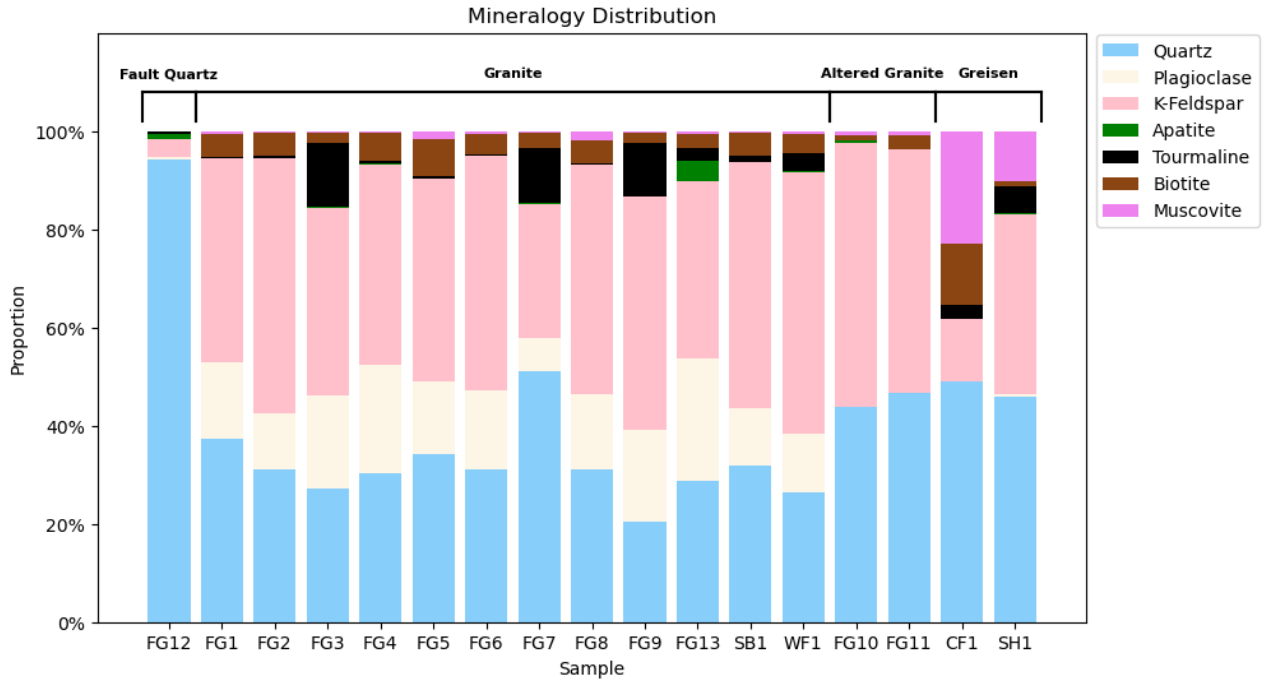


Figure 10: *Mineralogy calculated from XRF maps using manually set phase rules. Altered and greisenized samples contain significantly more micas.*

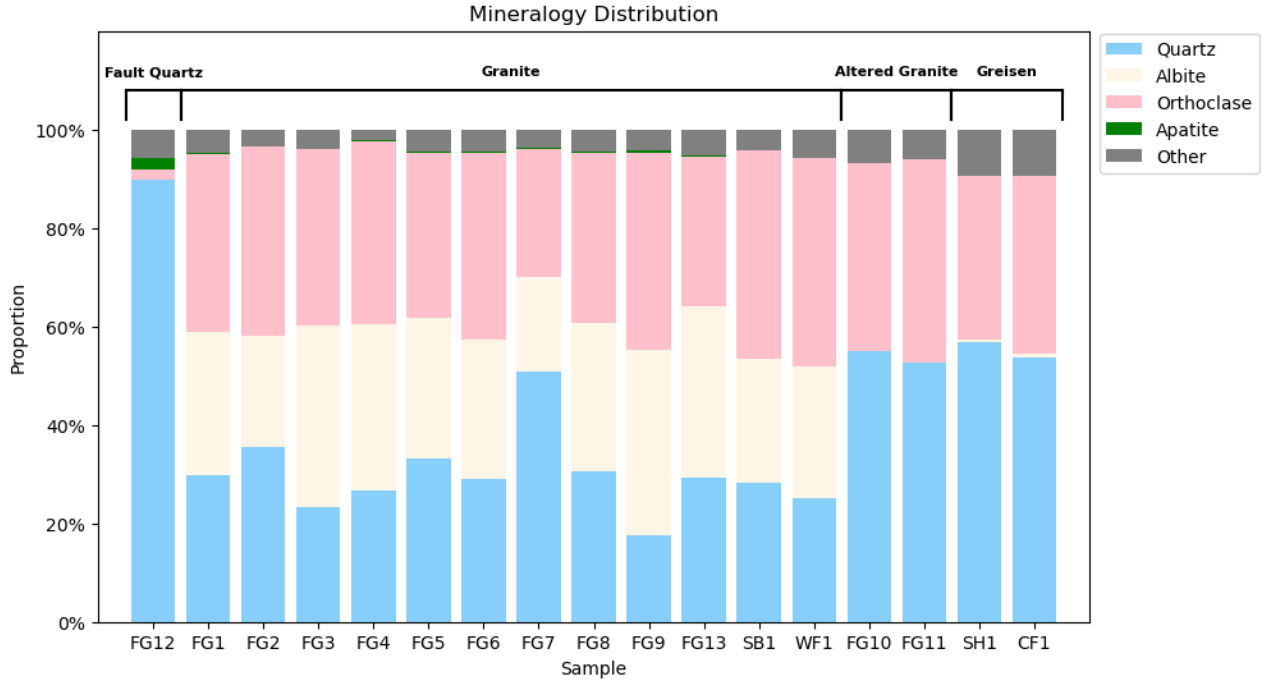


Figure 11: *Mineralogy calculated from CIPW norm using bulk oxide content of the samples.*

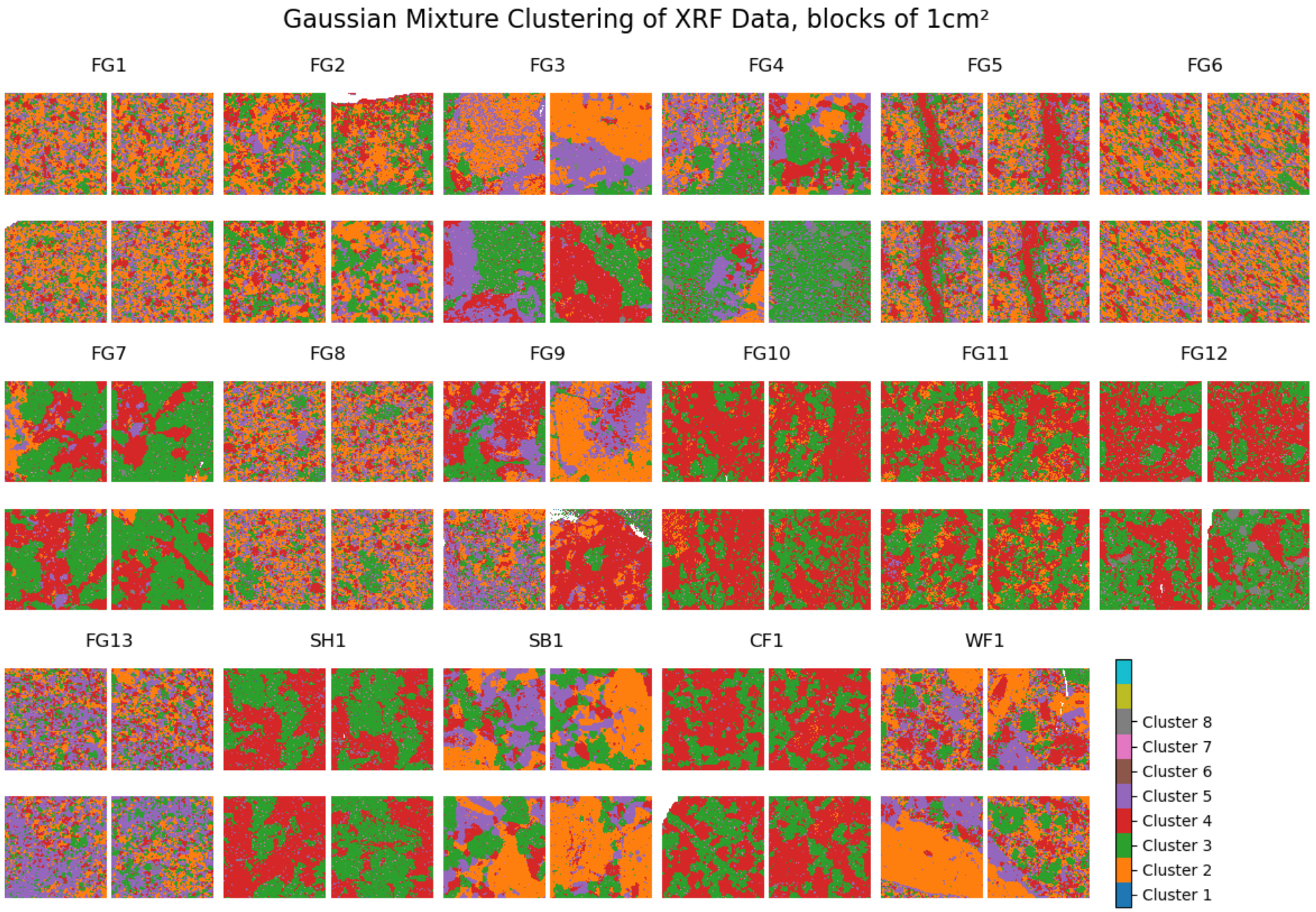


Figure 8: *GMM clustering results for 1x1cm squares of selected samples. The most common clusters in the samples are clusters 2, 3, 4 and 5. The other clusters are much less common. The altered and greisenized samples show a much lower quantity of clusters 2 and 5, and a higher quantity of clusters 3 and 4.*

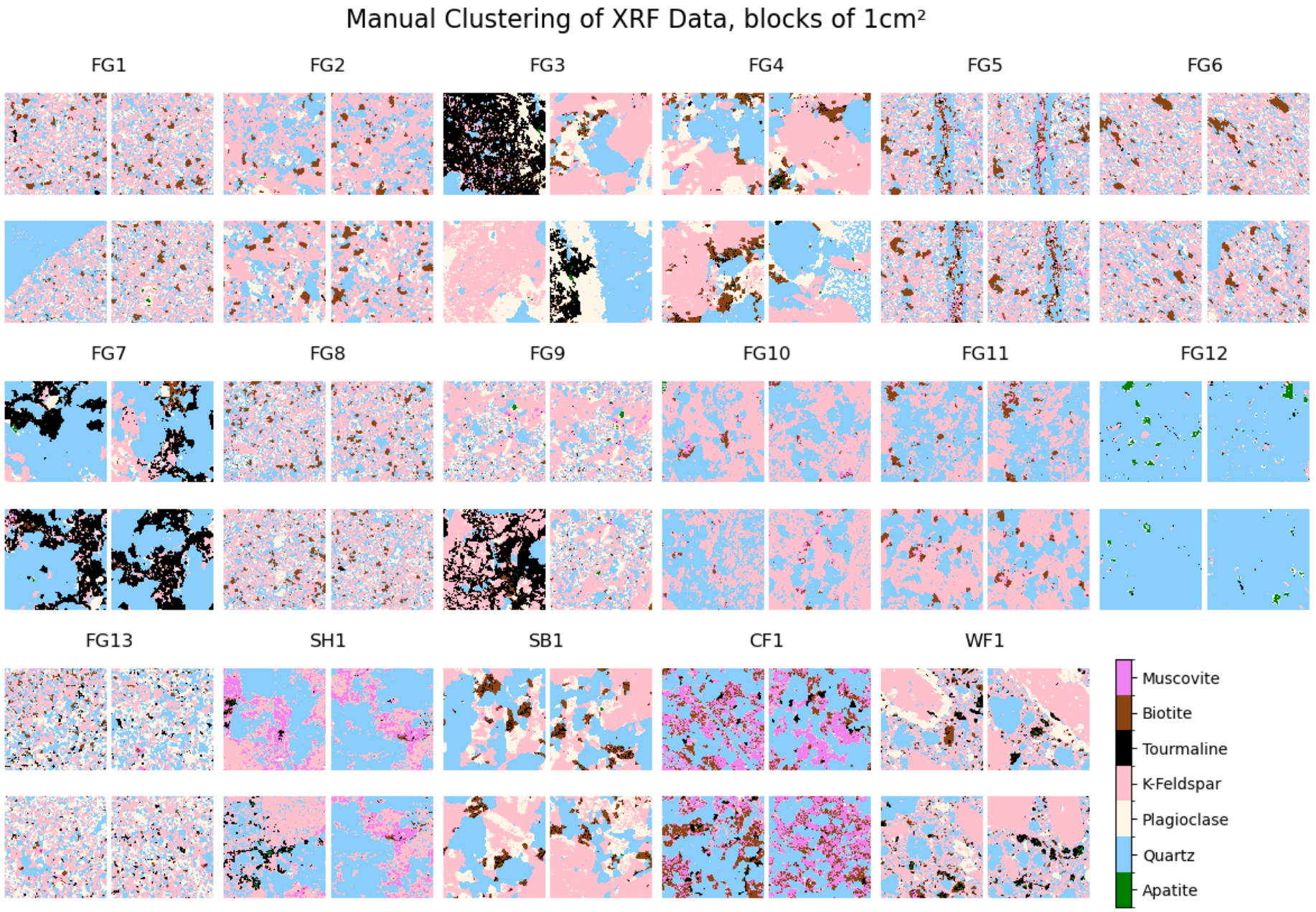


Figure 9: *Manual clustering results for 1x1cm squares of selected samples. The main minerals in the samples are quartz, plagioclase, and K-feldspar. Muscovite is common in greisen samples SH1 and CF1. Tourmaline is largely restricted to samples FG3, FG7, and FG9.*

7.2 Global textures

There is a large variety of textures in the samples even though most of the samples were collected from the same location. The grain size ranges from very fine to very coarse, with some samples being equigranular while others are more porphyritic.

The dominant texture in the samples from Fahsel quarry (FG) show a medium-grained to fine-grained equigranular texture, with rare phenocrysts of quartz or feldspar. More rarely, samples from this location show coarse-grained pegmatitic textures, or fine-grained aplitic textures, notably samples FG4 and FG9. The fine-grained aplitic and coarse-grained textures often appear close to one another, often in the same sample.

Grain boundaries between minerals can be straight and simple, but are more commonly curved, lobate, or sutured, varying per sample. The most developed lobate texture occurs as fingers of one mineral protruding into surrounding minerals. While straight grain boundaries do occur, they are uncommon and are mostly seen in samples showing little signs of hydrothermal alteration. The type of grain boundaries is highly variable however, and often changes even on the scale of a thin section.

Anhedral minerals are very common, and the trend is generally towards more anhedral grains in more altered sections. In particular, quartz shows serrated boundaries in nearly every thin section. In some samples, such as FG13, virtually all minerals are anhedral and the boundaries between them are amoeboid, rounded and ”fingers” of one mineral protrude into other minerals, sometimes forming exclaves. Although this texture seems to become more pronounced in more altered samples, the most altered samples do not have the most irregular grain boundaries. A good example of amoeboid and serrated mineral boundaries is seen in Figure 12. The CL view shows no zoning in the quartz, which excludes greisenization as an explanation for this phenomenon.

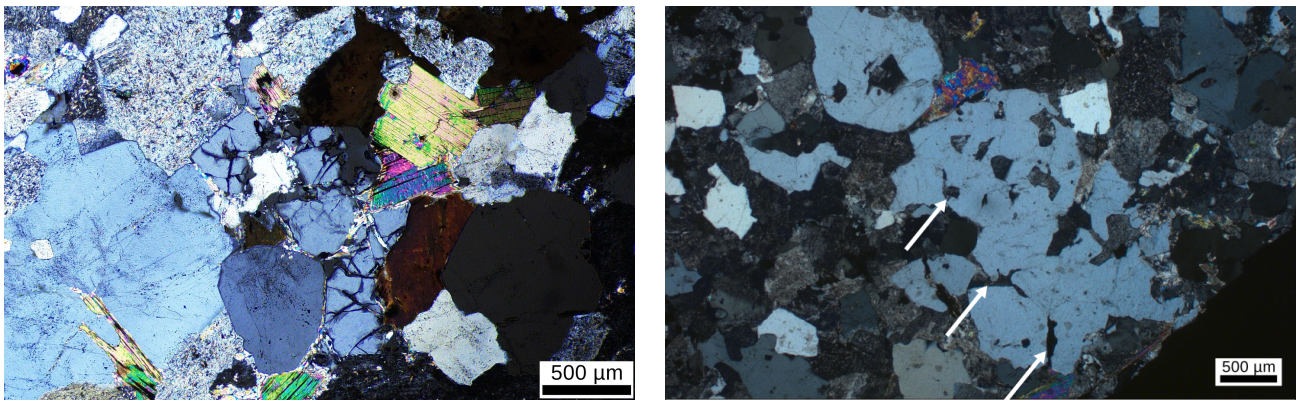


Figure 12: *Amoeboid textures in sample FG13 shown by XPL images of grain boundaries in thin section.* ***A)*** *Regular grain boundaries showing some curvature and a small degree of suturing.* ***B)*** *Lobate and amoeboid grain boundaries seen around large quartz crystal in gray are highly irregular and protrude into surrounding minerals.*

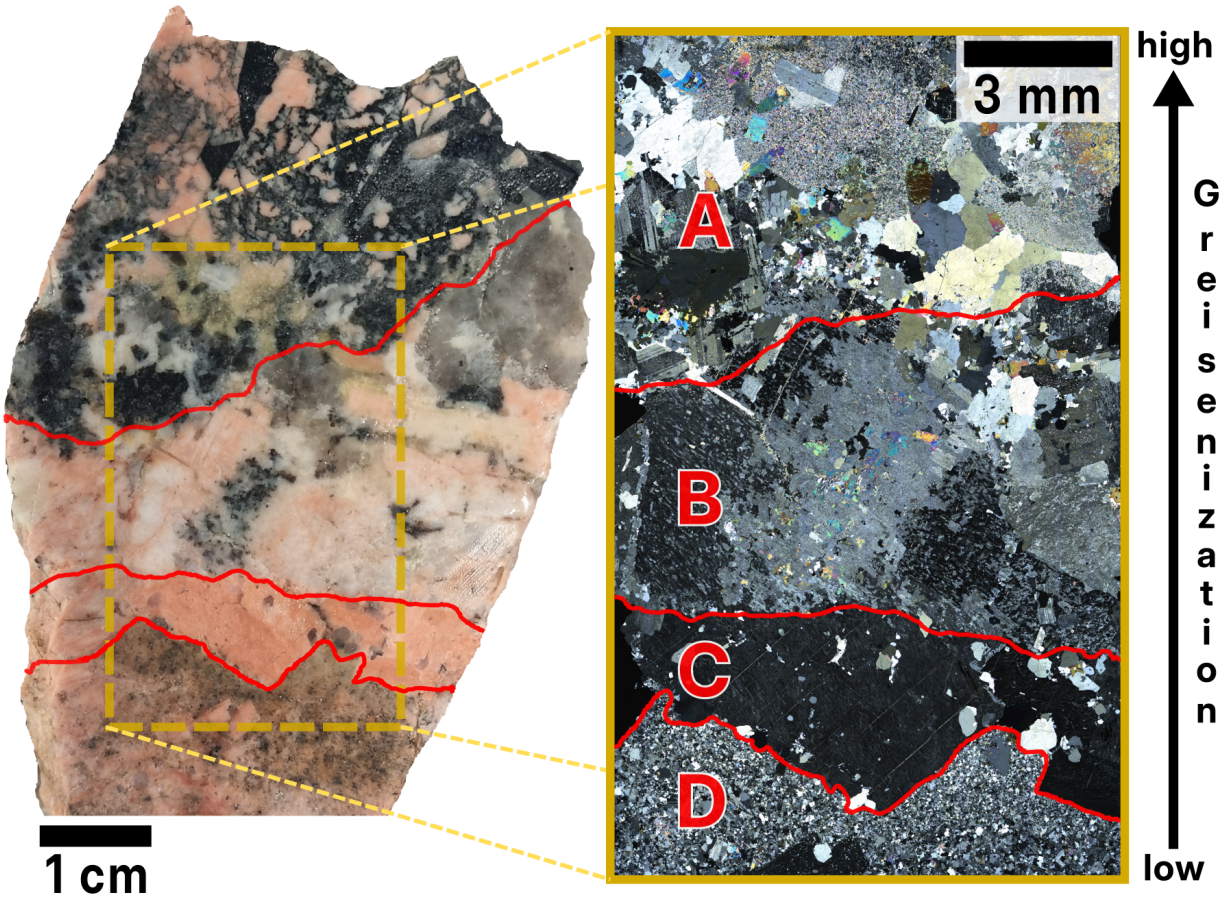


Figure 13: *Hand specimen and thin section scan of sample FG9 showing a distinct zonation as well as an increasing degree of greisenization from bottom to top.* ***A)*** *Strongly greisenized zone with a large grain size and brecciated texture. Feldspars are highly hydrolysed and replaced by white mica and tourmaline.* ***B)*** *Intermediately greisenized zone in which feldspars are partly hydrolysed.* ***C)*** *Non-greisenized, coarse grained zone where feldspars are completely intact.* ***D)*** *Non-greisenized zone with an aplitic texture.*

A number of samples from Fahsel contain tourmaline, and these samples are always coarser, or much finer-grained than the regular granite. The tourmaline either exists in a spherical shape, or in a brittle, brecciated texture, such as can be seen in Figure 13. This figure shows a transition from an aplitic texture, to a pegmatitic texture, to a greisenized texture with a brecciated appearance containing tourmaline.

7.3 Mineralogy

The mineralogy of the samples can be divided into three groups. The granites, the altered granites, and the greisens. The granites are predominantly composed of quartz, K-feldspar, plagioclase, biotite, and white mica, with the most common accessory minerals being apatite, topaz, tourmaline, cassiterite, zircon and opaque minerals. The reason for labeling the non-biotite micas white mica instead of muscovite is because with these methods there is no way to verify if the white mica is muscovite or another white mica such as zinnwaldite, siderophyllite, protolithionite. Tourmaline is only present in samples FG3, FG7 and FG9. In samples FG3 and FG7 it is present in spherical assemblages that radiate out from a single point. In these assemblages the tourmaline macroscopically occurs with quartz where both minerals are coarse and easy to recognize. Microscopically the picture is different, because microscopically, tourmaline is intergrown with feldspar in a kind of spiderweb-like pattern. In sample FG9 however, the tourmaline is the cemented matrix of a small-scale breccia-like facies in which the brecciated grains are part of the original granite.

In the altered granites the orthoclase and albite feldspars have partially altered to a sericitic assemblage of white mica, which is in turn largely altered to chlorite. The greisens consist mainly of quartz and muscovite. In these greisens biotite and feldspars have been destroyed and replaced by an assemblage of white mica and quartz.

Apatite and topaz are the most common accessory minerals, followed by cassiterite and opaque minerals such as hematite. The opaque minerals replace muscovite and follow the cleavage of the mica.

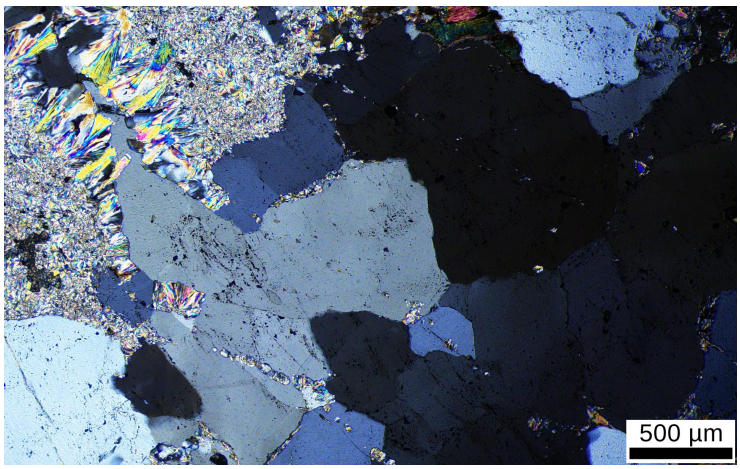
7.4 Detailed textural and compositional descriptions per mineral

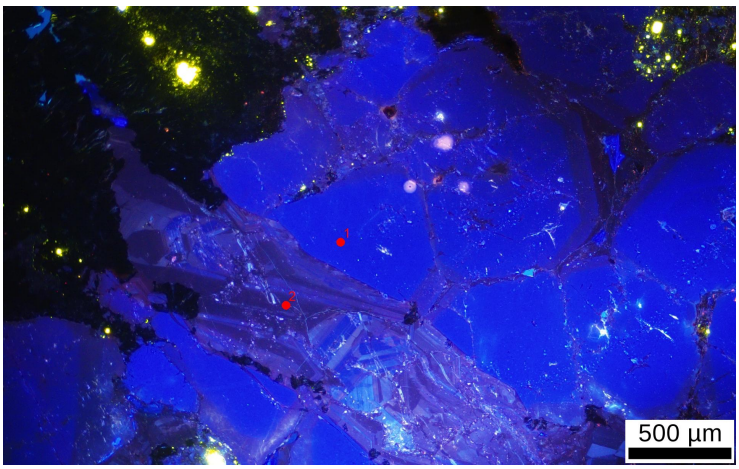
In the following section, detailed descriptions of main and accessory minerals can be found, which are based on all methods used. Five standalone sheets, found on the next pages, present a summary of the characteristics of the most important minerals. In addition to these sheets, the full descriptions for each mineral group can be found in the pages after.

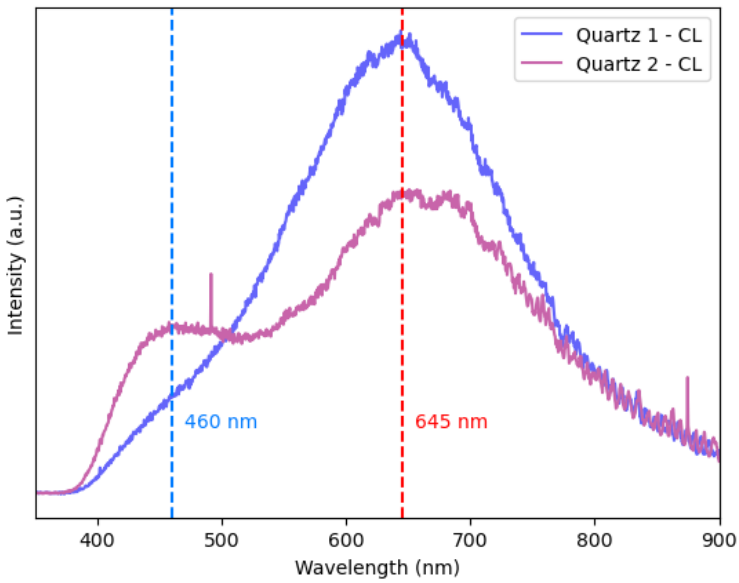
Location	**Mineral**	**Lithology**
Eibenstock granite, Saxony, Germany	Quartz	Greisenized granite

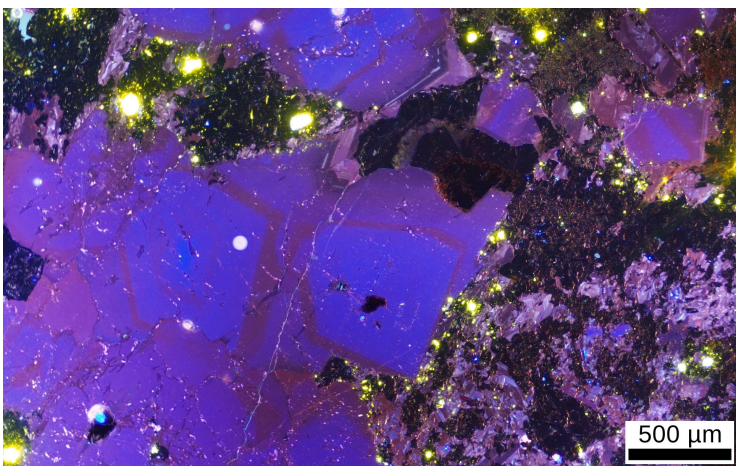
Transmitted-light Microscopy		**Optical Catholoduminescence Microscopy**		**Micro-XRF Spectrometry**	
Microscope	Zeiss Axio Imager.M2	**Microscope**	Lumic HC7-LM	**Spectrometer**	Bruker M4 Tornado Plus
Camera	Axio Cam MRc5	**Camera**	Olympus DP74	**Tube Parameters**	Rh, 50kV, 300 μA
Objective	EC Epiplan-Neoflur Zoom 2.5x/0.075 Pol M27	**Spectrometer**	Acton SpectraPro 2300i	**Resolution**	150 μm
				Dwell time	100 ms

Quartz is subhedral to anhedral, and tends to be more anhedral in more altered samples. In its anhedral form it has serrated boundaries to other grains. Fractures and inclusion trails are common, and these fractures are sometimes filled with micas. In greisenized samples the original edges of quartz grains are commonly overgrown with a layer of mica, which is then in turn overgrown by more quartz. This quartz overgrowth nearly always has the crystal orientation of the original grain, and in the absence of a layer of mica it is impossible to see where the boundary between the original grain and the overgrowth is.
Two phases of quartz exist in samples, a primary magmatic phase and a secondary hydrothermal phase. The difference between these phases is only visible in CL as the hydrothermal quartz generally crystallized from the edges of primary magmatic grains and thus shares the same crystal orientation. This means that the two phases have the same optical properties and are thus basically indistinguishable in XPL. The first phase is a primary magmatic quartz, which is weakly to strongly blue colored. This phase shows little to no zoning, and where present the transition between the zones is gradual. The second phase is a strongly zoned secondary quartz mainly present in greisenized feldspars. This phase is a lighter blue in CL with sharp transitions between the zones. Spectral measurements of these two phases show a distinct difference. Primary quartz has broad emission peaks at 460 and 645 nm, whereas in secondary quartz the peak at 460 nm is very small to absent.







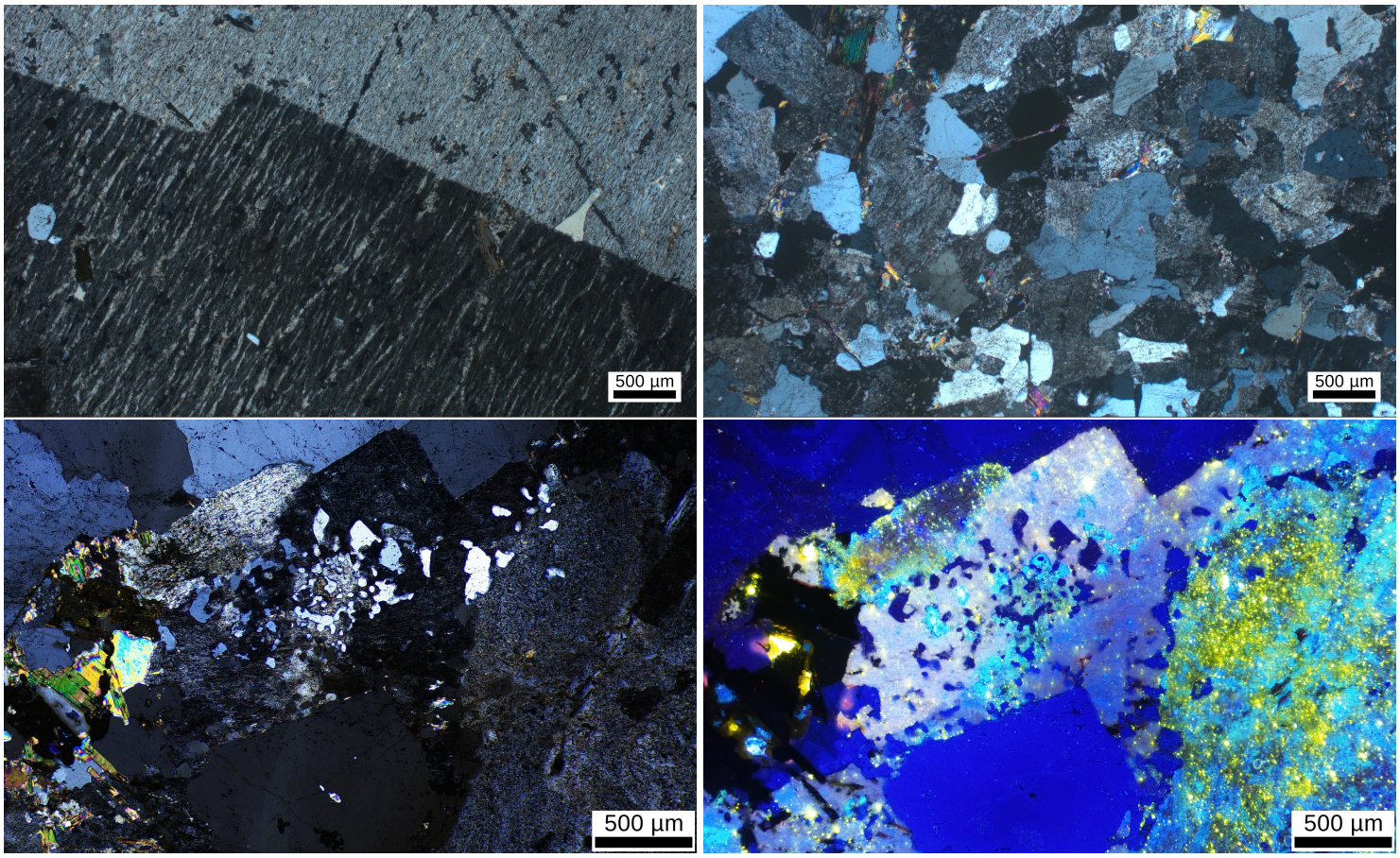


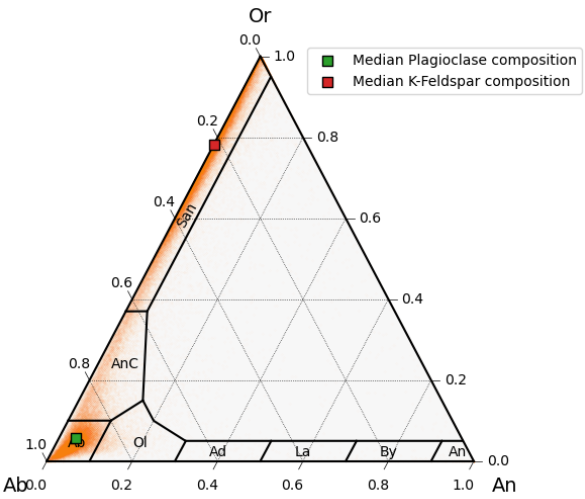
Top: *Left: XPL, right: CL. Primary magmatic quartz and secondary greisen quartz. As visible they have distinctly different appearances in CL. Primary quartz is only slightly zoned, with at maximum three different stages visible (Two stages in this view). Greisen quartz shows distinct zoning with many generations that have sharp transitions. Alongside this it has a different CL signal with a more purple hue.* ***Bottom:*** *Left: CL spectra corresponding to the top right image. As can be seen the greisen quartz has an additional peak at 460 nm that the primary quartz does not have. Right: a more clear example of zoned primary magmatic quartz. Three generations can be seen, with gradual transitions between them. Also visible is the overgrowth of greisen quartz, which is more distinctly zoned.*

Location	Sample ID	Lithology
Eibenstock granite, Saxony, Germany	Potassium Feldspar	Greisenized granite

Transmitted-light Microscopy		Optical Catholoduminescence Microscopy		Micro-XRF Spectrometry	
Microscope	Zeiss Axio Imager.M2	**Microscope**	Lumic HC7-LM	**Spectrometer**	Bruker M4 Tornado Plus
Camera	Axio Cam MRc5	**Camera**	Olympus DP74	**Tube Parameters**	Rh, 50kV, 300 μA
Objective	EC Epiplan-Neoflur Zoom 2.5x/0.075 Pol M27	**Spectrometer**	Acton SpectraPro 2300i	**Resolution**	150 μm
				Dwell time	100 ms

K-Feldspar is subhedral to euhedral in unaltered thin sections, which transitions to anhedral in altered thin sections. In both PPL and XPL the grains have a dirty look, which is different from the very homogeneous looking quartz grains. In unaltered thin sections most K-feldspars show a perthitic texture, which becomes more difficult to recognize as the sections get more altered. In these altered sections these feldspars are replaced in varying degrees by secondary minerals. Sericitic alteration (white mica replacement) is common, as well as replacement by apatite, quartz, or in places even topaz. In some samples, large crystals of tourmaline replace the feldspars. K-feldspathization of plagioclase feldspars is a common feature in most samples. Under CL the primary magmatic color of the K-feldspars is a deep blue. The alteration of many K-feldspars is clearly visible in CL. Parts altered by mica show short-lived red luminescence that dies out within a second. Secondary apatite is easy to see in CL by the bright yellow color of these apatites. Greisenized feldspars are additionally replaced by weakly luminescent violet zoned quartz.





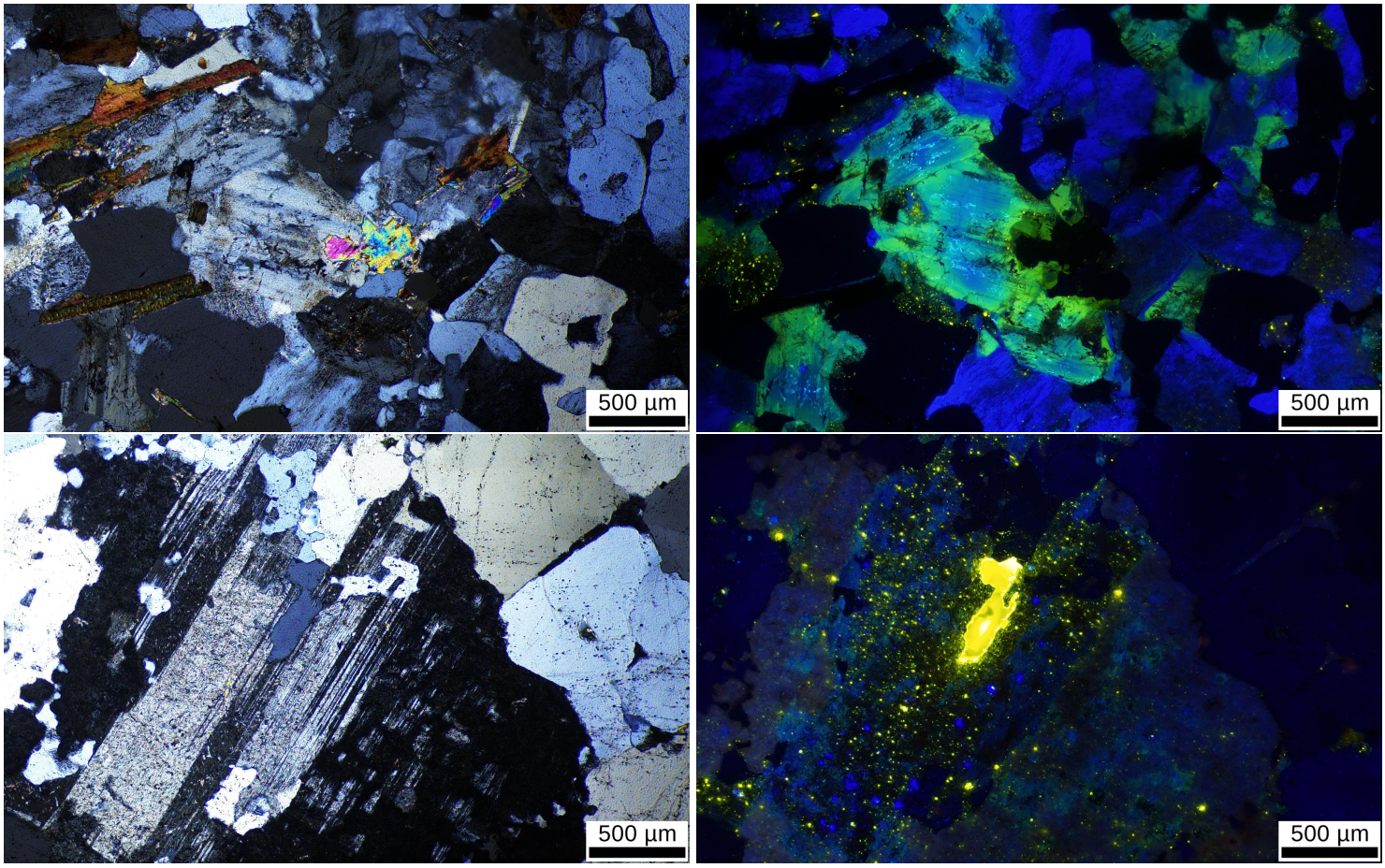
Top: *Left: A relatively clean twinned K-feldspar crystal. Clearly visible is the perthitic texture indicating solid-state exsolution of K-feldspar and plagioclase feldspar lamellae. Also visible are quartz inclusions near the left edge and along the twinning boundary. Right: Typical appearance of K-feldspar in greisenized granite. All of the feldspars have a dirty look due to fine-grained replacement by other minerals.* ***Bottom:*** *Left: XPL, Right: CL image of an altered K-feldspar crystal. The primary light blue CL color is replaced by alteration showing a lighter color, and in the other grains there are many brightly yellow-coloured apatites. The intergrowth texture with quartz is an interesting feature linked to the solid-state readjustment of crystal interfaces in order to minimize the interfacial energy.*

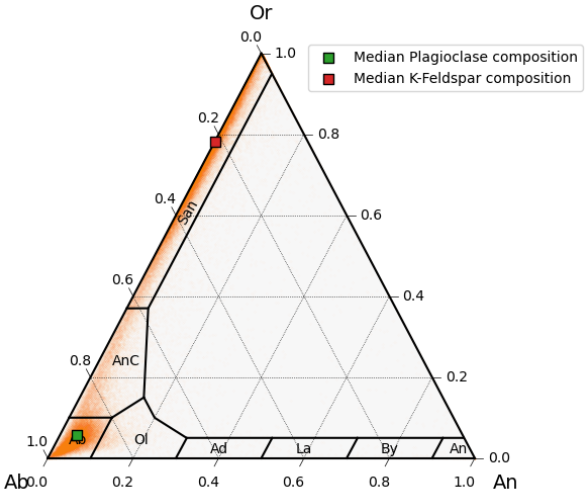
Left: *Ternary diagram of feldspar composition calculated from sample FG3. K-feldspar composition is primarily orthoclase with a large spread between pure albite and pure orthoclase. This reflects the perthitic texture in the K-feldspars, which the XRF resolution is unable to sample, which results in a spread between the two end-members, as there is no sanidine or anorthoclase present.*

Location	Mineral	Lithology
Eibenstock granite, Saxony, Germany	Plagioclase Feldspar	Greisenized granite

Transmitted-light Microscopy		Optical Catholoduminescence Microscopy		Micro-XRF Spectrometry	
Microscope	Zeiss Axio Imager.M2	**Microscope**	Lumic HC7-LM	**Spectrometer**	Bruker M4 Tornado Plus
Camera	Axio Cam MRc5	**Camera**	Olympus DP74	**Tube Parameters**	Rh, 50kV, 300 μA
Objective	EC Epiplan-Neoflur Zoom 2.5x/0.075 Pol M27	**Spectrometer**	Acton SpectraPro 2300i	**Resolution**	150 μm
				Dwell time	100 ms

Plagioclase feldspar is often heavily altered by various stages of greisenization or hydrothermal alteration. The grains are often anhedral and identification in XPL is made difficult by the absence of the characteristic twin lamellae. In CL this is easier, where plagioclase is distinguishable from K-feldspar by its green luminescence color. However, this green color disappears, alongside the twinning, with increasing K-feldspathization of plagioclase feldspars. This also makes plagioclase difficult to recognize in CL in some samples. Furthermore, plagioclase, like K-feldspar, is replaced often by bright luminescent apatites, quartz, white mica, and more rarely topaz. In general, plagioclase feldspars are more heavily affected than K-feldspars.





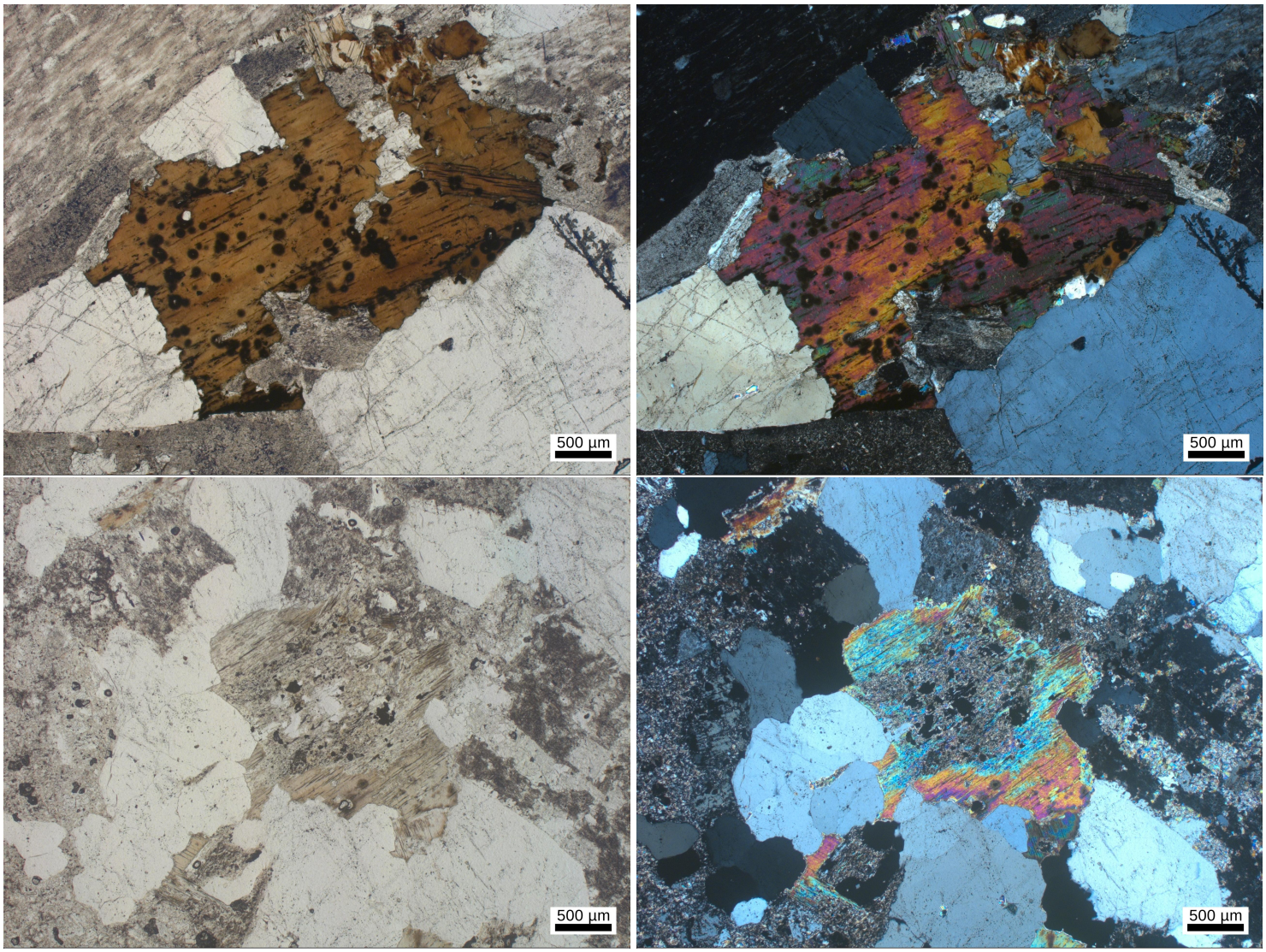
Top: *Left: XPL, Right: CL image of relatively unaltered plagioclase feldspar. In this section plagioclase can be discriminated from quarK-feldspar by its green color. The rims show more green CL than the cores of the grains, and the green CL is mutually exclusive with yellow luminescent apatite. Note the absence of twinning in the XPL image.* ***Bottom:*** *Left: XPL, Right: CL image of an plagioclase still showing twinning in XPL and replacement by bright yellow luminescent apatites in CL. Here the green CL color is very faint to absent. Brighter blue spots can also be seen, which could either be topaz or quartz.*

Left: *Ternary diagram of feldspar composition calculated from sample FG3. Plagioclase composition is albite on average with a small spread towards oligoclase and anorthoclase.*

Location	**Mineral**	**Lithology**
Eibenstock granite, Saxony, Germany	Biotite	Greisenized granite

Transmitted-light Microscopy		**Optical Catholoduminescence Microscopy**		**Micro-XRF Spectrometry**	
Microscope	Zeiss Axio Imager.M2	**Microscope**	Lumic HC7-LM	**Spectrometer**	Bruker M4 Tornado Plus
Camera	Axio Cam MRc5	**Camera**	Olympus DP74	**Tube Parameters**	Rh, 50kV, 300 μA
Objective	EC Epiplan-Neoflur Zoom 2.5x/0.075 Pol M27	**Spectrometer**	Acton SpectraPro 2300i	**Resolution**	150 μm
				Dwell time	100 ms

Biotite is anhedral to subhedral, and is easily seen in PPL by its brown-yellow color and distinct pleochroism. It often contains numerous inclusions of zircon, apatite, or other accessory minerals. Mainly the zircons additionally cause a dark radiation damage halo in the biotite. This can be seen in the top two pictures. Biotite is most common in non-greisenized or non-altered samples. In greisenized and altered samples in is often partially or fully replaced by white mica and/or opaques, as can be seen in the bottom right picture.

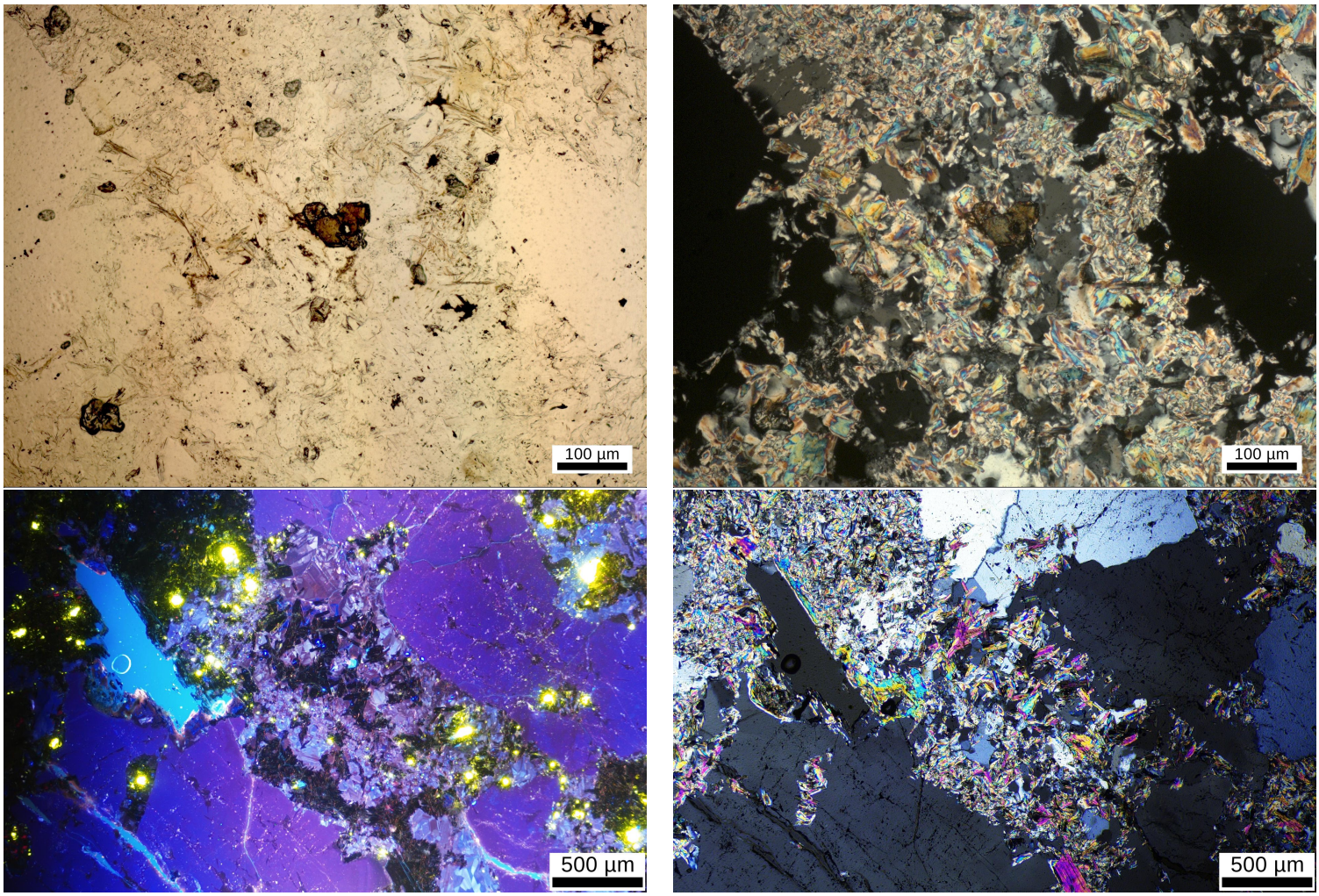


Top: *Left: PPL, Right: XPL image of practically unaltered biotite grain. The crystal shows a dark pleochroism in PPL alongside many radiation haloes around small zircon inclusions. In XPL the grain shows characteristic high interference colours.* ***Bottom:*** *Left: PPL, Right: XPL image of an altered biotite grain in a greisen. The sample shows little pleochroism due to alteration as well as due to the rotation of the grain relative to the polarizer. In XPL the secondary growth of white mica in the core of the grain is clearly visible.*

Location	Mineral	Lithology
Eibenstock granite, Saxony, Germany	White mica	Greisenized granite

Transmitted-light Microscopy		Optical Catholoduminescence Microscopy		Micro-XRF Spectrometry	
Microscope	Zeiss Axio Imager.M2	**Microscope**	Lumic HC7-LM	**Spectrometer**	Bruker M4 Tornado Plus
Camera	Axio Cam MRc5	**Camera**	Olympus DP74	**Tube Parameters**	Rh, 50kV, 300 μA
Objective	EC Epiplan-Neoflur Zoom 2.5x/0.075 Pol M27	**Spectrometer**	Acton SpectraPro 2300i	**Resolution**	150 μm
				Dwell time	100 ms

White mica is a common mineral in the greisenized samples and a less common mineral in the granite samples studied. It is mainly anhedral or subhedral. It is colorless in PPL but often shows a slightly rainbow-like pleochroism. It often occurs as fine-grained subhedral crystal assemblages together with quartz as a replacement texture of primary minerals such as feldspars due to greisenization. It also occurs as larger triangular or prismatic crystals that often fill space between quartz or feldspar. It tends to replace biotite in more greisenized samples.



Top: *Left: PPL, Right: XPL image of white mica in greisen. White mica forms small anhedral crystals in random orientations that are colorless in PPL. These crystals are often competing for space with quartz and replace primary magmatic feldspar. High relief brown crystal in PPL is cassiterite.* ***Bottom:*** *Left: CL, Right: XPL image of a typical greisen quartz-white mica assemblage. White mica has a slight red glow in CL but is mostly non-luminescent compared to the violet-blue quartz and bright yellow apatites shown in the section. This white mica is much more fine-grained than primary magmatic mica, which is also difficult to find.*

Location	**Mineral**	**Lithology**
Eibenstock granite, Saxony, Germany	Tourmaline	Greisenized granite

Transmitted-light Microscopy

Microscope	Zeiss Axio Imager.M2
Camera	Axio Cam MRc5
Objective	EC Epiplan-Neoflur Zoom 2.5x/0.075 Pol M27

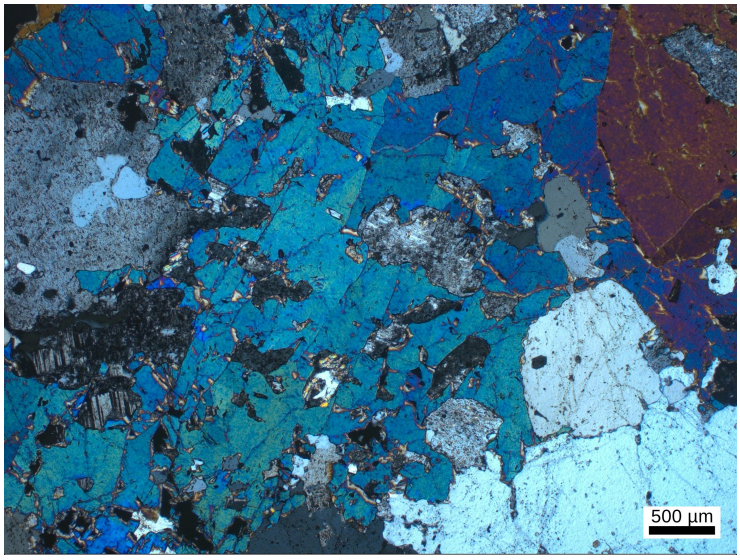
Optical Catholoduminescence Microscopy

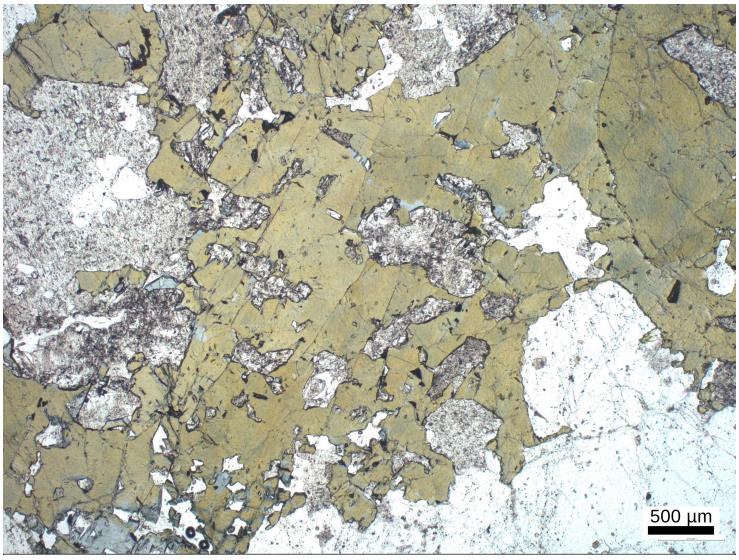
Microscope	Lumic HC7-LM
Camera	Olympus DP74
Spectrometer	Acton SpectraPro 2300i

Micro-XRF Spectrometry

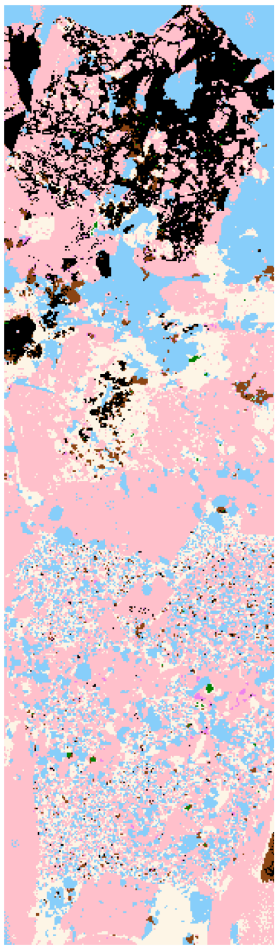
Spectrometer	Bruker M4 Tornado Plus
Tube Parameters	Rh, 50kV, 300 μA
Resolution	150 μm
Dwell time	100 ms

Tourmaline is not as common as the main minerals quartz, feldspar, and micas, but common enough to provide clues towards the formational environment of the samples. Tourmaline is anhedral, yet forms large crystals. In PPL it is yellow-green or light blue with clear pleochroism. In the hand samples it is mainly present in spherical assemblages that radiate out from a single point. In these assemblages the tourmaline macroscopically occurs with quartz where both minerals are coarse and easy to recognize. Microscopically the picture is different, because a microscopic view shows that tourmaline is intertwined with feldspar or quartz in a poikilitic pattern. In one sample tourmaline occurs as the cemented matrix of a small-scale breccia in which the brecciated grains are part of the original granite. Tourmaline is not luminescent in CL.

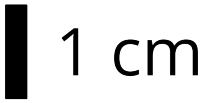












Top left: *XPL,* ***Top right:*** *PPL image of tourmaline in thin section. Tourmaline forms large crystals which encapsulate other minerals. The large crystals can be recognized by the same optical orientation. The blue part of the XPL image is a single crystal.* ***Left:*** *Sample FG9 containing tourmaline. Shown on the left is a picture of the sample, which shows an aplitic texture at the bottom and a pegmatitic texture towards the top. Tourmaline occurs only in the top part of the sample and can be recognized by the black color. On the right of this picture is a manually created mineral map from the XRF data, which also shows tourmaline in black. This map shows that tourmaline appears to fill in cracks in a breccia-like pattern.*

7.4.1 Quartz

Quartz is the most abundant mineral in the samples overall, and is present in large quantities in both the granite and greisen samples. Differences in textures in quartz can be diagnostic to determine if a sample is greisenized if it is not immediately clear.

Transmitted Light Microscopy Quartz is mainly anhedral with serrated boundaries to other grains. Fractures and inclusion trails are common, and these fractures are sometimes filled with micas. In the more greisenized samples the original edge of quartz grains can be overgrown with a layer of mica, which is then in turn overgrown by more quartz. This quartz overgrowth nearly always has the crystal orientation of the original grain, and in the absence of a layer of mica it is impossible to see where the boundary between the original grain and the overgrowth is. An example of an overgrown quartz with a layer of mica can be seen in Figure 14d.

Cathodoluminescence Microscopy Two phases of quartz exist in most samples, which is only visible in CL as the secondary generation of quartz generally crystallized from the edges of primary grains and thus shares the same crystal orientation. This means that the two phases have the same optical properties in XPL and are thus basically indistinguishable. The first phase is a primary magmatic quartz, which is weakly to strongly blue colored. This phase shows little to no zoning, and where present the transition between the zones is gradual. The second phase is a strongly zoned secondary quartz mainly present in greisenized feldspars. This phase is a lighter blue in CL with sharp transitions between the zones. Spectral measurements of these two phases show a distinct difference. Primary quartz has broad emission peaks at 460 and 645 nm, whereas in secondary quartz the peak at 460 nm is very small to absent. Figure 15 shows spectral measurements of different quartz phases, with primary quartz having a stronger emission around 645 nm and little or no emission around 460 nm, while secondary quartz has a much more pronounced emission at 460 nm.

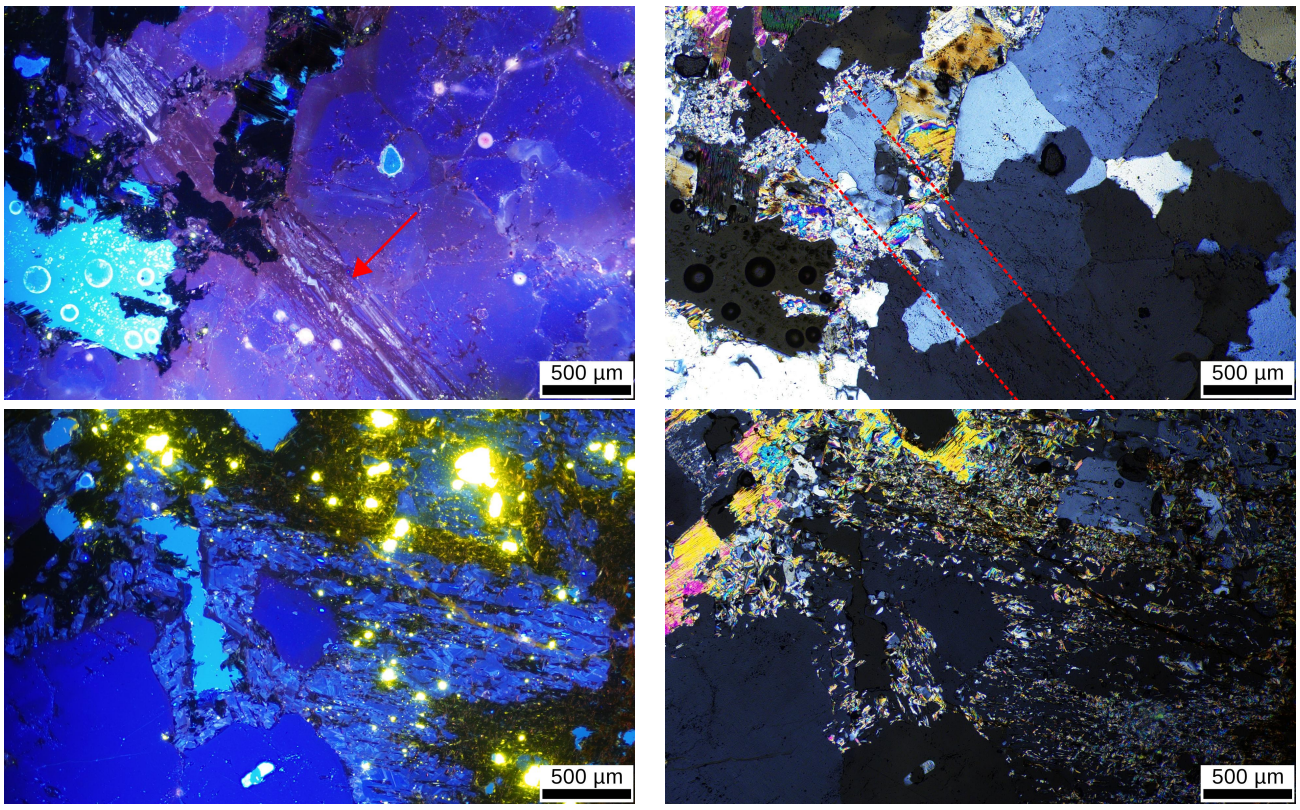


Figure 14: *Quartz textures in CL (left) and XPL (right). The lightest blue in both CL pictures is not a mineral but the mounting epoxy resin.* ***A)*** *Primary, lightly zoned quartz in pinkish blue CL (top right) with secondary, strongly zoned pinkish to light blue quartz associated with greisenization. Sample CF2a.* ***B)*** *Same view as A) in XPL. Vein is almost invisible, as secondary quartz has the same optical properties.* ***C)*** *Primary quartz in bright blue CL in the bottom left. Greisen quartz is a lighter blue and shows strong zoning. Note the bright yellow apatites in the top right and bottom. Sample SH1.* ***D)*** *Same view as C) in XPL. Different quartz types are indistinguishable, and apatites are much harder to identify.*

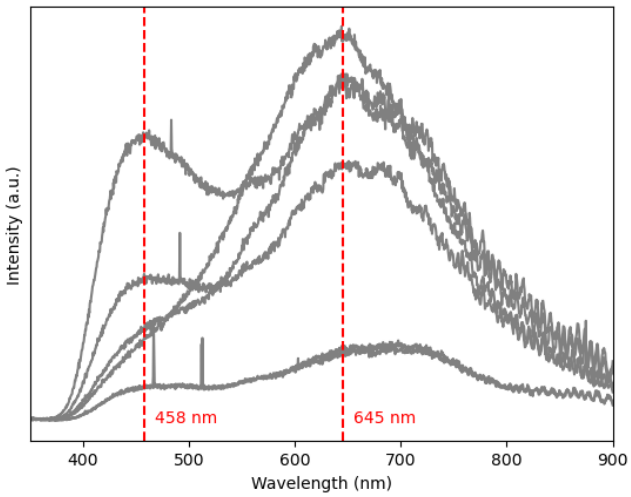


Figure 15: *Spectral CL measurements of quartz grains in the samples. The main quartz emissions occur around 460 nm and 645 nm. The brightness of these emissions varies in both bands, and some quartz are more strongly luminescent than others*

7.4.2 Feldspars

Feldspars are completely destroyed and replaced as greisenization intensifies. This is why the mechanism of feldspar hydrolysis and the associated textures are important characteristics aiding determination of the intensity of greisenization.

Transmitted-light microscopy Feldspars in the studied thin sections show many signs of alteration such as the destruction of plagioclase twinning and replacement by quartz and/or mica. In plane polarized light both plagioclase and orthoclase feldspars appear dirty, which is different from quartz grains, which are smooth and homogeneous. Cross-polarized light shows that feldspars with this dirty appearance are partially replaced by fine white mica, quartz, or both. In some samples such as FG3 and FG9, tourmaline, instead of quartz or mica, replaces feldspars. This seems to be constrained to mainly plagioclase feldspars. However, it is difficult to tell apart plagioclase and potassium feldspar in the thin sections, as the majority of plagioclase feldspars have lost their characteristic lamellar twinning. This is attributed to alteration as some plagioclase grains do still show twinning, whereas other grains only partially show twinning or show none at all, and the absence of twinning correlates with more altered samples.

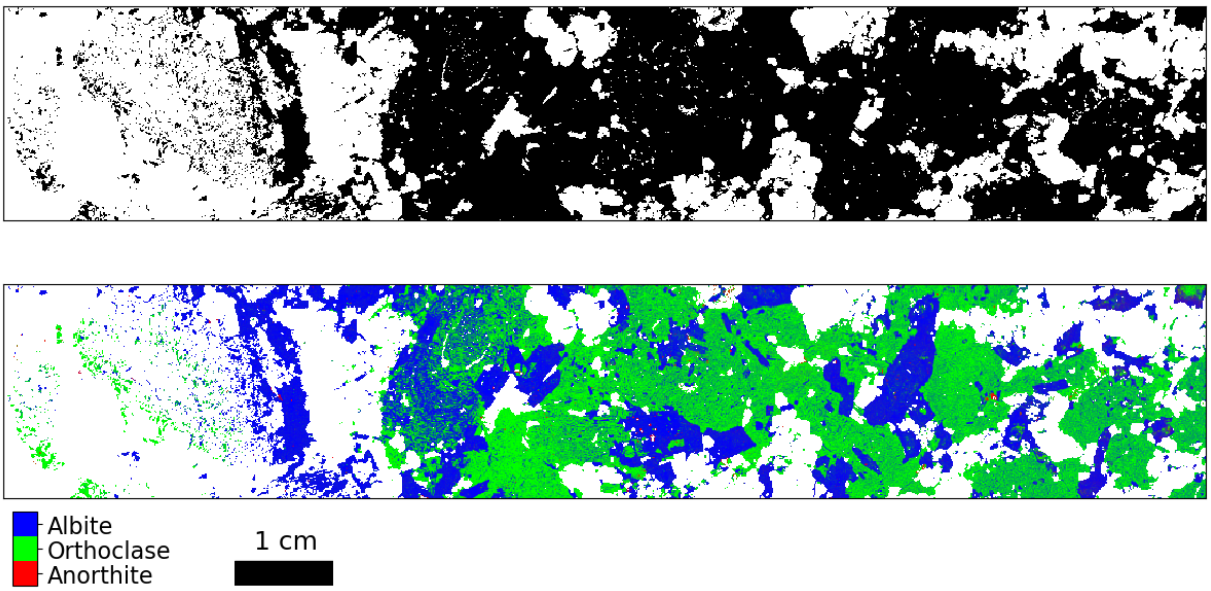


Figure 16: *False colour RGB map of feldspar varieties. Shown is sample FG3, where the blue channel corresponds to pure albite, green corresponds to pure orthoclase, and red corresponds to pure anorthite. K-feldspars are notably mixtures of albite and orthoclase, whereas plagioclase feldspars are closer to pure albite.*

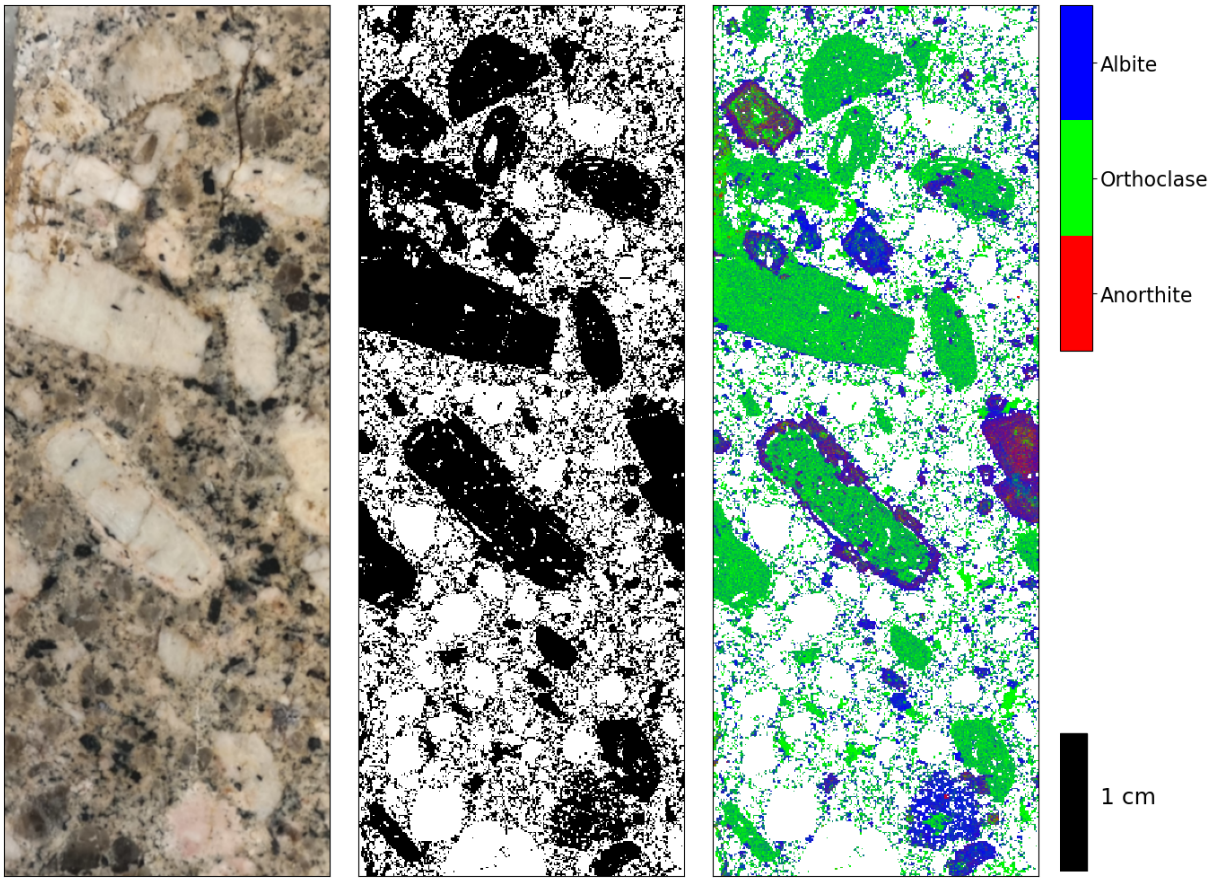


Figure 17: *Detailed look of feldspar varieties in sample WF1. Left: Photograph, Middle: Mask from XRF data showing all feldspars, right: False colour RGB map of feldspar varieties, where the blue channel corresponds to pure albite, green corresponds to pure orthoclase, and red corresponds to pure anorthite. The mainly orthoclase K-feldspar in the middle shows an albite rim with some Ca-rich zones included. The plagioclase feldspar in the center right is also a more Ca-rich variant.*

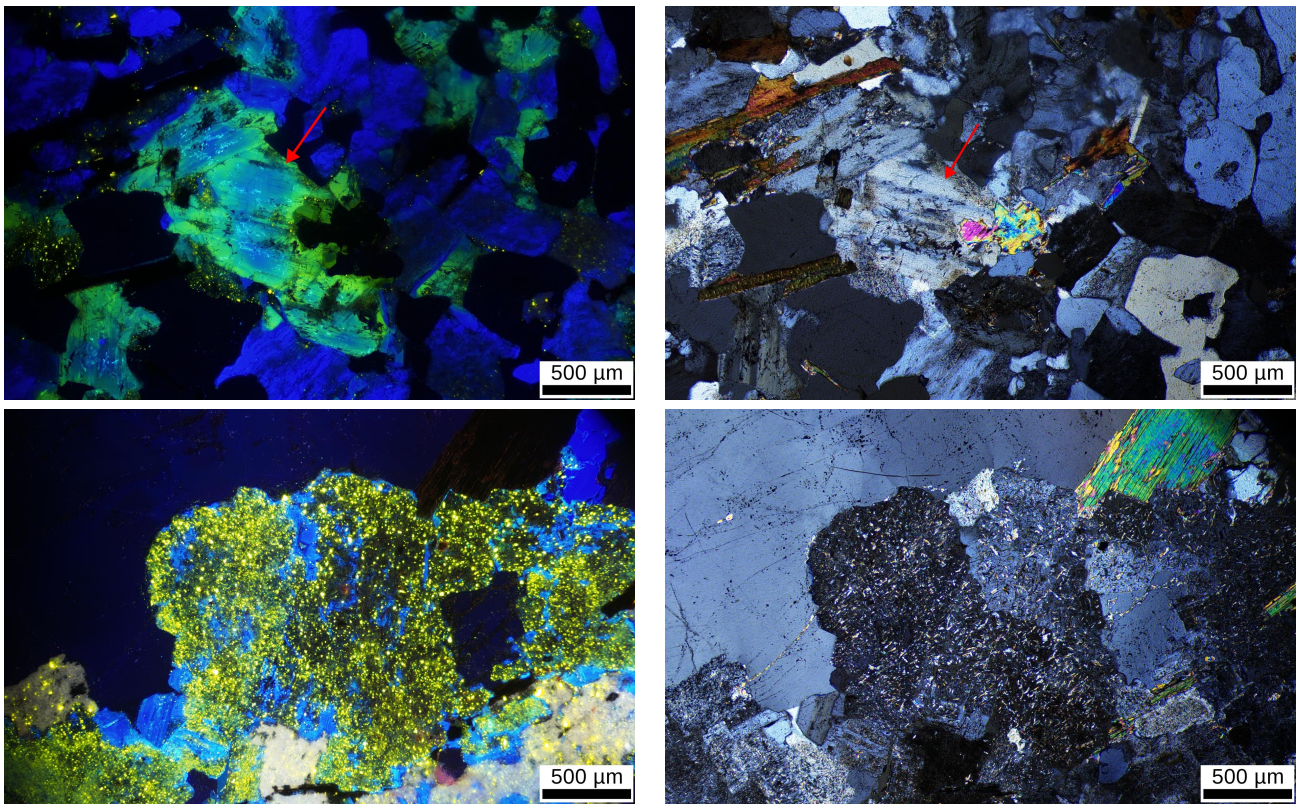


Figure 18: *Feldspars in thin section FG13a. Left: CL, right: XPL* ***A)*** *Altered plagioclase where the rims are less affected than the core. CL colors of the core resemble more a K-feldspar than a plagioclase.* ***B)*** *Same view as A. The characteristic plagioclase twinning can still be seen, but it is mainly destroyed due to the alteration.* ***C)*** *An orthoclase crystal in the same sample showing severe alteration by yellow apatite.* ***D)*** *Same view as C. In XPL it is clearly visible that alongside apatite the feldspar is also largely replaced by muscovite.*

Cathodoluminescence Microscopy Individual feldspar grains show a variety of colours in CL. K-feldspars grains show deep blue, pale yellow, or cyan colors. Plagioclase feldspar grains show green or blue colours. Single grains often show multiple colors, such as a blue core and green rim. Spectral measurement of the CL emission show that the green color of the plagioclase feldspars is caused by two emission peaks: A blue emission around 450 nm and a yellow emission at 560 nm. This yellow and blue light mixes to become the green color that is often observed. In some plagioclase grains this yellow emission band is removed, which makes the grain appear blue. Measurement of K-feldspar grains shows a light blue emission peak around 450 nm and a dark-red emission peak around 710 nm. Together these emissions create the deep blue colour that is observed in the majority of K-feldspars. This visual overview of feldspar CL emissions can be seen in Figure 20. Bright yellow luminescent apatite inclusions are very common, and are mainly found in plagioclase feldspars grains. These inclusions are only found in feldspars with a blue CL color, and not in feldspars with a green colour. These two appearances seem to be mutually exclusive, meaning they are not observed together. This is illustrated in Figure 18, where green plagioclase grains contain no apatite, while plagioclase grains containing apatite inclusions are blue.

XRF mapping The compositional differences in feldspars in the system anorthite-orthoclase-albite, can be calculated and visualized using the XRF maps. A visual overview of this system can be seen in Figure 19. This figure shows that plagioclase is predominantly of albite composition and that K-feldspar is composed of 20$ albite and 80% orthoclase. This does not mean that the K-feldspar is a sanidine however, as K-feldspar is perthitic and thus composed of lamellae of pure albite and pure orthoclase. The average composition explains that 80 % of the volume of the perthitic K-feldspar crystal is occupied by orthoclase lamellae, and 20% of the volume is occupied by albite lamellae. A visual overview of feldspar compositions is shown for sample FG3 in Figure 16. This sample is representative for the samples from Fahsel and shows that plagioclase feldspars are close to pure albite composition, whereas K-feldspars are perthitic mixtures of albite and orthoclase. Notable in sample FG3 is the

large phenocryst of K-feldspar which shows a zonation starting with a perthitic core, overgrown by an orthoclase rim, which is again overgrown by an albite rich feldspar. Plagioclase feldspars in WF1 are a of a slightly different composition than other samples, as they contain a higher amount of anorthite. This can also be seen in Figure 17 by the more reddish tint of the plagioclase feldspars. Another notable feature in this figure is the plagioclase rims which indicate two periods of feldspar growth under different conditions. These rims are only observed in sample WF1.

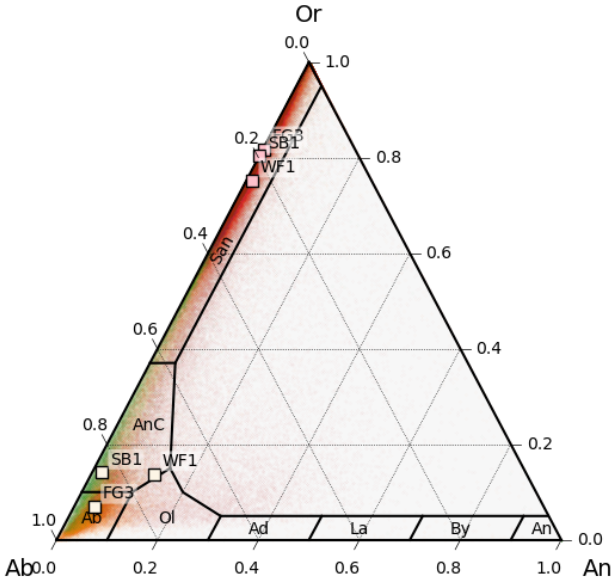


Figure 19: *Ternary scatterplot of feldspars in the system orthoclase-albite-anorthite. Data shown is for samples WF1, SB1 and FG3, which are relatively unaltered granites from three different locations. average K-feldspar composition is shown with pink squares, and average plagioclase compositioin is shown in white squares.*

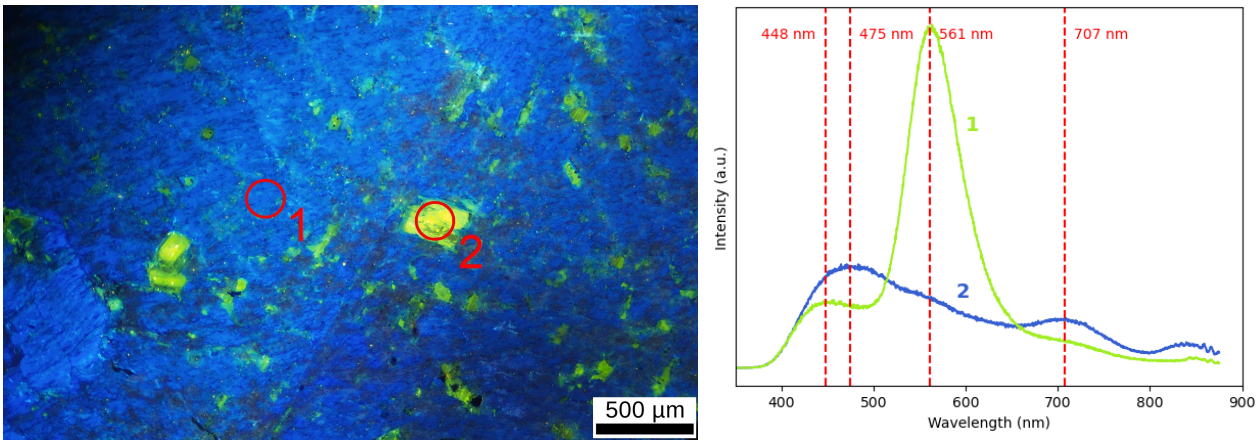


Figure 20: *CL image and associated CL spectra of a K-feldspar crystal (blue) with small inclusions of plagioclase (green). The K-feldspar shows a slight perthitic texture with exsolution zones of plagioclase. Plagioclase shows a very strong emission band at 561 nm as well as a small emission at 448 nm, whereas K-feldspar shows weaker emission bands at 475 and 707 nm.*

7.4.3 Biotite

Transmitted-light Microscopy Biotite is subhedral or anhedral and occurs to limited extent in the samples. It tends to get removed early in greisenization, during which it is replaced by other minerals such as white mica, topaz, or quartz. This means that less greisenized samples or zones can be recognized by the more frequent occurrence of biotite. In plane-polarized light the biotites are easily recognized by a brownish red colour which is pleochroic. Biotites often contain small inclusions of other minerals such as zircons or apatites. These, mainly

the zircons, can be radioactive and cause radiation damage haloes in the biotite. In some samples the biotite is replaced by opaques, following the cleavage plane of the crystal. Biotite shows no cathodoluminescence.

7.4.4 White mica and alteration-related micas

Transmitted-light Microscopy Alongside biotite, white mica is common in the samples, increasing in occurrence with increasing greisenization. This white mica occurs in a range of grain sizes. In the most pervasively greisenized samples this white mica forms an assemblage of small flaky crystals that are subhedral. It also occurs in larger anhedral crystals that often fill space between other minerals, forming triangular or prismatic shapes. This white mica is colourless in plane-polarized light, but rarely shows some pleochroism. Upon rotation in PPL, many white mica crystals do show a slight rainbow-like color change. White mica is a common replacement mineral of biotite and replacement occurs along cleavage planes. In addition to white mica, alteration-related micas can be observed in some of the samples. A very fine-grained talc-like mica occurs in sample FG2, and in samples FG10 and FG11 a chlorite mica is observed. This chlorite mica has a greenish-yellow tint in PPL and shows lower-order interference colours in XPL.

Cathodoluminescence Microscopy White and alteration-related mica show a very short-lived red cathodoluminescence. This emission is very weak in the white micas and stronger in chlorite mica. On average, this luminescence fades away in less than five seconds.

XRF mapping The white micas identified using XRF mapping are not homogeneous. Their composition changes from the granites to the greisenized samples. The white micas in the greisen samples are more Fe-rich than the white micas in the granites and slightly greisenized samples. They also contain more Mn and Al. Figure 21 shows an overview of the Mg / (Mg + Fe) for micas in several samples. It shows that there are virtually no Mg micas in the greisenized and altered samples.

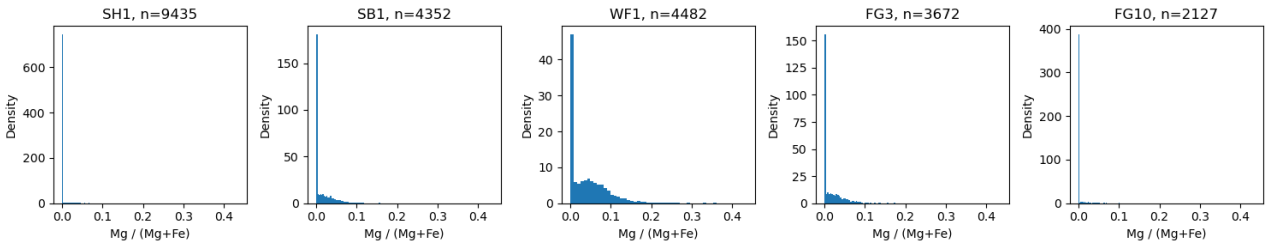


Figure 21: *Mg / (Mg + Fe) ratios for micas in selected samples calculated from XRF maps. Samples SH1 (greisen) and FG10 (altered granite) contain no magnesium micas, unlike the granites, that contain a small amount of magnesium mica. N represents the sample size per histogram.*

7.4.5 Accessory minerals

Transmitted-light Microscopy The main accessory minerals observed in the samples are tourmaline, apatite, topaz, cassiterite, zircon and opaque minerals. The occurrence of tourmaline and cassiterite is limited to specific samples, whereas the other accessory minerals can be found in all samples.

Tourmaline is anhedral and has a poikilitic texture either replacing or intergrowing with quartz or feldspar. Its occurrence is limited to near-spherical zones or brecciated zones. It is pleochroic in plane-polarized light, with the majority of tourmaline showing a yellow-green color, often rimmed by a light blue variety. **Apatite** is anhedral or subhedral and is observed with difficulty in transmitted light due to its optical similarites to quartz. Crystals of apatite are small and dispersed and only rare larger crystals can be identified more easily. **Topaz** is easier to observe than apatite even though it is also optically similar to quartz. Topaz crystals are similar in size to the main rock forming minerals, and are often fractured and replaced by white micas. Cleavage is rarely seen in topaz. **Cassiterite** is subhedral or euhedral and is found as small crystals in greisen samples, mainly from Carlsfeld. It has a brown color in plane-polarized light and a very high relief. In cross-polarized light it has very high interference

colours, which makes it difficult to distinguish from the similarly sized white micas that often surround it. **Zircon** forms small euhedral grains that can most easily be seen in biotites, where they are surrounded by radiation damage haloes. They can also be found as small inclusions in other minerals. **Opaque** minerals occur in multiple forms, but most commonly replace parts of micas as bands perpendicular to cleavage planes. They are anhedral and show little colour in plane-polarized light, except for some red edges in certain samples. There are brightness differences between opaque minerals in reflected light, as well as the red color in polarized reflected light for some crystals. These reflected-light observations were made from thin sections however, so the quality of these observations might be questionable. In any case, the most likely opaque minerals found in the sections are hematite and pyrite.

Cathodoluminescence Microscopy Apatite and topaz are the only accessory minerals that show cathodoluminescence. Apatites are the strongest luminescent mineral in the samples and show a very bright emission peak in CL at around $575\ nm$. This is the only peak for all apatites measured across the samples. While the wavelength of this peak is always around $575\ nm$, the intensity varies significantly. This is illustrated in Figure 22, which shows a large apatite grain as well as a number of spectral measurements of various apatites. Both of these show the variation in intensity of the apatite luminescence, with darker regions in the apatite grain shown corresponding to smaller peaks in the spectral measurements. Many apatite grains are zoned, which can be seen by changes in luminosity of the CL emission. This zonation is also observable in the grain shown in Figure 22. However, the zonation seen in this grain is complex and chaotic as the grain is anhedral. For many apatite subhedral or euhedral apatite grains the zonation pattern neatly follows the crystal structure, forming concentric rings or bands.

Topaz shows a bright blue luminescence color that outshines quartz, making it easy to identify in CL. It also shows distinct growth and sector zoning. The blue color is due to an emission at $465\ nm$, along with a small emission at $700\ nm$.

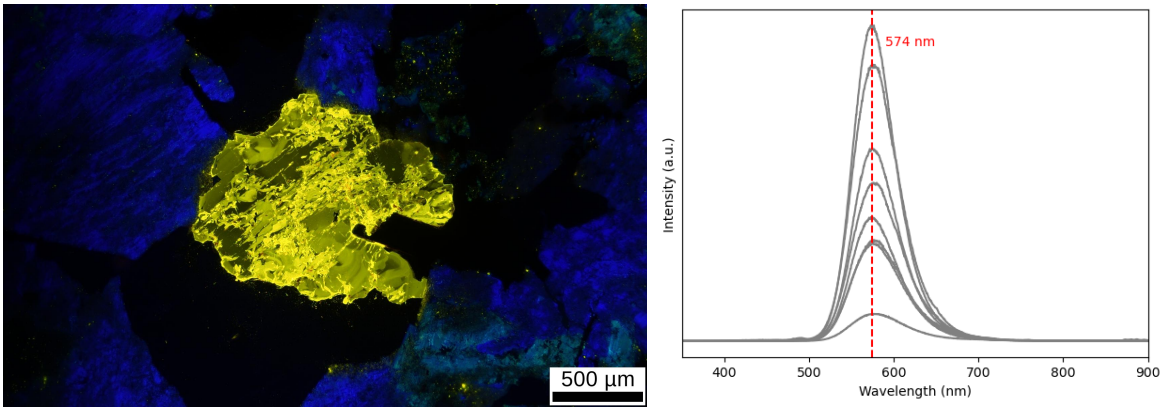


Figure 22: *CL image of a large apatite crystal, with spectral CL measurements shown on the right. The crystal shows weakly luminescent zones, as well as strongly luminescent zones that appear more chaotic. The crystal shows growth zoning in the weakly-luminescent zones. The spectra show that all apatite has a single emission at 574 nm, varying in intensity per crystal or growth zone.*

8 Discussion

In the previous section the analysis of XRF maps, transmitted-light microscopy, and cathodoluminescence microscopy were presented, aiming to gain a deeper understanding of the formation of greisen deposits. This understanding is vital to effective exploration for these deposits. In this section the findings of the previous chapter will be discussed and explained, by trying to link these findings to literature.

8.1 Additions to the Genetic Model of Greisen Formation

In this study, tourmaline was observed in a number of samples, and was found exclusively in granites from Fahsel with a pegmatitic or aplitic texture. Tourmaline was not observed in the much more common medium-grained

granite from Fahsel. This implies that the occurrence of pegmatitic or aplitic facies granite is correlated to the occurrence of tourmaline. This phenomenon could be explained by a threefold evolution of the intrusion; The main crystallization of the intrusion leading to volatile enrichment producing a pegmatitic phase, which crystallizes and enriches further in volatiles until it exsolves a hydrothermal, greisenizing fluid. This three step process implies that evidence of hydrothermal fluids should be found close to pegmatites in the intrusion, which is what was observed in this study, as samples FG3 and especially FG9 show a clear pegmatitic texture as well as extensive greisenization and tourmaline formation. This threefold intrusion evolution is described in more detail below and can be seen visually in Figure 23. A similar intrusion evolution was proposed by (Breiter et al., 2005) for the Podlesí stock in the Czech Republic, not far from the Eibenstock granite. This granite stock and surrounding rocks contain abundant tourmaline, said to have crystallized from B-rich fluids emanating from the crystallizing granite.

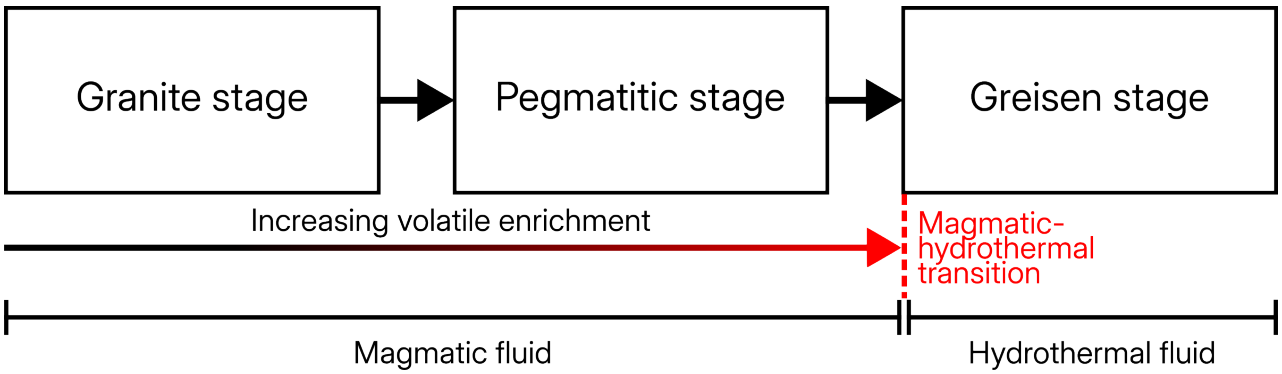


Figure 23: *Evolution of a greisen system. As the magma cools, it becomes enriched in volatiles until it has a pegmatitic composition with a low viscosity. As this magma crystallizes further, it eventually becomes saturated with water, which marks the magmatic-hydrothermal transition. This hydrothermal fluid then causes greisenization of the host granite or the surrounding rock.*

The first stage in the evolution of a greisen system is the emplacement and partial crystallization of the granitic magma. In this stage, anhydrous minerals such as feldspars and quartz begin to crystallize. These minerals do not readily incorporate water or other volatiles into their crystal lattices, which causes the magma to slowly become saturated in volatiles as it crystallizes.

The high water content depolymerizes the pegmatitic melt because water molecules bond to silicate tetrahedra, which causes the long chains of connected silicate ions to become shorter. The other volatiles have the same effect. These volatiles thus drastically lower the viscosity of the melt, which allows this pegmatitic magma to move more easily than the original magma. This enriched magma also has a lower density than the parent magma, which causes an upward force due to buoyancy. These buoyancy forces drive the pegmatitic fluid upwards, concentrating this fluid in the apical regions of the intrusion. Here, the pegmatitic melt can intrude weak points or microscopic cracks in the host rock, which could help the development of fractures and the propagation of the intrusion.

Stockscheider pegmatites could be an early occurrence of this phenomenon. The coldest parts of the intrusion, which are often the edges, should crystallize first. This region should then go through the process described above and produce a pegmatitic phase, which, when crystallized in place, should form the stockscheider pegmatite.

As the pegmatitic phase is crystallizing, the system moves into the third stage of its evolution: The saturation of volatiles in the pegmatitic fluid. The pegmatitic magma is already highly enriched in water and other volatiles, and when it starts to crystallize, it will eventually reach volatile saturation. This is when a hydrothermal phase separates from the pegmatitic magma. This magmatic-hydrothermal transition in pegmatites has been observed in pegmatites from Rwanda (Prado Araujo et al., 2023). In existing literature this process is known as second boiling. Magmas can expel a volatile phase due to oversaturation of volatiles due to pressure differences during ascent, which is called first boiling. Second boiling is the exsolution of a volatile phase at near constant pressure during crystallization (Candela, 1997).

The mechanics of the system during the magmatic-hydrothermal transition should dictate the style of greisenization. If the confining pressure is low enough, the hydrothermal fluid can fracture the host rock and produce veins or even a breccia, and we obtain an exogreisen. If the confining pressure is too high for the fluid to escape, the fluid will remain in place and produce a self-altered endogreisen.

A summary of these styles of greisenization and what such a system would like, is given as a conceptual model in Figure 24. Presented in this figure are two exogreisens, one from the main granitic intrusion and one from a smaller secondary intrusion. These exogreisens can be recognized by their vein-style greisenization. The third greisen body is an endogreisen where the fluid did not have enough pressure to escape, altering its source granite instead. The vein systems of exogreisens can be very large, which makes it difficult to observe the spatial connection between the greisen veins and the source granite. For endogreisens, the greisen phase can also alter the pegmatite or aplite phase that it originated from, erasing evidence of its existence.

8.2 Location markers in a greisen system

In the previous chapter, multiple textures were observed that are related to greisen formation, both at the microscopic and the macroscopic scale. At the **microscopic** scale, the most important and pronounced features were irregular amoeboid-like grain boundaries, varying degrees of feldspar hydrolysis, overgrowths of quartz and mica, and the occurrence of greisen-related minerals such as cassiterite.

Amoeboid-like grain boundaries are likely a solid-state or sub-solid-state readjustment of mineral interfaces which takes place after crystallization. This occurs because mineral interfaces formed during crystallization do not minimize the energy between the minerals, because the driving force during crystallization is not pressure but rather the kinetis of crystallization. After crystallization this pressure becomes the greatest factor, forming a pressure gradient between minerals. Given enough heat, time and possibly presence of fluids, the mineral interfaces can readjust to accommodate this pressure. This is likely what explains the observation of lobate mineral boundaries in the majority of the thin sections studied, and indicates that a heat source affected parts of the granite for a long time. This mechanism may be thus be regarded as a contact metamorphic feature affecting granites. This feature has been observed in hornfels surrounding intrusions before (Wirth, 1985). The fact that this occurs within granites as well indicates multiple intrusion episodes, or a slow, uneven rate of crystallization, causing early crystalline regions to readjust. This is illustrated in Figure 24 by a hornfels layer of granite surrounding a younger intrusion than the main intrusion shown.

Feldspars in the samples studied show a varying degree of alteration, ranging from being pristine, with no replacement textures or minerals and intact twinning in plagioclase grains, to fully hydrolysed, with mica or quartz completely replacing the feldspar. In these cases the previous feldspar can only be recognized by the outline of its original crystal structure.

Cassiterite was only observed in samples from Carlsfeld. These samples, along with the specimen from Schönheide, are the most significantly greisenized of the samples studied. These samples do not contain a single intact feldspar, and the micas in these samples contain mica that is more iron rich than in the greisenized granites samples. Thus, it seems that the mineralization style in these samples is different. This could be explained by a larger distance from these locations to the source granite of their greisenizing fluids, although this depends on many factors such as the composition, temperature, and pressure of these fluids.

At the **macroscopic** scale, observations were tourmaline formation in radial aggregates or breccias, greisen veins crosscutting granite, and small lenses or sheets of pegmatite. Tourmaline formation can be linked to greisenization, as specified in the previous section. However, this did not fully explain the formation of radial aggregates, or 'suns' as found in sample FG7, and the brecciated tourmaline found in samples FG9, and to a lesser extent, FG3. The radial tourmaline aggregates show no signs of vein formation or other brittle behaviour. Therefore, it is likely that these formed as part of an endogreisen, with the hydrothermal fluid forming a bubble in the near-fully crystallized granite. The other tourmaline occurrences most likely involve a breaching of the surrounding granite, resulting in a brecciated texture, which can be characterized as an exogreisen. Greisen veins crosscutting existing granite can also be viewed as exogreisens, because the hydrothermal fluid propagates through fractures in a fully

crystallized granite. Examples of these location markers and where they are located in the conceptual model can be seen in Figure 24, which shows both the endogreisen and exogreisen tourmaline, as well as an exogreisen vein.

Tourmaline occurrence related to greisen systems are not solely observed in the Eibenstock granite. Tourmaline-bearing aplites have been described in a greisen system in the Highiş granitoids in Romania. At this location, the authors describe tourmaline nests within aplites veins in the hornfels, as well as tourmaline bearing pegmatites (Varga et al., 2023). This is highly similar to what is observed in this study, and aligns with the ideas presented in the previous section.

The thin layers or shells of pegmatite observed at Fahsel quarry, as seen in Figure 5 could indicate the presence of multiple 'mini-stocks'. This coincides with the many small greisen veins and greisen breccias found at this location, which are difficult to explain given a single intrusion.

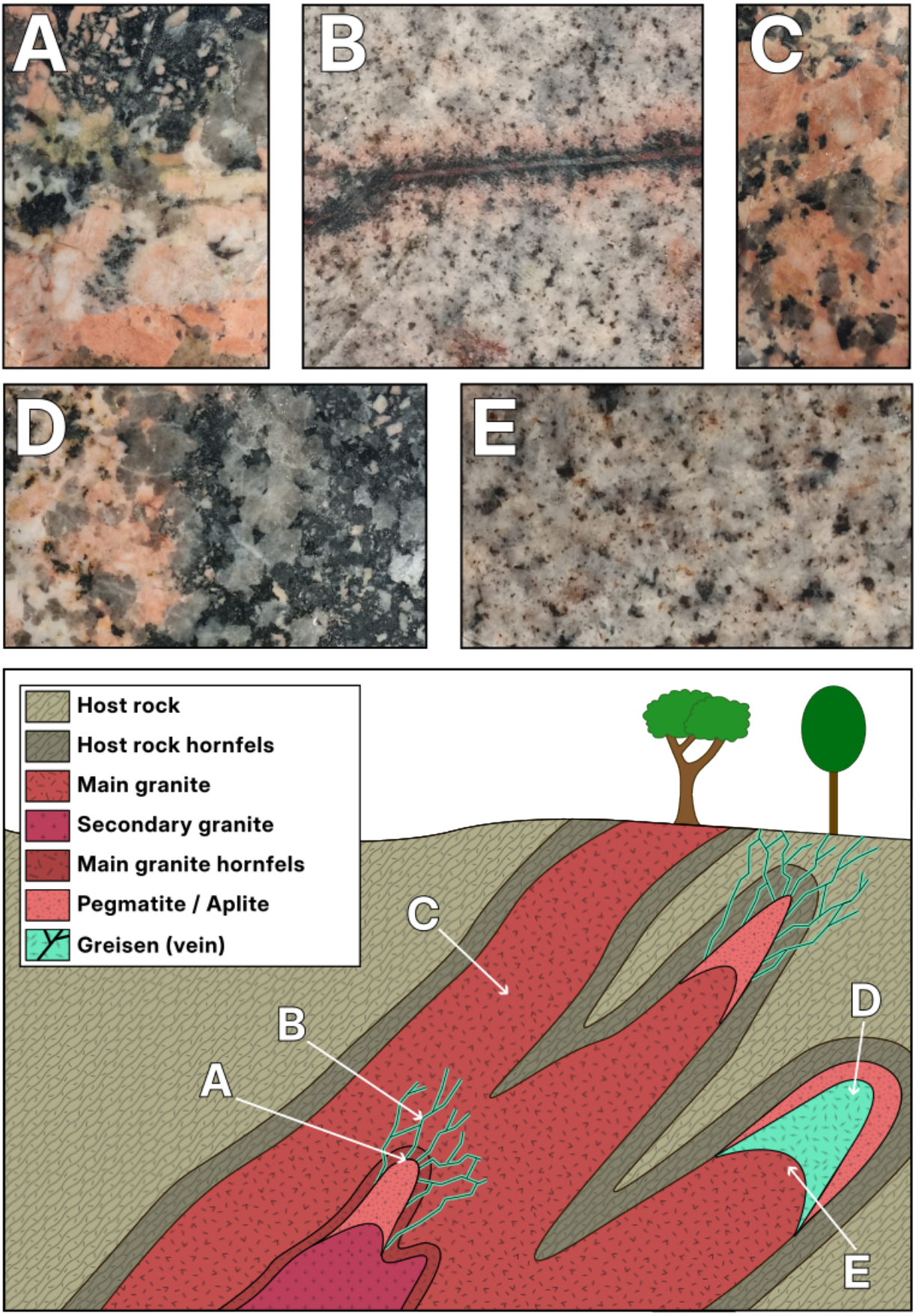


Figure 24: *Conceptual model of a greisen system with representative rock textures for different parts of the system.* ***A)*** *Pegmatite facies granite at the magmatic-hydrothermal transition showing tourmaline and greisenization in upper part, in a brittle, breccia-like texture, and non-altered pegmatite in the bottom part.* ***B)*** *Exogreisen vein in granite.* ***C)*** *Unaltered granite.* ***D)*** *Endogreisen showing tourmaline without any brittle deformation.* ***E)*** *Slightly greisenized granite.*

8.3 Clustering of µXRF data

The two approaches taking to clustering XRF data in the previous chapter are very useful for understanding the data and the samples, but both have their limitations. Benefits of the manual method are that the results are very interpretable, as rules for different minerals have been set explicitly. This makes it easy to see at a glance which minerals are present in which sample. A disadvantage of this method is that it is biased. Minerals rules have been set up by interpretation of the data using knowledge of what minerals should be present.

This is not the case for the unsupervised machine learning clustering of the data, which is unbiased. The model has no knowledge of the samples at hand and separates the data purely using the relationships in the data. This however that some interpretability is lost, and that the mineral phases have to be interpreted afterwards. This can be done, but is time-consuming and difficult. Figure 25 compares the manual and automated clustering results. The model is able to separate the main phases well. These are quartz, albite and orthoclase, represented by clusters 4, 5, and 2 respectively. Furthermore, the model is able to separate tourmaline, represented by cluster 2, from micas, which are represented in cluster 6. Different types of mica are not differentiated, and tourmaline is often misclassified as micas and vice versa. Apatite is not assigned to a single cluster, and seems to be assigned cluster 3, which mostly includes tourmaline. This could indicate that there aren't enough clusters to represent all minerals present, even though clusters 1, 7, and 8 are assigned very little pixels. This can be explained by the fact that the model appears to have trouble with noise. This noise appears at the edges of samples, or in locations with defects that scatter the x-rays, such as fractures or small holes. This noise has a larger variance than the data itself, which explains why the model assigns it a large amount of clusters. Handling of this noise could be improved upon in the future.

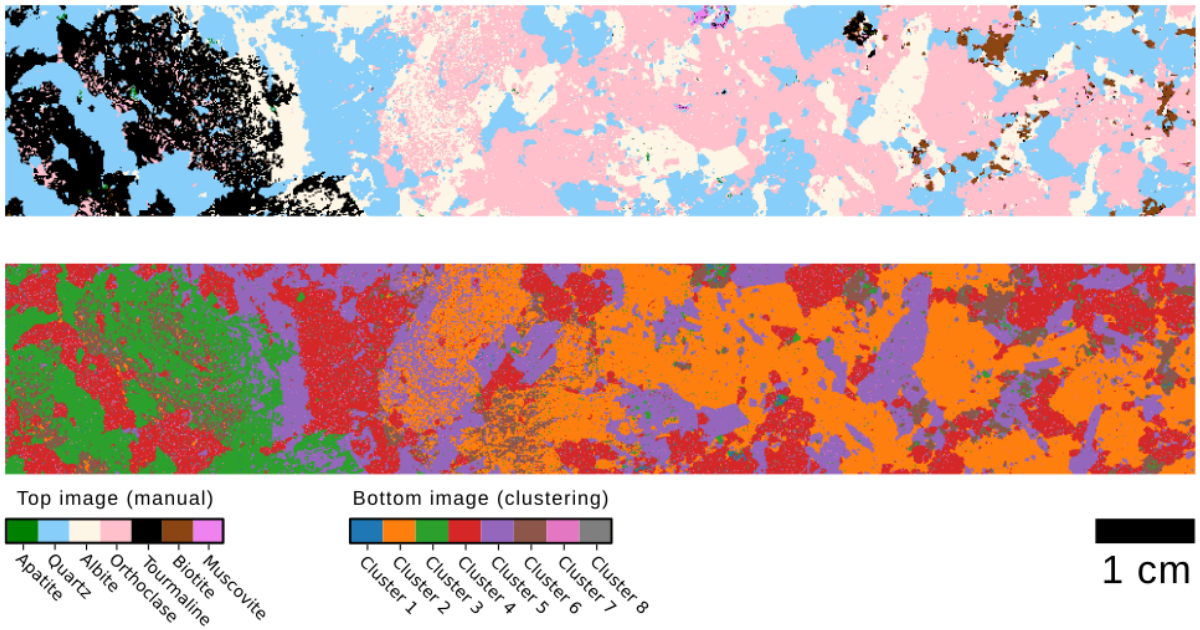


Figure 25: *Comparison between machine-learning clustering (top) and manual clustering (bottom) of XRF data. The automated model separates the main mineral phases such as quartz, albite, and orthoclase very well, but groups together Fe-rich phases such as tourmaline, biotite and muscovite (cluster 4). However, altered parts of feldspars are recognized better in automated model than in the manual one, and are subsequently put in cluster 4.*

8.4 Practical Implications for Mineral Exploration

The methods and workflows presented in this study may be of use in mineral exploration. Though, methods such as µXRF spectrometry and CL may be unfeasible for most exploration enterprises due to the high cost of the associated equipment. However, the presented workflow of manual and unsupervised clustering can still be used with point measurements from a handheld XRF device, which many exploration firms have access to. This is

possible because μXRF maps used in this study are simply arrays of point measurements. Both the manual and automated workflows treat each of these point measurements individually. This means that these methods can be applied to an individual measurement, without the need for a full two-dimensional map. While this doesn't yield the full maps presented in this study, it can still be useful to characterize specific minerals in, for example, drill cores or hand samples. The only caveat is that special care should be taken regarding the spot size and location of the measurement, as accidental measurement of two different minerals at once will yield untrustworthy or wrong results. This means that the method may not be feasible for very fine-grained samples or for large spot-size XRF devices. Furthermore, if the unsupervised clustering model is used, this model should be pre-trained on an existing dataset to function properly.

The textures described in this thesis, which occur throughout different parts of greisen systems, can also be used in exploration as additional geological information. These textures can be recognized from hand samples, drill cores, and in thin sections. The spatial distribution of these textures gives an estimate of the number of hydrothermal events, the complexity of the intrusion, and the distance to the location of hydrothermal fluid release. For example, a greisen veins crosscutting a main granite could suggest multiple intrusion episodes, which will affect the distribution of metals. If such later intrusions did not release metals, then these greisen veins can easily be characterized as barren just by their texture alone.

8.5 Petrogenesis of the Eibenstock granite

The regular occurrence of small crystals of apatite in plagioclase feldspars is most likely an alteration-related feature, as more intensely altered thin sections show a larger amount of apatites in plagioclase feldspars. As such, during alteration, hydrolysis of these feldspars results in the formation of apatite. The fact that apatite occurrence is constrained to within the feldspars suggests that the crystal structure of the feldspars contains either phosphate or calcium, which leads to favourable conditions for apatite formation upon hydrolysis. Calcium ions are naturally present in plagioclase feldspars, although the majority of plagioclase feldspars in this study are of albite composition, which means these feldspars are calcium-poor. On the other hand, phosphate is not commonly incorporated into feldspars. However, this incorporation of phosphate into feldspars has been described in P-rich, Ca-poor granites such as the Podlesí granite, which is compositionally and geographically close to the Eibenstock-Nejdek pluton (Breiter et al., 2002). In such granites, apatite is not able to crystallize directly from the melt as the Ca concentration is too low, which is why it is incorporated into the crystal structure of feldspars instead. It is very likely that this also happened in the Eibenstock granite, as the XRF data shows that Ca values are very low (<0.4 Wt%) in the samples studied.

Textures observed in the samples indicate that the Eibenstock granite had a complex intrusion history. Different granite facies can be found in close proximity, and exogreisen veins crosscut the granite frequently, which indicates that intrusion and greisenization occured in multiple, distinct episodes. This is further supported by the complex grain boundaries observed mainly in quartz, which have been characterized as a type of granite hornfels in a previous section. The three types of Eibenstock granite introduced by (Förster et al., 1999) confirm this, though there may be more subtypes than initially identified. Using the geochemical data available in this study it is not possible to separate these different intrusion episodes chemically. It is also not possible to identify different episodes using cathodoluminescence, as minerals studied in the samples show very similar luminescence properties throughout the samples.

9 Conclusions

Detailed analysis of greisenized granites from the Eibenstock region highlighted important information about the formation of greisen deposits. The very large Eibenstock intrusion proved to be a complex, multi-stage granite system with many heterogeneities, making it difficult to characterize. The proposed additions to the greisen formation model and findings specific to the Eibenstock granite are the following:

1. Greisen systems appear to go through a pegmatitic phase before the magmatic-hydrothermal transition and onset of greisenization, because of volatile enrichment due to crystallization.

2. Textures such as greisen veins, irregular grain boundaries, or endogreisen, can be used as location markers in greisen systems. These textures alone provide a large amount of information about the style of greisenization and the related intrusion.

3. The Eibenstock granite has had a complex petrogenetic history featuring many intrusion episodes. It is unknown at this time how many intrusion episodes occured or how conditions favouring metal deposition evolved during this time.

Clustering of μXRF data and detailed study of rock textures are viable methods that can both be used in exploration for greisen deposits. Using these methods provides geological knowledge about the intrusion and the style of greisenization that can be of great use for mineral resource modelling. The key results for mineral exploration are as follows:

4. Clustering of XRF data is a viable way of obtaining automated mineralogy. However, handling of noise in the data is currently suboptimal, and requires careful tuning.

5. Macroscopic and microscopic rock textures, as well as clustering of μXRF data, are feasible sources of geological information for exploration. If μXRF equipment is not available, the method can still be used, given that an XRF device with a small enough spot size is available and a pre-trained model is used.

10 Recommendations

The study of greisen deposits is made difficult by two factors. The first factor is the complex nature of many granites such as the Eibenstock, which have seen many different episodes of intrusion, each partially overprinting minerals and textures from the previous intrusion, which makes these granites hard to study. The second factor is the fact that metal deportment in greisens is not fully understood. It is known that base metals are often deposited further from the intrusion than metals such as Li, W, and Sn, yet there is no good model of what controls this metal deposition. These two factors lead to two major areas of interest for future work, namely:

1. Studying of a single, less complicated granite stock can provide answers to many open questions without the difficulty of overprinting. In this thesis the majority of the sample material came from Fahsel quarry. While this is a very interesting location with a lot of research potential, it is part of the very large and complex Eibenstock pluton. To truly study the greisen system well, it would be easier to focus on a smaller, standalone intrusion. This would allow for more detailed analysis of different domains in the greisen system, without having to deal with different intrusions overprinting each other and producing a very complex geology in the process. One candidate is the Podlesí stock, which has been mentioned several times in this study (e.g. (Breiter et al., 2005), (Breiter et al., 2002)). This granite stock has the potential to answer many questions that are difficult to answer in a composite granite body such as the Eibenstock. In such an isolated stock it would be interesting to focus on pegmatites and aplites and their spatial relation with greisenization. If the ideas presented in the previous chapter are true, then one would observe the onset of greisenization only near pegmatites or aplitic facies granite. In such a system, it would be worthwhile to examine whether pegmatitic magmas play any role in the formation of fractures, or whether this is constrained to hydrothermal fluids only. A very interesting finding would be to find a gradient moving from pegmatite or aplite facies to hydrothermal facies in a vein or at the microscopic level. This would very clearly mark the magmatic-hydrothermal transition. Furthermore, if one would go back to Fahsel and observes tourmaline in the regular, fine-grained granite unrelated to aplites or pegmatites, it would disprove the theories proposed here easily.
2. Another region of improvement is chemical and thermodynamic modelling of hydrothermal fluids related to greisenization. It is unclear at this point which variables control the deposition of cassiterite, wolframite, zinnwaldite, and other ore minerals, and to what extent the composition of the parent granite influences the formation of these minerals. Better knowledge of these fluid systems would allow for more targeted exploration for greisen deposits, as it could provide estimates of how far around an intrusion one should explore for a given mineral phase. It seems, from this study, and other studies by e.g. (Launay et al., 2021), (Varga et al., 2023), or (Burisch et al., 2025) that there is a general trend of mineralization of B-rich phases (tourmaline), moving into Li-rich phases (Zinnwaldite), then W-Sn (Wolframite, cassiterite) and finally base metals (e.g. pyrite, chalcopyrite), however there also seem to be many exceptions to this trend. To better understand when this trend is true, and when a system deviates from it, chemical and thermodynamic modelling would be of use.

References

Abart, R., Petrishcheva, E., Käßner, S., & Milke, R. (2009). Perthite microstructure in magmatic alkali feldspar with oscillatory zoning; Weinsberg Granite, Upper Austria. *Mineralogy and Petrology*, *97*(3), 251–263. https://doi.org/10.1007/s00710-009-0090-1

Achtziger-Zupančič, P., Loew, S., & Hiller, A. (2017). Factors controlling the permeability distribution in fault vein zones surrounding granitic intrusions (ore mountains/germany). *Journal of Geophysical Research: Solid Earth*, *122*(3), 1876–1899. https://doi.org/10.1002/2016JB013619

Beaufort, D., Rigault, C., Billon, S., Billault, V., Inoue, A., Inoué, S., & Patrier, P. (2015). Chlorite and chloritization processes through mixed-layer mineral series in low-temperature geological systems – a review. *Clay Minerals*, *50*, 497–523. https://doi.org/10.1180/claymin.2015.050.4.06

Boscaini, A., Davies, J. H. F. L., Perrot, M. G., Sassi, R., Mazzoli, C., De Min, A., Morelli, C., Kustatscher, E., Blanchet-Gavouyère, T., & Marzoli, A. (2025). Early permian post-collisional magmatism induced by extensive removal of the variscan lithospheric mantle. *Contributions to Mineralogy and Petrology*, *180*(2), 10. https://doi.org/10.1007/s00410-024-02196-z

Breiter, K., Ďurišová, J., Korbelová, Z., Lima, A., Vašinová Galiová, M., Hložková, M., & Dosbaba, M. (2022). Rock textures and mineral zoning – a clue to understanding rare-metal granite evolution: Argemela stock, central-eastern portugal. *Lithos*, *410-411*, 106562. https://doi.org/10.1016/j.lithos.2021.106562

Breiter, K., Frýda, J., & Leichmann, J. (2002). Phosphorus and rubidium in alkali feldspars:case studies and possible genetic interpretation. *Bulletin of the Czech Geological Survey*, *77*(2), 93–104. Retrieved April 3, 2026, from https://www.muni.cz/en/research/publications/406909

Breiter, K., Hložková, M., Korbelová, Z., & Galiová, M. V. (2019). Diversity of lithium mica compositions in mineralized granite–greisen system: Cínovec li-sn-w deposit, erzgebirge. *Ore Geology Reviews*, *106*, 12–27. https://doi.org/10.1016/j.oregeorev.2019.01.013

Breiter, K., Müller, A., Leichmann, J., & Gabašová, A. (2005). Textural and chemical evolution of a fractionated granitic system: The podlesí stock, czech republic. *Lithos*, *80*(1), 323–345. https://doi.org/10.1016/j.lithos.2003.11.004

Bruker Nano GmbH. (2026). *Bruker m4 tornado high performance micro-xrf spectrometer*. Retrieved December 29, 2025, from https://www.bruker.com/en/products-and-solutions/elemental-analyzers/micro-xrf-spectrometers/m4-tornado-plus.html

Burisch, M., Leopardi, D., Guilcher, M., Šešulka, V., Dittrich, T., & Lehmann, B. (2025). Greisen-hosted lithium resources of the erzgebirge/krušné hory province (germany and czech republic). *Economic Geology*, *120*(3), 627–647. https://doi.org/10.5382/econgeo.5136

Buzzi, L., & Gaggero, L. (2008). Petrogenesis of post – orogenic lower permian andesites in southern europe: Insights into the collapse of the variscan range. *Geodinamica Acta*, *21*(5), 273–290. https://doi.org/10.3166/ga.21.273-290

Candela, P. A. (1997). A review of shallow, ore-related granites: Textures, volatiles, and ore metals. *Journal of Petrology*, *38*(12), 1619–1633. https://doi.org/10.1093/petroj/38.12.1619

Chen, R., Siidra, O. I., Shilovskikh, V. V., Firsova, V. A., Ugolkov, V. L., & Kotova, E. L. (2025). Metamict thorium orthosilicates from the syenite pegmatites of the Larvic Plutonic Complex, Norway: Phase transformations and thermal behaviour. *Mineralogical Magazine*, *89*(3), 393–410. https://doi.org/10.1180/mgm.2024.88

Cummings, D. (1965). Kink-Bands: Shock Deformation of Biotite Resulting from a Nuclear Explosion. *Science*, *148*(3672), 950–952. https://doi.org/10.1126/science.148.3672.950

Dharmapriya, P. L., Malaviarachchi, S. P. K., Kriegsman, L. M., Galli, A., Dyck, B., Sajeev, K., Su, B.-X., & Pitawala, A. (2020). Symplectite growth in the presence of alkaline fluids: Evidence from high-aluminous metasediments of the Highland Complex, Sri Lanka. *Mineralogy and Petrology*, *114*(6), 515–538. https://doi.org/10.1007/s00710-020-00710-2

Erko, A., Arkadiev, V., Bjeoumikhov, A., Antonov, A., Beckhoff, B., Grigorieva, I., Kanngießer, h. B., & Vidal, B. (2006). X-ray optics. In B. Beckhoff, B. Kanngießer, N. Langhoff, R. Wedell, & H. Wolff (Eds.), *Handbook of practical x-ray fluorescence analysis* (pp. 85–198). Springer. https://doi.org/10.1007/978-3-540-36722-2_3

Finger, F., Schiller, D., Lindner, M., Hauzenberger, C., Verner, K., & Žák, J. (2022). Ultrahigh-temperature granites and a curious thermal eye in the post-collisional south bohemian batholith of the variscan orogenic belt (europe). *Geology*, *50*(5), 542–546. https://doi.org/10.1130/G49645.1

First Tin PLC. (2025, October 13). *Gottesberg project MRE update*. https://www.lse.co.uk/rns/gottesberg-project-mre-update-k8rz2mb54adk3ei.html

Förster, H.-J. (1998). The chemical composition of REE-y-th-u-rich accessory minerals in peraluminous granites of the erzgebirge-fichtelgebirge region, germany, part i: The monazite-(ce)-brabantite solid solution series. *American Mineralogist*, *83*(3), 259–272. https://doi.org/10.2138/am-1998-3-409

Förster, H.-J. (2018). Accessory minerals in felsic igneous rocks - part 2: Composition of monazite-(ce), xenotime-(y) and zircon from the multi-stage, strongly peraluminous, p-f-rich li-mica granite massif of eibenstock (erzgebirge-vogtland metallogenic province, germany). https://doi.org/10.5880/GFZ.6.2.2018.002

Förster, H.-J., Tischendorf, G., Trumbull, R. B., & Gottesmann, B. (1999). Late-collisional granites in the variscan erzgebirge, germany. *Journal of Petrology*, *40*(11), 1613–1645. https://doi.org/10.1093/petroj/40.11.1613

Förster, H.-J., Tischendorf, G., Seltmann, R., & Gottesmann, B. (1998). Die variszischen granite des erzgebirges: Neue aspekte aus stofflicher sicht. *Zeitschrift für Geologische Wissenschaften*, *26*, 31–60.

Franke, W. (1989, January 1). Tectonostratigraphic units in the variscan belt of central europe. In R. D. Dallmeyer (Ed.), *Terranes in the circum-atlantic paleozoic orogens* (Vol. 230). Geological Society of America. https://doi.org/10.1130/SPE230-p67

Franke, W., & Żelaźniewicz, A. (2023). Variscan evolution of the bohemian massif (central europe): Fiction, facts and problems. *Gondwana Research*, *124*, 351–377. https://doi.org/10.1016/j.gr.2023.06.012

Halter, W. E., Williams-Jones, A. E., & Kontak, D. J. (1998). Modeling fluid–rock interaction during greisenization at the east kemptville tin deposit: Implications for mineralization. *Chemical Geology*, *150*(1), 1–17. https://doi.org/10.1016/S0009-2541(98)00050-3

Henderson, G. H. (1939). A quantitative study of pleochroic haloes. V. The genesis of haloes. *Proceedings of the Royal Society of London. Series A. Mathematical and Physical Sciences*, *173*(953), 250–264. https://doi.org/10.1098/rspa.1939.0143

Houseman, G. A., McKenzie, D. P., & Molnar, P. (1981). Convective instability of a thickened boundary layer and its relevance for the thermal evolution of continental convergent belts. *Journal of Geophysical Research: Solid Earth*, *86*, 6115–6132. https://doi.org/10.1029/JB086iB07p06115

Kästner, F., Pierdominici, S., Zappone, A., Morales, L. F. G., Schleicher, A. M., Wilke, F. D. H., & Berndt, C. (2021). Cross-scale seismic anisotropy analysis in metamorphic rocks from the COSC-1 borehole in the scandinavian caledonides. *Journal of Geophysical Research: Solid Earth*, *126*(5), e2020JB021154. https://doi.org/10.1029/2020JB021154

Kempe, U., Bombach, K., Matukov, D., Schlothauer, T., Hutschenreuter, J., Wolf, D., & Sergeev, S. (2004). Pb/pb and u/pb zircon dating of subvolcanic rhyolite as a time marker for hercynian granite magmatism and sn mineralisation in the eibenstock granite, erzgebirge, germany: Considering effects of zircon alteration. *Mineralium Deposita*, *39*(5), 646–669. https://doi.org/10.1007/s00126-004-0435-y

Komatani, S., Nakamachi, K., Nakano, K., Ohzawa, S., Uchihara, H., Bando, A., & Tsuji, K. (2013). Fundamental characteristics of hybrid x-ray focusing optics for micro x-ray fluorescence analysis. *Nuclear Instruments and Methods in Physics Research Section B: Beam Interactions with Materials and Atoms*, *309*, 260–263. https://doi.org/10.1016/j.nimb.2013.02.023

Korges, M., Weis, P., Lüders, V., & Laurent, O. (2020). Sequential evolution of sn–zn–in mineralization at the skarn-hosted hämmerlein deposit, erzgebirge, germany, from fluid inclusions in ore and gangue minerals. *Mineralium Deposita*, *55*(5), 937–952. https://doi.org/10.1007/s00126-019-00905-4

Krejčí Kotlánová, M., Dolníček, Z., René, M., Prochaska, W., Ulmanová, J., Kapusta, J., Mašek, V., & Kropáč, K. (2024). Fluid evolution of greisens from krupka sn-w ore district, bohemian massif (czech republic). *Minerals*, *14*(1), 86. https://doi.org/10.3390/min14010086

Kröner, A., & Willner, A. P. (1998). Time of formation and peak of variscan HP-HT metamorphism of quartz-feldspar rocks in the central erzgebirge, saxony, germany. *Contributions to Mineralogy and Petrology*, *132*(1), 1–20. https://doi.org/10.1007/s004100050401

Kroner, U., & Romer, R. L. (2013). Two plates — many subduction zones: The variscan orogeny reconsidered. *Gondwana Research*, *24*(1), 298–329. https://doi.org/10.1016/j.gr.2013.03.001

Langhoff, N., Simionovici, A., Arkadiev, V., Knüpfer, W., Čechák, T., Leonhardt, J., & Chavanne, J. (2006). X-ray sources. In B. Beckhoff, B. Kanngießer, N. Langhoff, R. Wedell, & H. Wolff (Eds.), *Handbook of practical x-ray fluorescence analysis* (pp. 33–83). Springer. https://doi.org/10.1007/978-3-540-36722-2_2

Launay, G., Sizaret, S., Lach, P., Melleton, J., Gloaguen, E., & Poujol, M. (2021). Genetic relationship between greisenization and sn–w mineralization in vein and greisen deposits: Insights from the panasqueira deposit (portugal). *BSGF - Earth Sciences Bulletin*, *192*, 2. https://doi.org/10.1051/bsgf/2020046

Lefebvre, M. G., Romer, R. L., Glodny, J., Kroner, U., & Roscher, M. (2019). The hämmerlein skarn-hosted polymetallic deposit and the eibenstock granite associated greisen, western erzgebirge, germany: Two phases of mineralization—two sn sources. *Mineralium Deposita*, *54*(2), 193–216. https://doi.org/10.1007/s00126-018-0830-4

Mantler, M., Willis, J., Lachance, G., Vrebos, B. A. R., Mauser, K.-E., Kawahara, N., Rousseau, R. M., & Brouwer, P. N. (2006). Quantitative analysis. In B. Beckhoff, B. Kanngießer, N. Langhoff, R. Wedell, & H. Wolff (Eds.), *Handbook of practical x-ray fluorescence analysis* (pp. 309–410). Springer. https://doi.org/10.1007/978-3-540-36722-2_5

Markovic, S., Szymanowski, D., Tavazzani, L., Torró, L., Kouzmanov, K., Kalinaj, M., & Chelle-Michou, C. (2025). Timescales of magmatic-hydrothermal activity at the giant san rafael tin deposit (peru). *Earth and Planetary Science Letters*, *671*, 119624. https://doi.org/10.1016/j.epsl.2025.119624

Mathieu, L. (2018). Quantifying hydrothermal alteration: A review of methods. *Geosciences*, *8*(7), 245. https://doi.org/10.3390/geosciences8070245

Matte, P. (1986). Tectonics and plate tectonics model for the variscan belt of europe. *Tectonophysics*, *126*(2), 329–374. https://doi.org/10.1016/0040-1951(86)90237-4

Mirijam, V., Nastja, R. S., & Marko, V. (2018). Calcite deformation twins in Pohorje marbles. *Geologija*, *61*(1), 73–84. https://doi.org/10.5474/geologija.2018.005

Nasdala, L., Wildner, M., Wirth, R., Groschopf, N., Pal, D. C., & Möller, A. (2006). Alpha particle haloes in chlorite and cordierite. *Mineralogy and Petrology*, *86*(1), 1–27. https://doi.org/10.1007/s00710-005-0104-6

Neuser, R., Bruhn, F., Götze, J., Habermann, D., & Richter, D. (1995). Kathodolumineszenz: Methodik und anwendung. *Zentralblatt für Geologie und Paläontologie*, *1995*, 287–306.

Passchier, C. W., & Trouw, R. A. J. (1998). Dilatation Sites: Fibrous Veins, Strain Shadows, Strain Fringes and Boudins. In C. W. Passchier & R. A. J. Trouw (Eds.), *Microtectonics* (pp. 131–151). Springer. https://doi.org/10.1007/978-3-662-08734-3_6

Pattrick, R. a. D., Charnock, J. M., Geraki, T., Mosselmans, J. F. W., Pearce, C. I., Pimblott, S., & Droop, G. T. R. (2013). Alpha particle damage in biotite characterized by microfocus X-ray diffraction and Fe K-edge X-ray absorption spectroscopy. *Mineralogical Magazine*, *77*(6), 2867–2882. https://doi.org/10.1180/minmag.2013.077.6.12

Peterková, T., & Dolejš, D. (2019). Magmatic-hydrothermal transition of mo-w-mineralized granite-pegmatite-greisen system recorded by trace elements in quartz: Krupka district, eastern krušné hory/erzgebirge. *Chemical Geology*, *523*, 179–202. https://doi.org/10.1016/j.chemgeo.2019.04.009

Phillips, W. J. (1965). The deformation of quartz in a granite. *Geological Journal*, *4*(2), 391–414. https://doi.org/10.1002/gj.3350040213

Philpotts, A. R., & Ague, J. J. (2021). *Principles of igneous and metamorphic petrology* (Third edition). Cambridge University Press.

Pirajno, F. (2009). *Hydrothermal processes and mineral systems.* Springer.

Poirier, J.-P., & Guillopé, M. (1979). Deformation induced recrystallization of minerals. *Bulletin de Minéralogie*, *102*(2), 67–74. https://doi.org/10.3406/bulmi.1979.7256

Pongrac, P., Jeřábek, P., Stünitz, H., Raimbourg, H., Heilbronner, R., Racek, M., & Nègre, L. (2022). Mechanical properties and recrystallization of quartz in presence of H2O: Combination of cracking, subgrain rotation and dissolution-precipitation processes. *Journal of Structural Geology*, *160*, 104630. https://doi.org/10.1016/j.jsg.2022.104630

Prado Araujo, F., Muchez, P., & Hulsbosch, N. (2023). The magmatic-hydrothermal transition in p-rich pegmatitic melts: Crystal-melt-fluid interactions recorded by phosphate minerals. *Geochimica et Cosmochimica Acta*, *356*, 129–148. https://doi.org/10.1016/j.gca.2023.07.009

Rast, N. (1988). Tectonic implications of the timing of the variscan orogeny. *Geological Society, London, Special Publications*, *38*(1), 585–595. https://doi.org/10.1144/GSL.SP.1988.038.01.40

Ribeiro, B. V., Kirkland, C. L., Finch, M. A., Faleiros, F. M., Reddy, S. M., Rickard, W. D. A., & Hartnady, M. I. H. (2023). Microstructures, geochemistry, and geochronology of mica fish: Review and advances. *Journal of Structural Geology*, *175*, 104947. https://doi.org/10.1016/j.jsg.2023.104947

Rohrer, G. S., Chesser, I., Krause, A. R., Naghibzadeh, S. K., Xu, Z., Dayal, K., & Holm, E. A. (2023). Grain Boundary Migration in Polycrystals. *Annual Review of Materials Research*, *53*(1), 347–369. https://doi.org/10.1146/annurev-matsci-080921-091511

Romer, R. L., Förster, H., & Štemprok, M. (2010). Age constraints for the late-variscan magmatism in the altenberg-teplice caldera (eastern erzgebirge/krusne hory). *Neues Jahrbuch Fur Mineralogie-abhandlungen*, *187*, 289–305. https://api.semanticscholar.org/CorpusID:130647576

Rötzler, K. (2025). Die geologische entwicklung und metamorphose im erzgebirge, ein exkursionsführer durch das erzgebirge. *Geologica Saxonica – Journal of Central European Geology*, *71*, 31–59. https://doi.org/10.3897/gs.71.e147496

Schönig, J., von Eynatten, H., Meinhold, G., & Lünsdorf, N. K. (2019). Diamond and coesite inclusions in detrital garnet of the saxonian erzgebirge, germany. *Geology*, *47*(8), 715–718. https://doi.org/10.1130/G46253.1

Schust, F., & Wasternack, J. (2002). Granitoid-typen in postkinematischen granitoidplutonen: Abbilder von autonomen intrusionsschuben. beispiele vom nordrand des bohmischen massivs (erzgebirge-harz-flechtinger scholle-lausitz). *Zeitschrift für geologische Wissenschaften*, *30*, 77–118.

Seifert, T. (2017). Lamprophyres, f-sn-rhyolites and -explosive breccia pipes and their relationship to sn-polymetallic mineralization in the muehlleithen-gottesberg district (germany) – indications for late-variscan mantle-derived rare metal-enriched fluid pulses. *International Kimberlite Conference: Extended Abstracts*, *11*. https://doi.org/10.29173/ikc3992

Sherlock, S. C., Kelley, S. P., Zalasiewicz, J. A., Schofield, D. I., Evans, J. A., Merriman, R. J., & Kemp, S. J. (2003). Precise dating of low-temperature deformation: Strain-fringe analysis by 40Ar-39Ar laser microprobe. *Geology*, *31*(3), 219–222. https://doi.org/10.1130/0091-7613(2003)031<0219:PDOLTD>2.0.CO;2

Song, Y., Griffiths, T. A., Zhao, S., & Abart, R. (2025). Myrmekite and antiperthite formation in deformed granite: Chemical and crystallographic constraints on formation mechanisms. *American Mineralogist*. https://doi.org/10.2138/am-2024-9715

Štemprok, M. (1987). Greisenization (a review). *Geologische Rundschau*, *76*(1), 169–175. https://doi.org/10.1007/BF01820580

Štemprok, M., & Blecha, V. (2015). Variscan sn–w–mo metallogeny in the gravity picture of the krušné hory/erzgebirge granite batholith (central europe). *Ore Geology Reviews*, *69*, 285–300. https://doi.org/10.1016/j.oregeorev.2015.02.014

Thomas, R., & Klemm, W. (1997). Microthermometric study of silicate melt inclusions in variscan granites from SE germany: Volatile contents and entrapment conditions. *Journal of Petrology*, *38*(12), 1753–1765. https://doi.org/10.1093/petroj/38.12.1753

Tichomirowa, M., Käßner, A., Sperner, B., Lapp, M., Leonhardt, D., Linnemann, U., Münker, C., Ovtcharova, M., Pfänder, J. A., Schaltegger, U., Sergeev, S., von Quadt, A., & Whitehouse, M. (2019). Dating multiply overprinted granites: The effect of protracted magmatism and fluid flow on dating systems (zircon u-pb: SHRIMP/SIMS, LA-ICP-MS, CA-ID-TIMS; and rb–sr, ar–ar) – granites from the western erzgebirge (bohemian massif, germany). *Chemical Geology*, *519*, 11–38. https://doi.org/10.1016/j.chemgeo.2019.04.024

Tichomirowa, M., Gerdes, A., Lapp, M., Leonhardt, D., & Whitehouse, M. (2019). The chemical evolution from older (323–318 ma) towards younger highly evolved tin granites (315–314 ma)—sources and metal enrichment in variscan granites of the western erzgebirge (central european variscides, germany). *Minerals*, *9*(12), 769. https://doi.org/10.3390/min9120769

Tischendorf, G., & Förster, H.-J. (1994). Hercynian granite magmatism and related metallogenesis in the erzgebirge: A status report. In *Monograph series on mineral deposits* (pp. 5–23, Vol. 31). Borntraeger.

Varga, A., Pozsár, A., Zajzon, N., Topa, B., Benkó, Z., Pál-Molnár, E., & Raucsik, B. (2023). Effects of metasomatism on granite-related mineral systems: A boron-rich open greisen system in the highiş granitoids (apuseni mountains, romania). *Minerals*, *13*(8), 1083. https://doi.org/10.3390/min13081083

Wang, C., Song, S., Su, L., Allen, M. B., & Dong, J. (2021). Lithospheric modification at the onset of the destruction of the north china craton: Evidence from late triassic mafic dykes. *Chemical Geology*, *566*, 120105. https://doi.org/10.1016/j.chemgeo.2021.120105

Wang, H., Jiang, Y., Yang, C., Zhang, B., Gu, Y., Luo, X., Zhou, L., & Wang, Z. (2023). Hydrothermal silicification in Ediacaran Dengying Formation fourth member deep dolomite reservoir, Central Sichuan Basin, China: Implications for reservoir quality. *Geological Journal*, *58*(11), 4257–4270. https://doi.org/10.1002/gj.4757

Weil, A., Pastor-Galán, D., Johnston, S. T., & Gutiérrez-Alonso, G. (2019). Late/post variscan orocline formation and widespread magmatism. In C. Quesada & J. T. Oliveira (Eds.), *The geology of iberia: A geodynamic approach: Volume 2: The variscan cycle* (pp. 527–542). Springer International Publishing. https://doi.org/10.1007/978-3-030-10519-8_14

Wirth, R. (1985). The influence of the low-high quartz transformation on recrystallization and grain growth during contact metamorphism (traversella intrusion, north italy). *Tectonophysics*, *120*(1), 107–117. https://doi.org/10.1016/0040-1951(85)90089-7

Wolff, R., Dunkl, I., Lange, J.-M., Tonk, C., Voigt, T., & von Eynatten, H. (2015). Superposition of burial and hydrothermal events: Post-variscan thermal evolution of the erzgebirge, germany. *Terra Nova*, *27*(4), 292–299. https://doi.org/10.1111/ter.12159

Young, K. E., Evans, C. A., Hodges, K. V., Bleacher, J. E., & Graff, T. G. (2016). A review of the handheld x-ray fluorescence spectrometer as a tool for field geologic investigations on earth and in planetary surface exploration. *Applied Geochemistry*, *72*, 77–87. https://doi.org/10.1016/j.apgeochem.2016.07.003

Yu, H.-C., Qiu, K.-F., Hetherington, C. J., Chew, D., Huang, Y.-Q., He, D.-Y., Geng, J.-Z., & Xian, H.-Y. (2021). Apatite as an alternative petrochronometer to trace the evolution of magmatic systems containing metamict zircon. *Contributions to Mineralogy and Petrology*, *176*(9), 68. https://doi.org/10.1007/s00410-021-01827-z

Yund, R. A., & Ackermand, D. (1979). Development of perthite microstructures in the Storm King granite, N.Y. *Contributions to Mineralogy and Petrology*, *70*(3), 273–280. https://doi.org/10.1007/BF00375357

Zajacz, Z., Halter, W. E., Pettke, T., & Guillong, M. (2008). Determination of fluid/melt partition coefficients by LA-ICPMS analysis of co-existing fluid and silicate melt inclusions: Controls on element partitioning. *Geochimica et Cosmochimica Acta*, *72*(8), 2169–2197. https://doi.org/10.1016/j.gca.2008.01.034

Zamiatina, D. A., Mandrygina, D. A., Mikhaylovskaya, Z. A., Bulatov, V. A., Medvedeva, E. V., & Zamyatin, D. A. (2025). Metamict fergusonite-(Y) and samarskite-(Y) from the Ilmeny mountains (South urals, Russia): Secondary alterations and thermal annealing. *Mineralogy and Petrology*. https://doi.org/10.1007/s00710-025-00954-w

11 Appendix

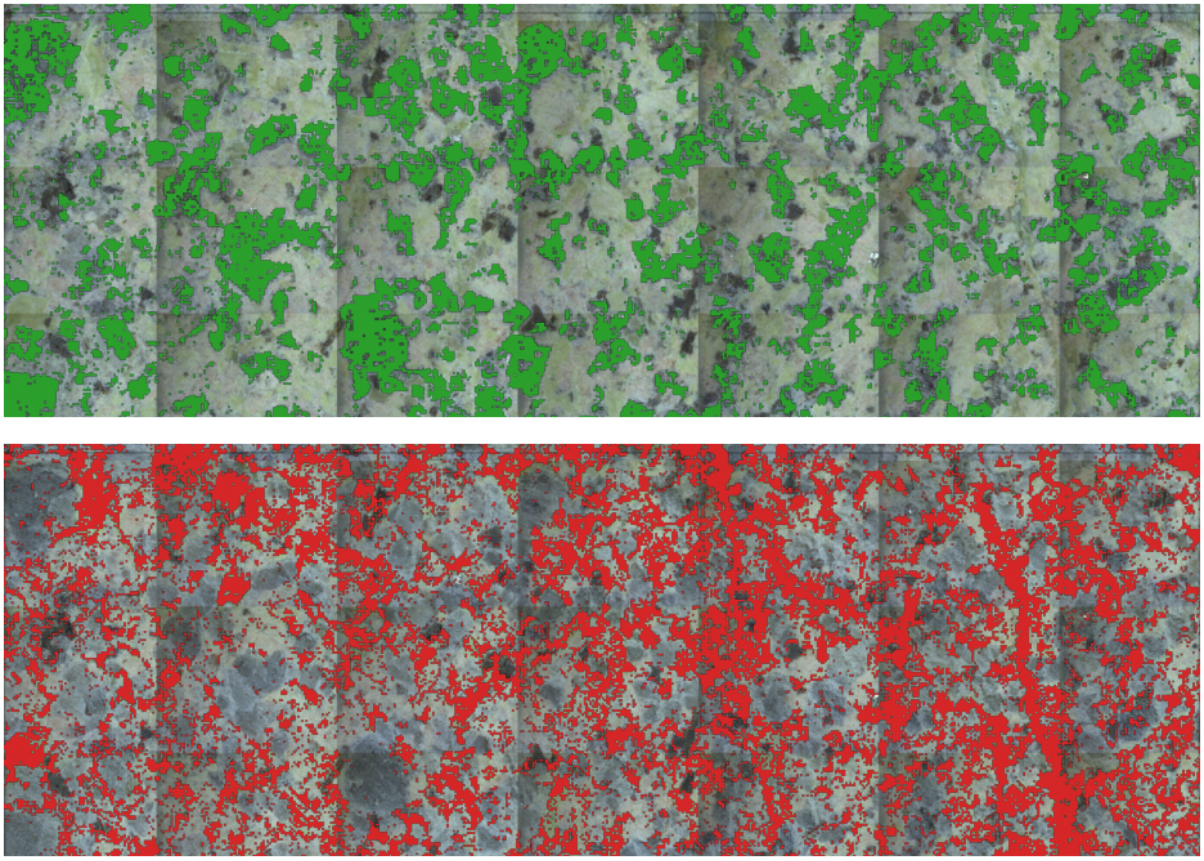


Figure 26: *Selected clusters overlayed on image of FG11 slab.* ***A)*** *cluster 2,* ***B)*** *cluster 3.*

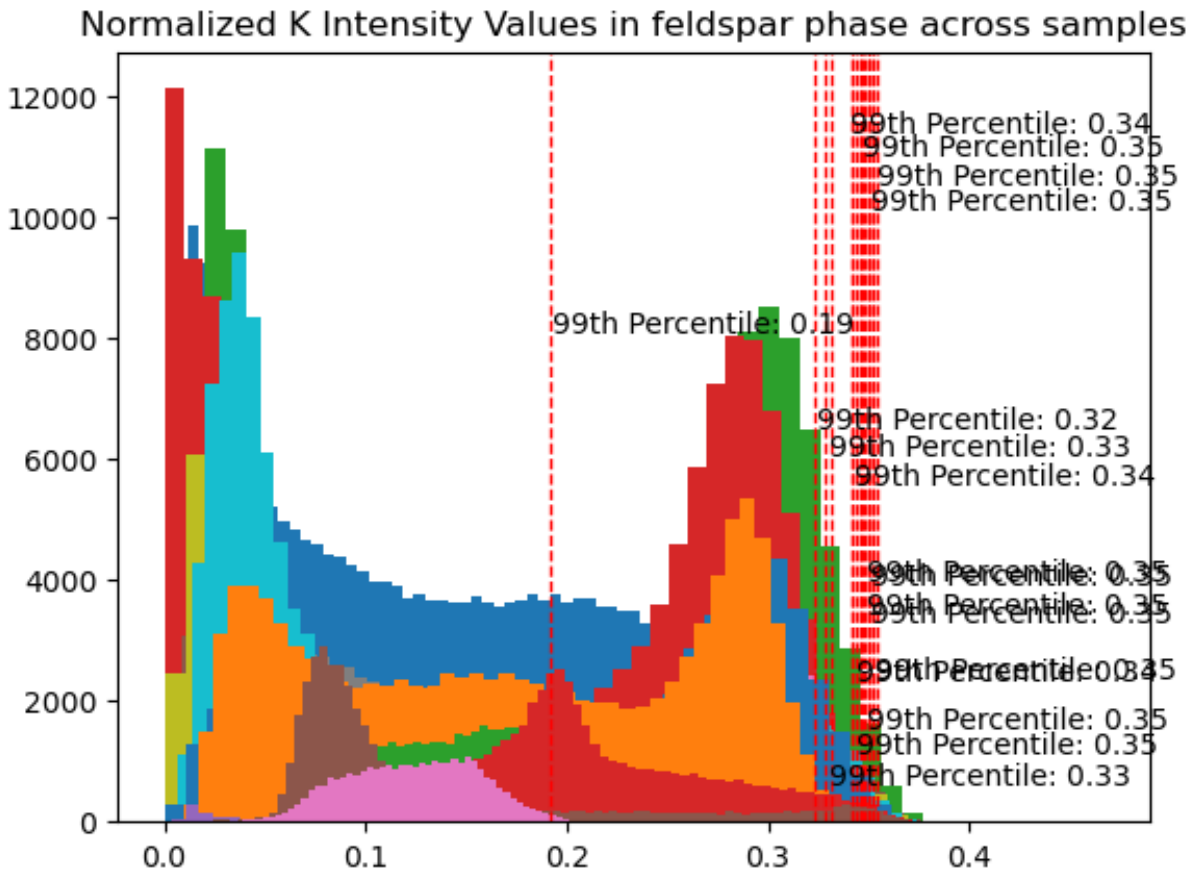


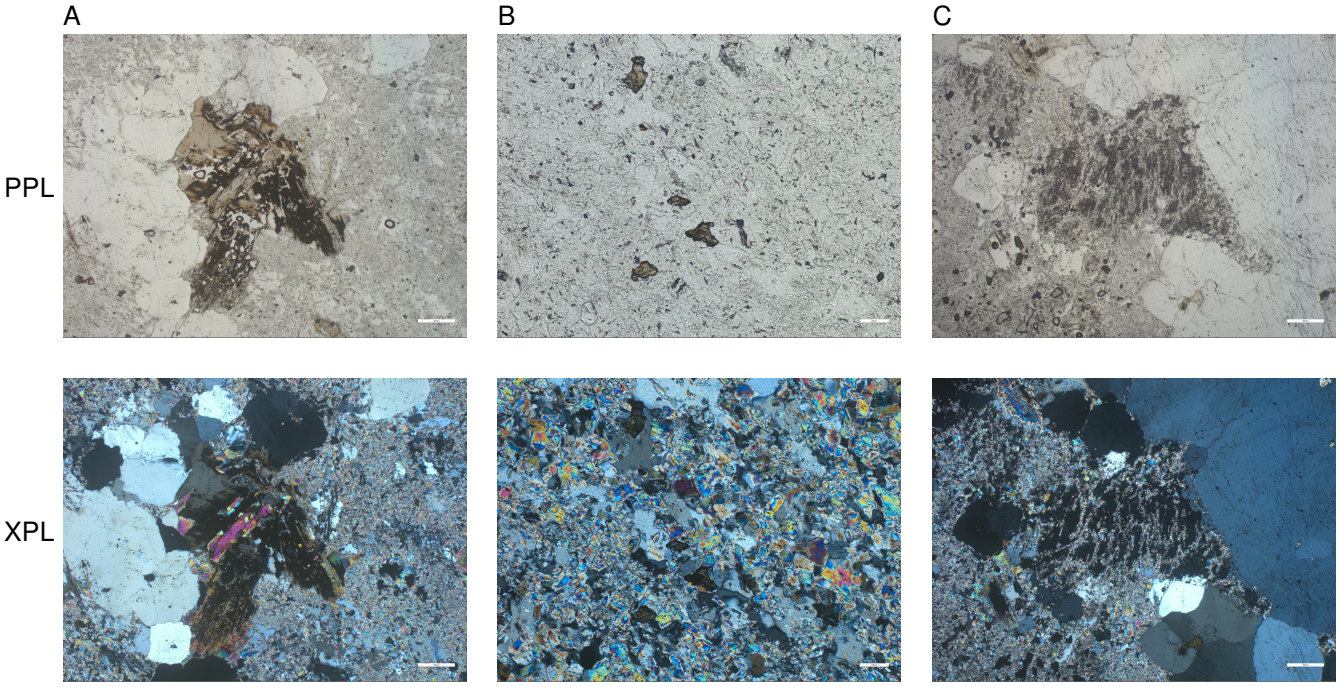
Figure 27: *Histogram of K intensities for feldspars in manual clustering. It shows clearly the bimodal distribution of K-feldspars and plagioclase feldspars in the samples.*

12 µXRF Element maps

The following figures show the raw element intensities for each element identified in the M4 software. The only processing that has been performed on these maps is normalizing each pixel by the total X-ray intensity for that pixel.

Location	Sample ID	Lithology
Carlsfeld, Saxony, Germany	CF2a	Greisen

Microscope	Zeiss Axio Imager.M2
Camera	Axio Cam MRc5
Objective	EC Epiplan-Neoflur Zoom 2.5x/0.075 Pol M27



A) B) C)

Description / Notes

General
Very heavily greisenized, mostly muscovite greisen, some cassiterites and other ore minerals

Quartz	Orthoclase	Plagioclase	Biotite	Muscovite	Other / Accessory Minerals
m.g., subhedral, serrated edges common,	completely replaced by msc+qz	completely replaced by msc+qz	Uncommon, anh, pale in PPL, pleochroic haloes,	completely replaces feldspars, radial aggregates, fine grained	cst,

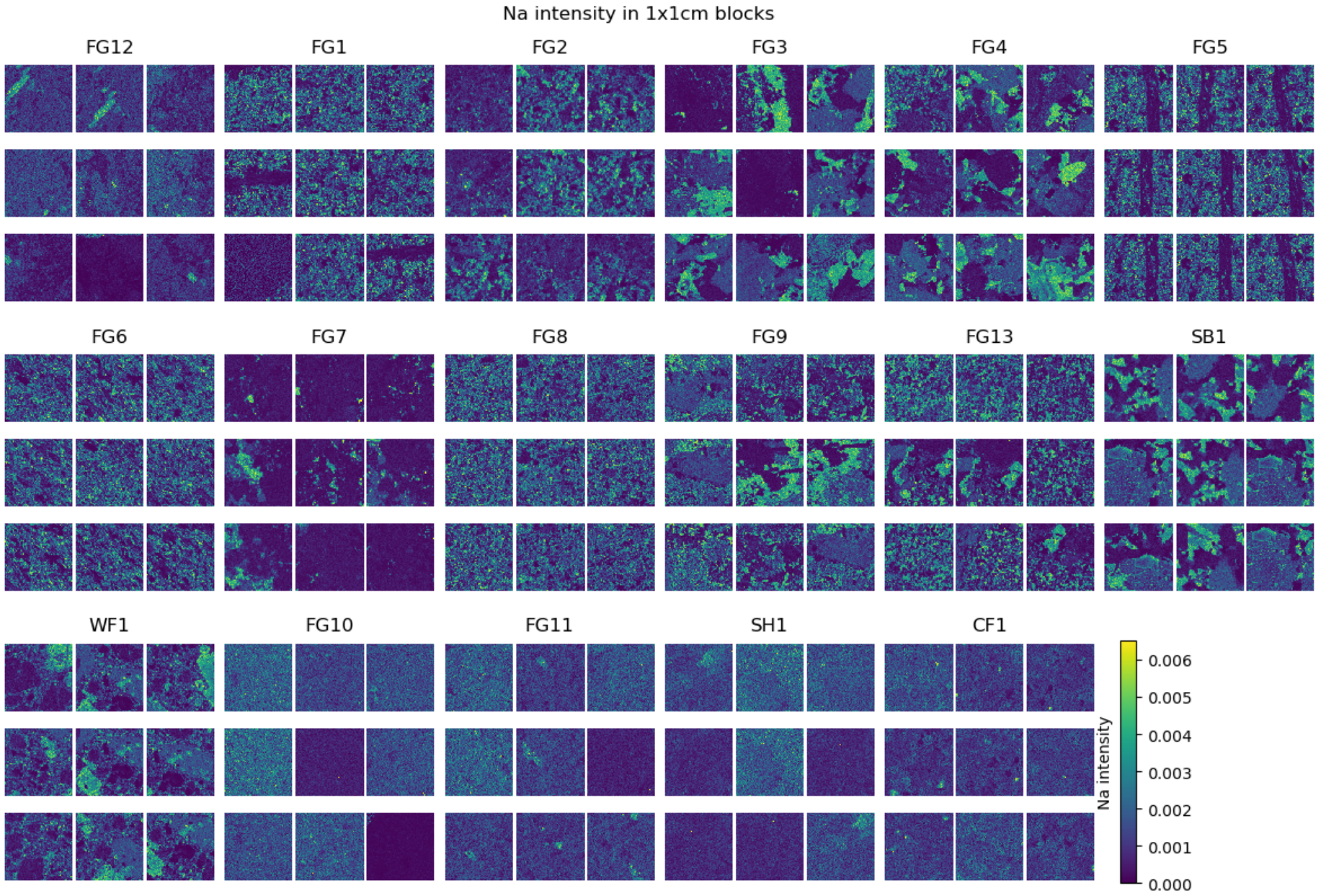


Figure 28: *1x1cm squares of selected samples colored by ratio of Na counts to total counts per pixel.*

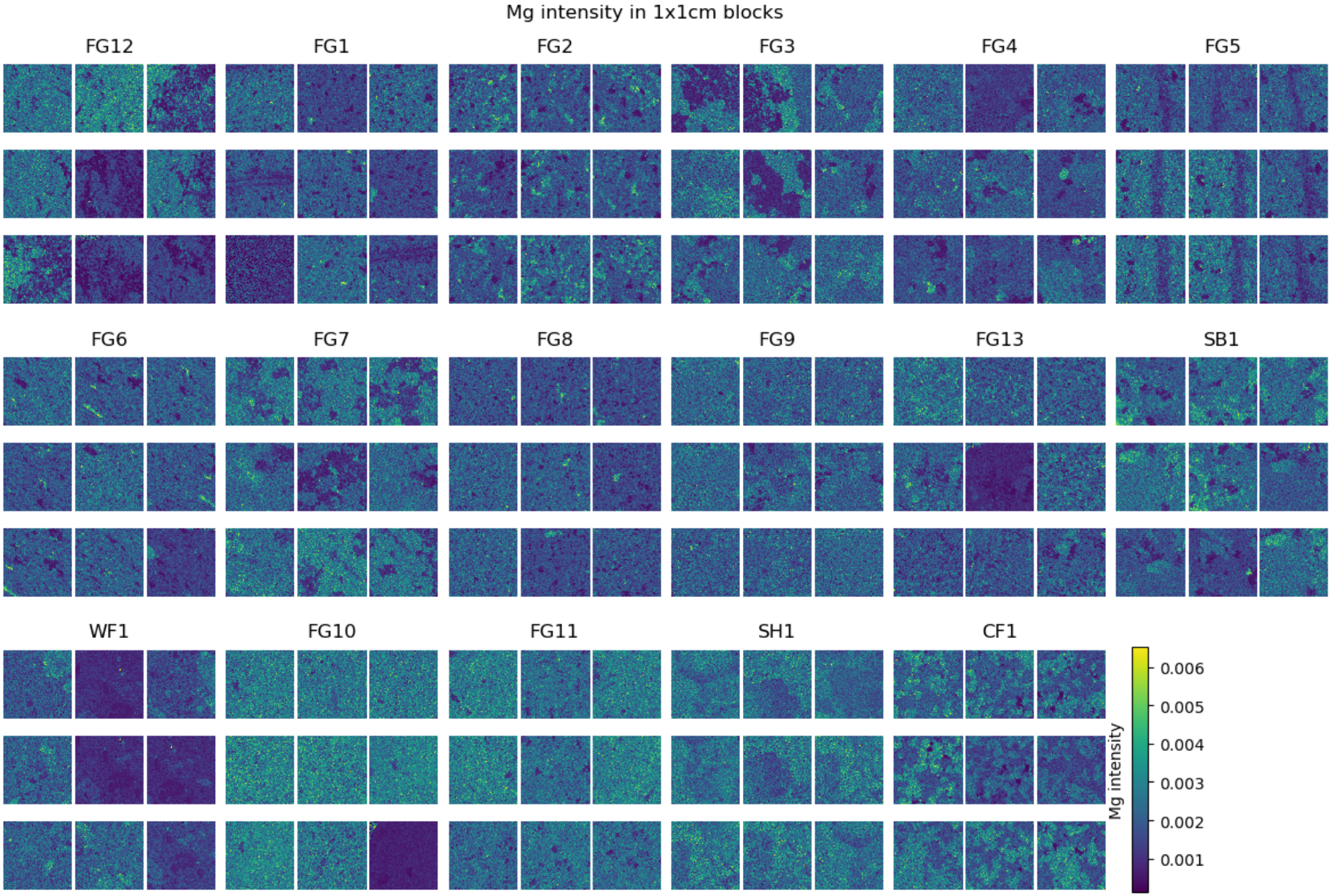


Figure 29: *1x1cm squares of selected samples colored by ratio of Mg counts to total counts per pixel.*

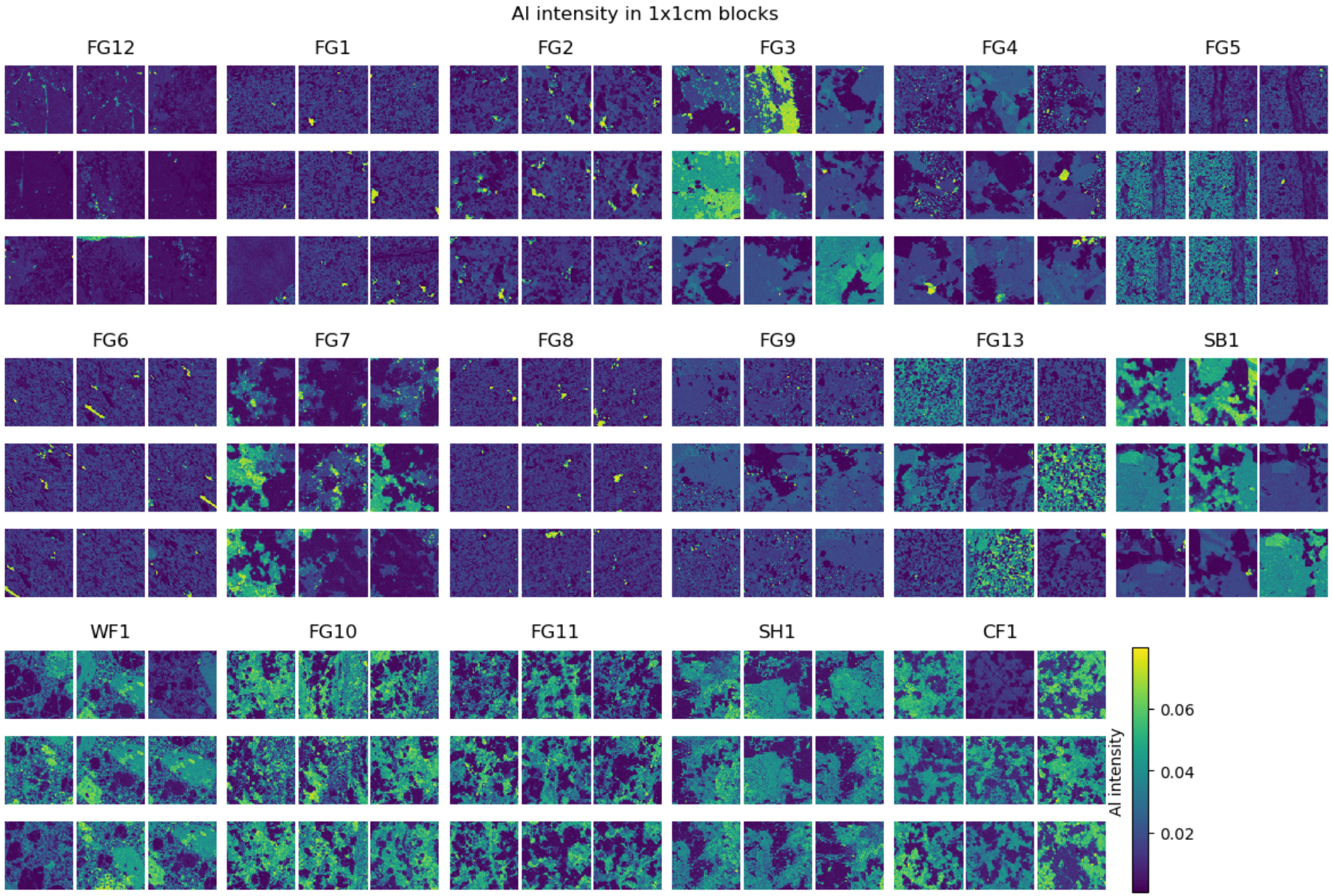


Figure 30: *1x1cm squares of selected samples colored by ratio of Al counts to total counts per pixel.*

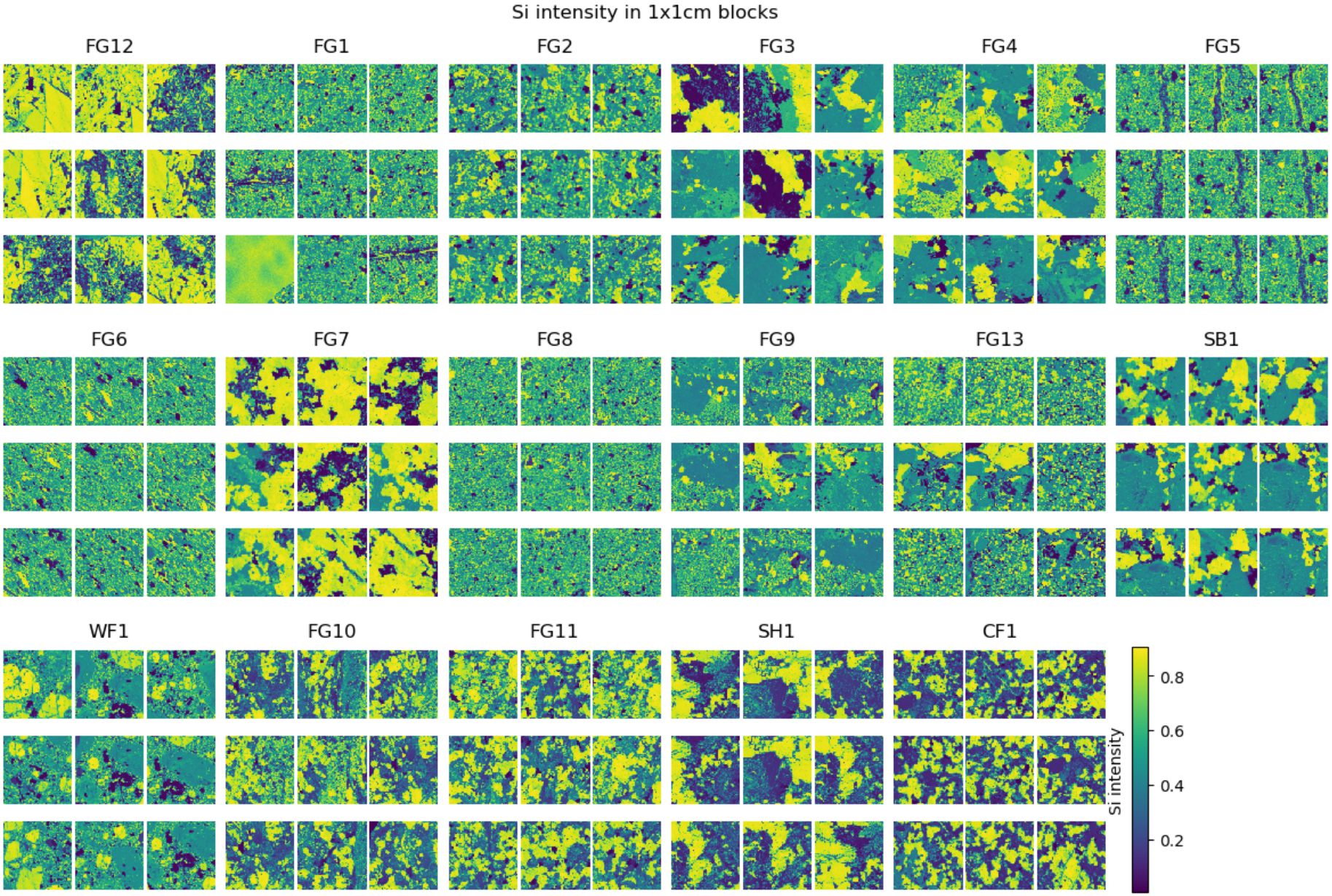


Figure 31: *1x1cm squares of selected samples colored by ratio of Si counts to total counts per pixel.*



Figure 32: *1x1cm squares of selected samples colored by ratio of P counts to total counts per pixel.*

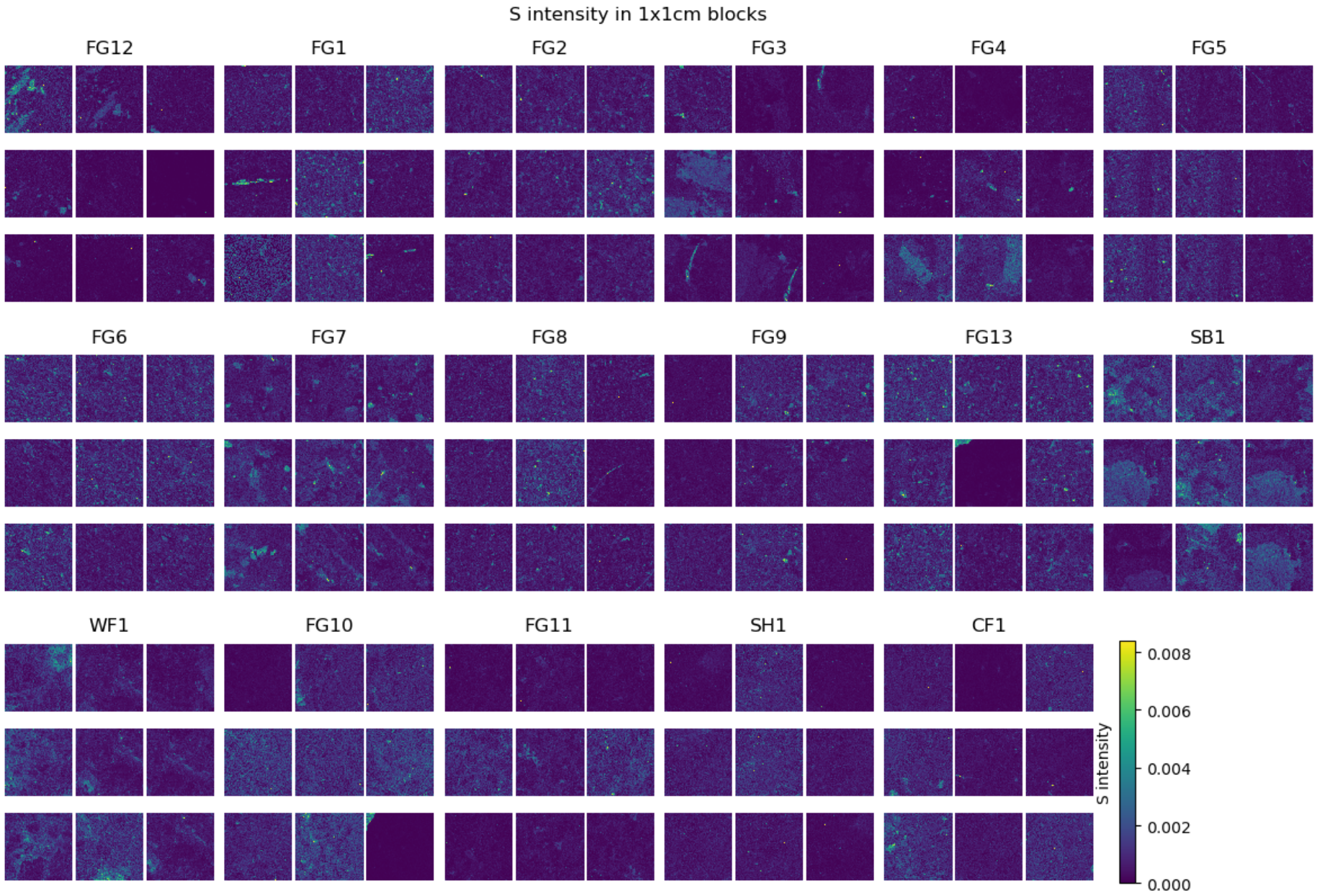


Figure 33: *1x1cm squares of selected samples colored by ratio of S counts to total counts per pixel.*

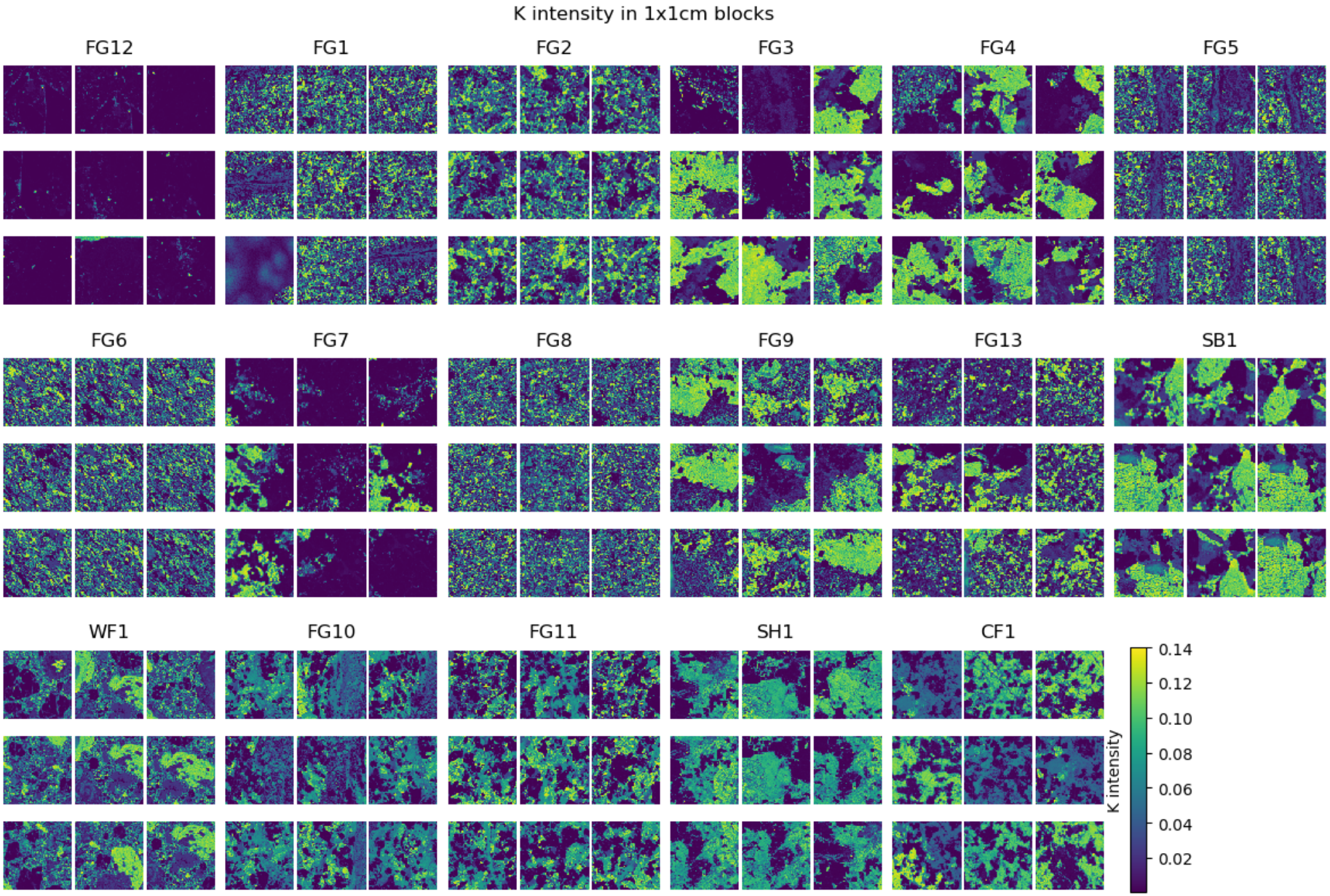


Figure 34: *1x1cm squares of selected samples colored by ratio of K counts to total counts per pixel.*



Figure 35: *1x1cm squares of selected samples colored by ratio of Ca counts to total counts per pixel.*

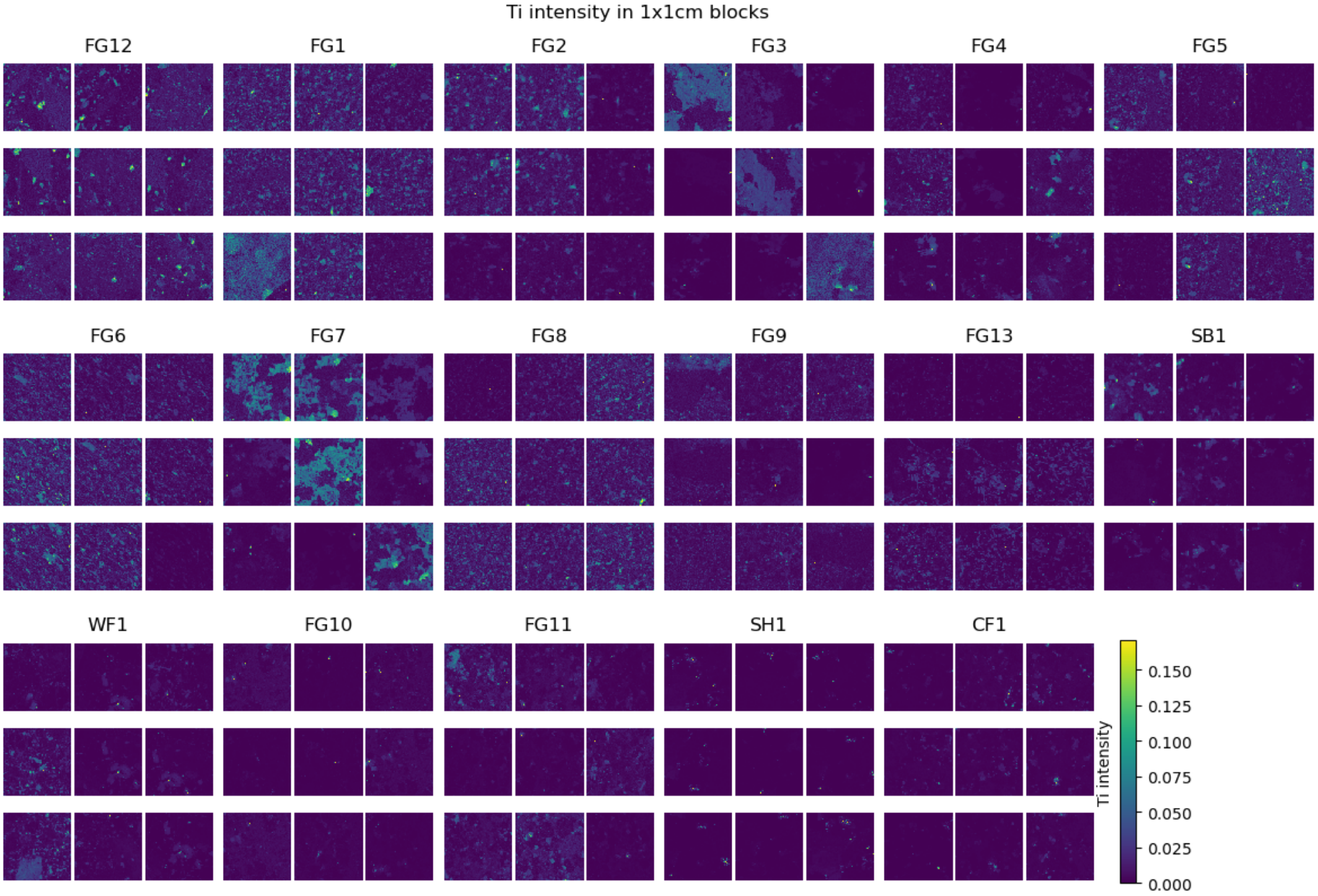


Figure 36: *1x1cm squares of selected samples colored by ratio of Ti counts to total counts per pixel.*

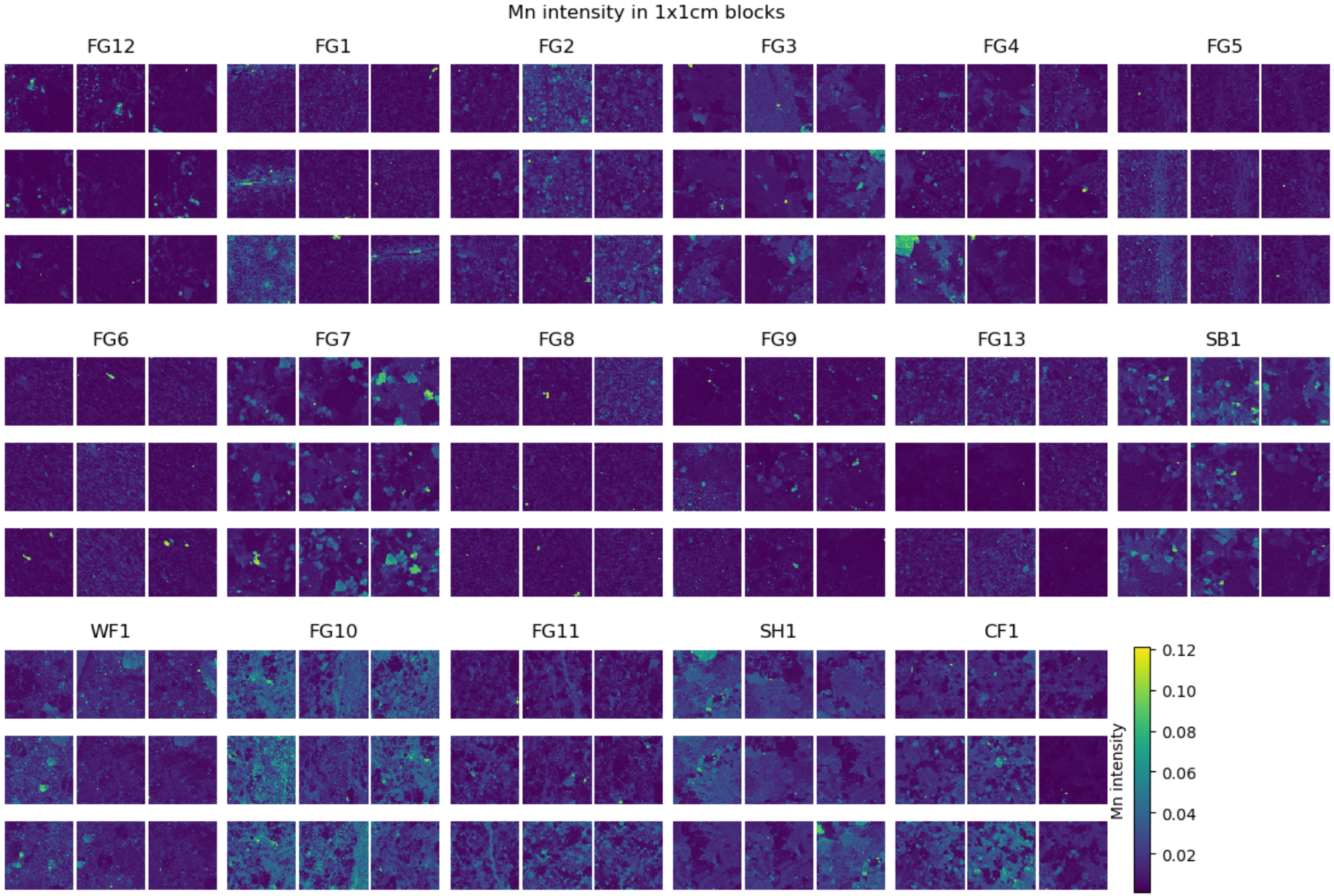


Figure 37: *1x1cm squares of selected samples colored by ratio of Mn counts to total counts per pixel.*

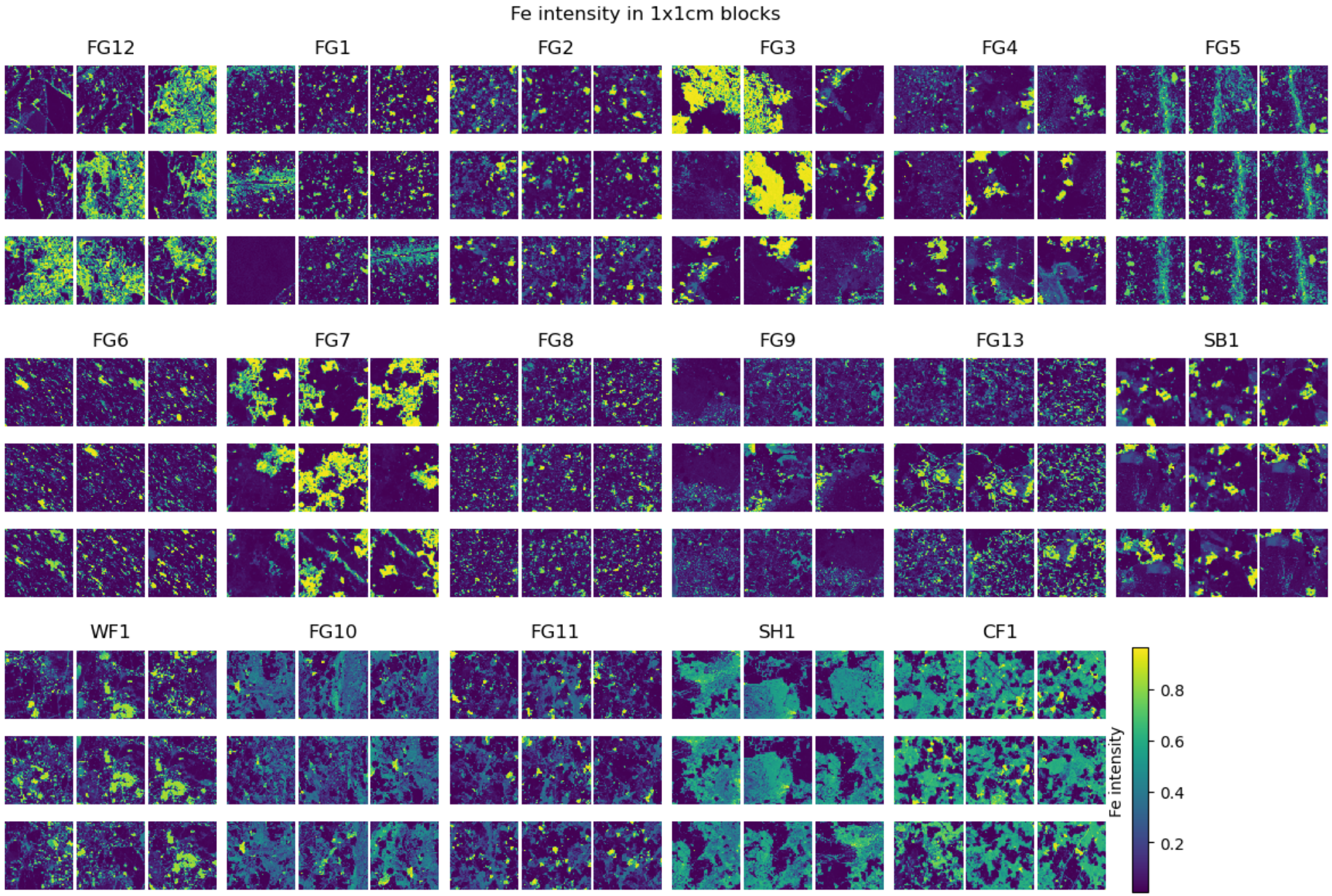


Figure 38: *1x1cm squares of selected samples colored by ratio of Fe counts to total counts per pixel.*

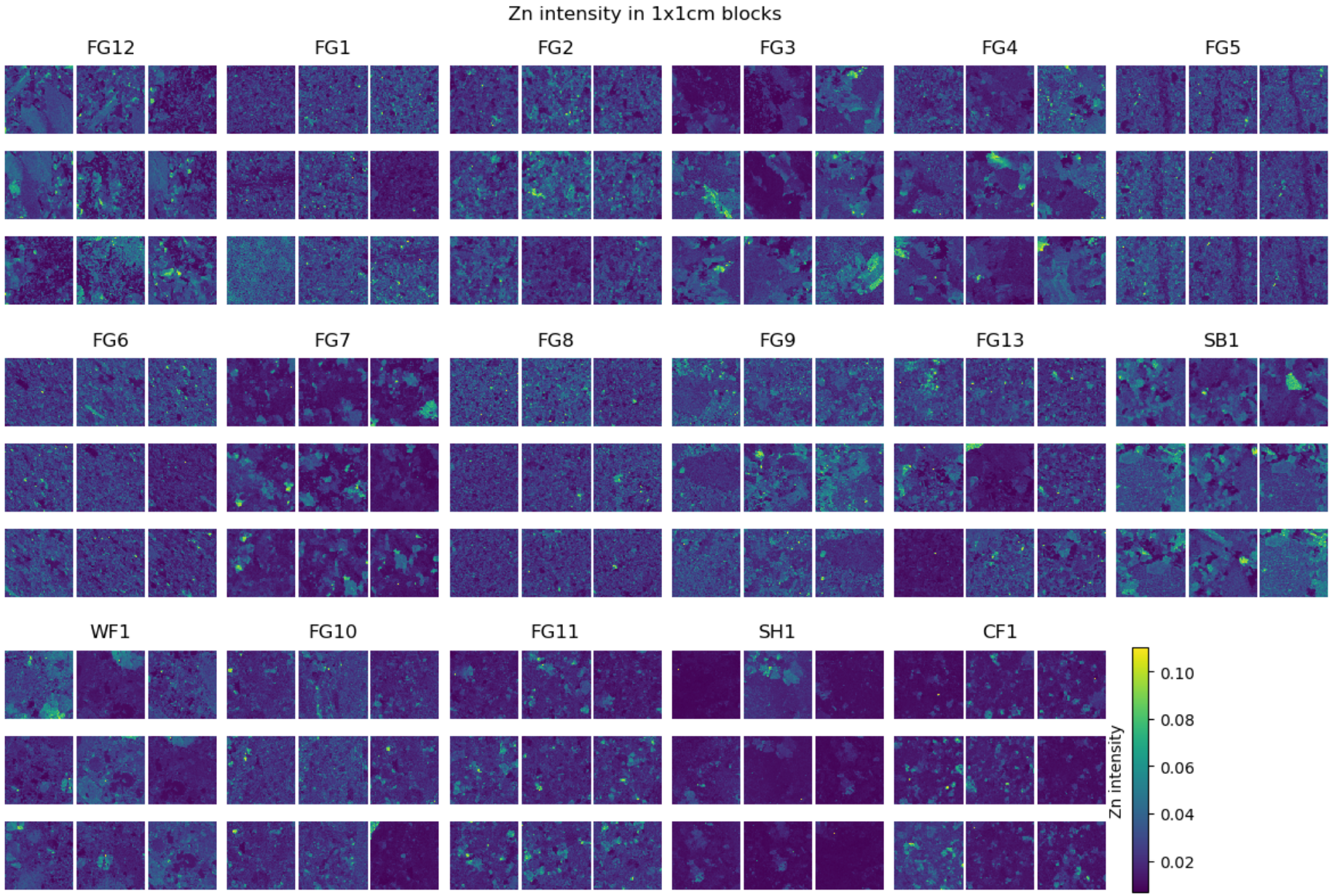


Figure 39: *1x1cm squares of selected samples colored by ratio of Zn counts to total counts per pixel.*

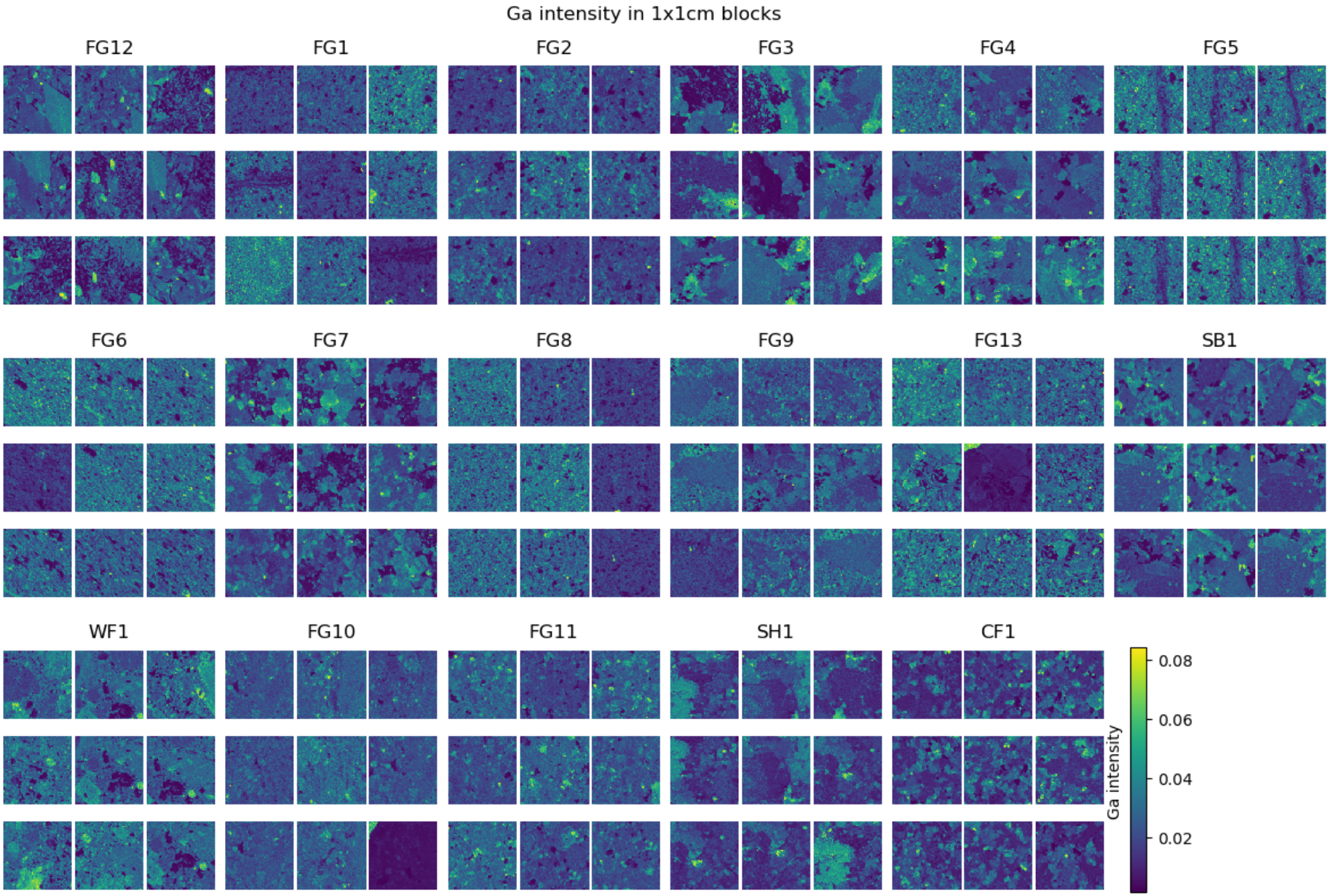


Figure 40: *1x1cm squares of selected samples colored by ratio of Ga counts to total counts per pixel.*

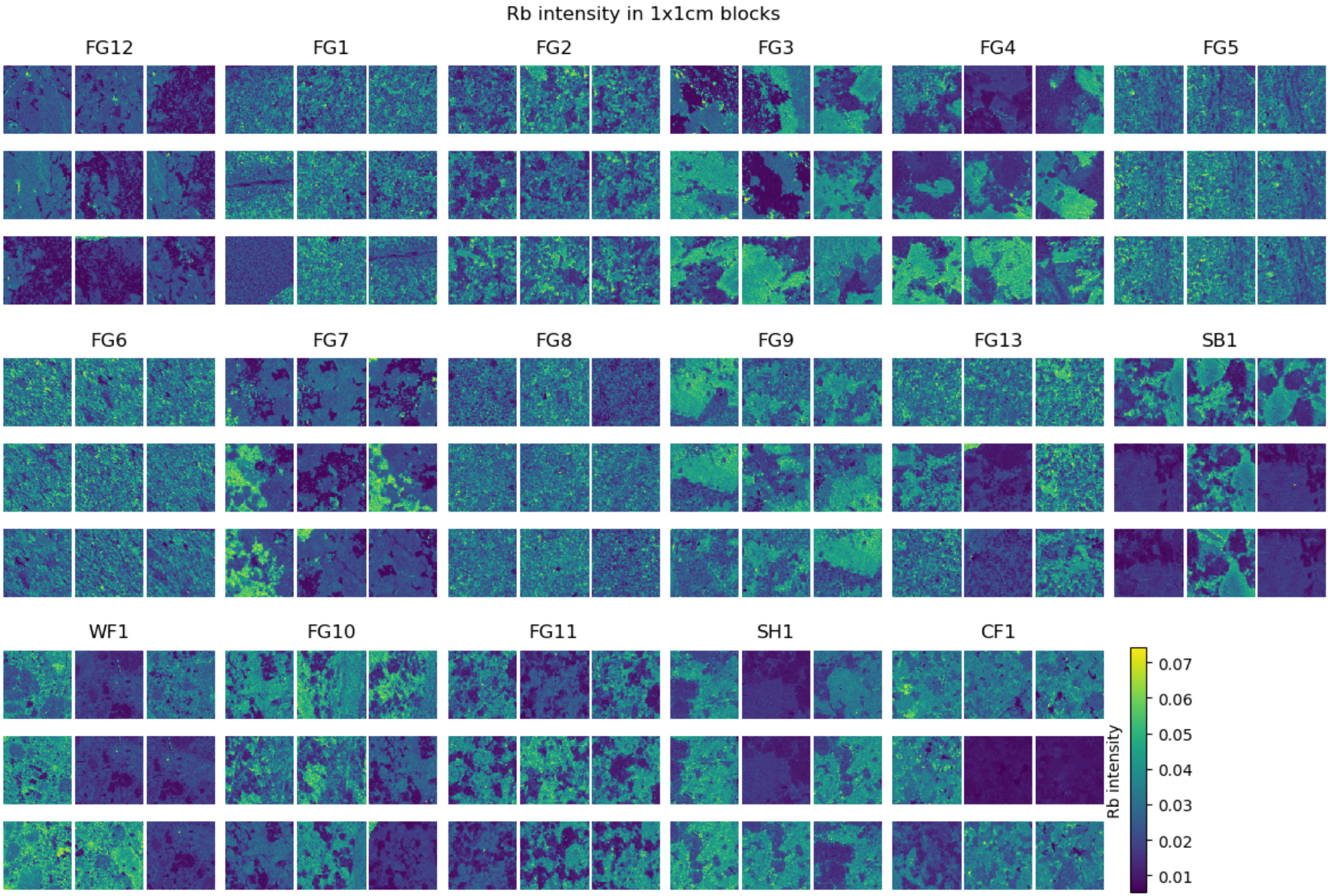


Figure 41: *1x1cm squares of selected samples colored by ratio of Rb counts to total counts per pixel.*

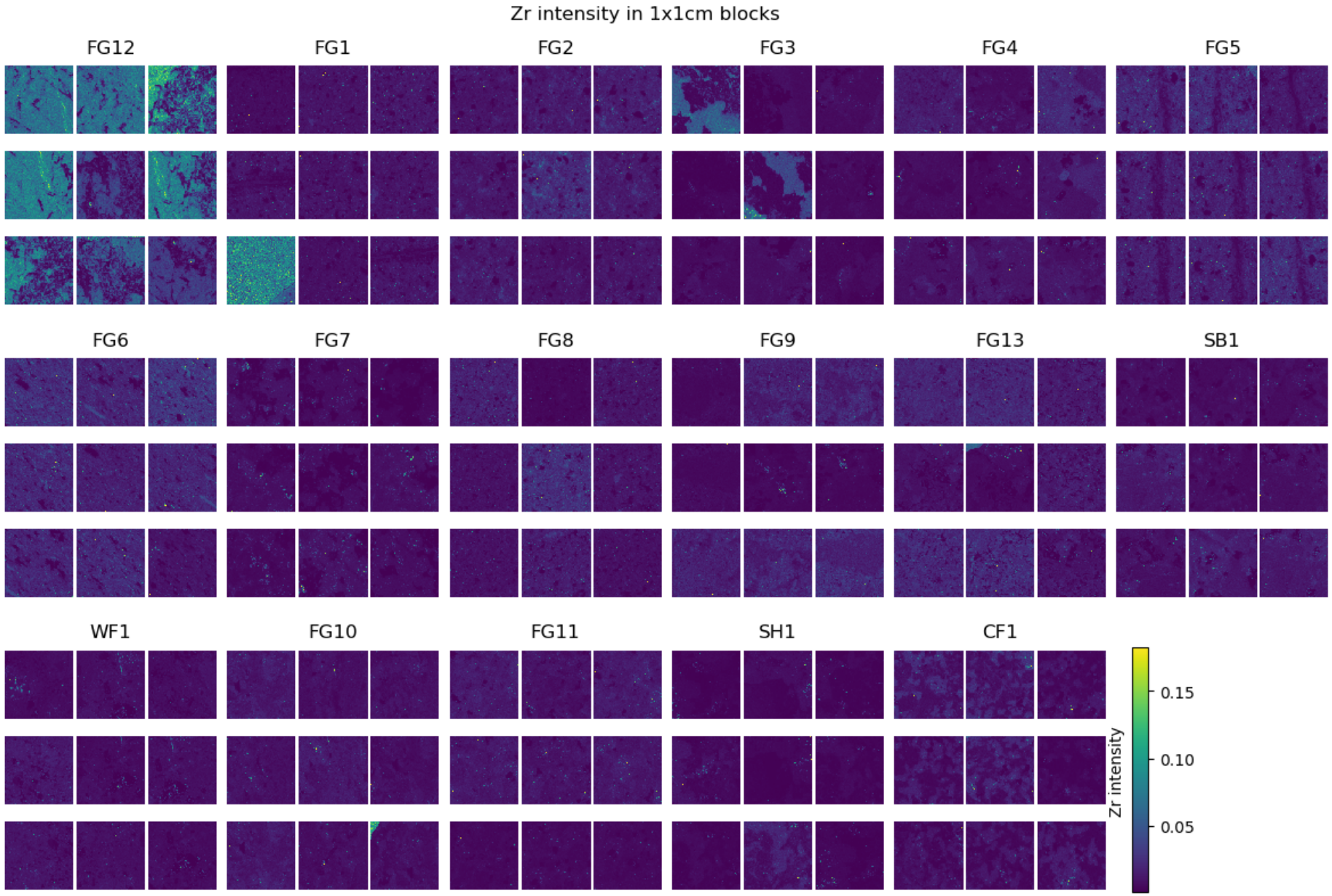
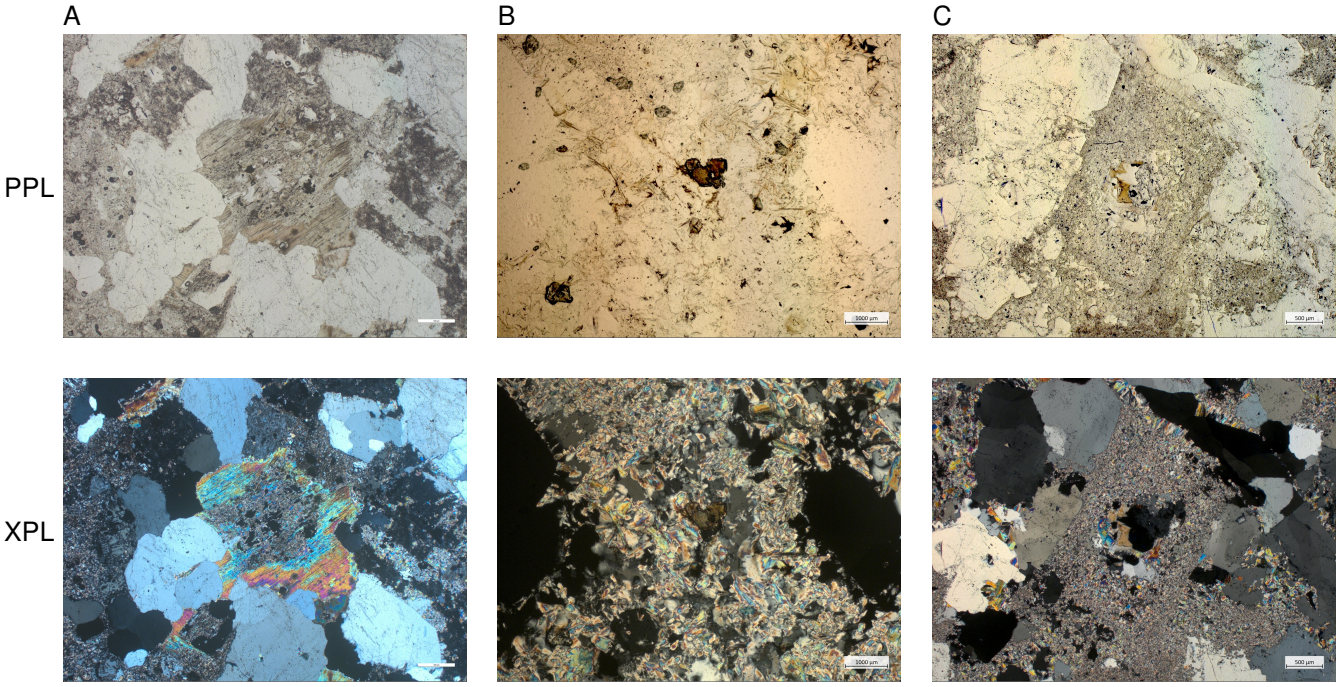


Figure 42: *1x1cm squares of selected samples colored by ratio of Zr counts to total counts per pixel.*

Location	Sample ID	Lithology
Carlsfeld, Saxony, Germany	CF2b	Greisen

Microscope	Zeiss Axio Imager.M2
Camera	Axio Cam MRc5
Objective	EC Epiplan-Neoflur Zoom 2.5x/0.075 Pol M27



A) B) C)

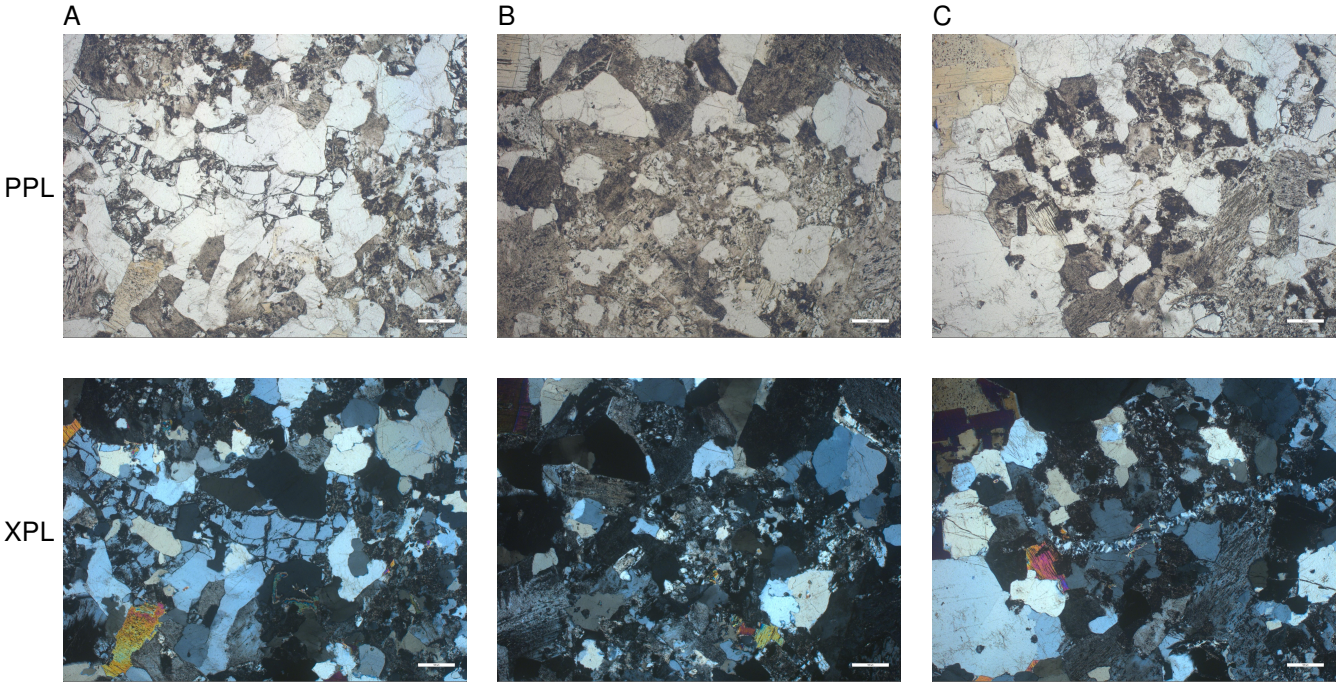
Description / Notes

General
Very heavily greisenized, mostly muscovite greisen, some cassiterites and other ore minerals

Quartz	Orthoclase	Plagioclase	Biotite	Muscovite	Other / Accessory Minerals
m.g., subhedral, serrated edges common,	completely replaced by msc+qz	completely replaced by msc+qz	Uncommon, anh, pale in PPL, pleochroic haloes,	completely replaces feldspars, radial aggregates, fine grained	zrc, cst, crd, mnt

Location	Sample ID	Lithology
Fahsel Quarry, Saxony, Germany	FG2	Greisenized Granite

Microscope	Zeiss Axio Imager.M2
Camera	Axio Cam MRc5
Objective	EC Epiplan-Neoflur Zoom 2.5x/0.075 Pol M27



A) B) C)

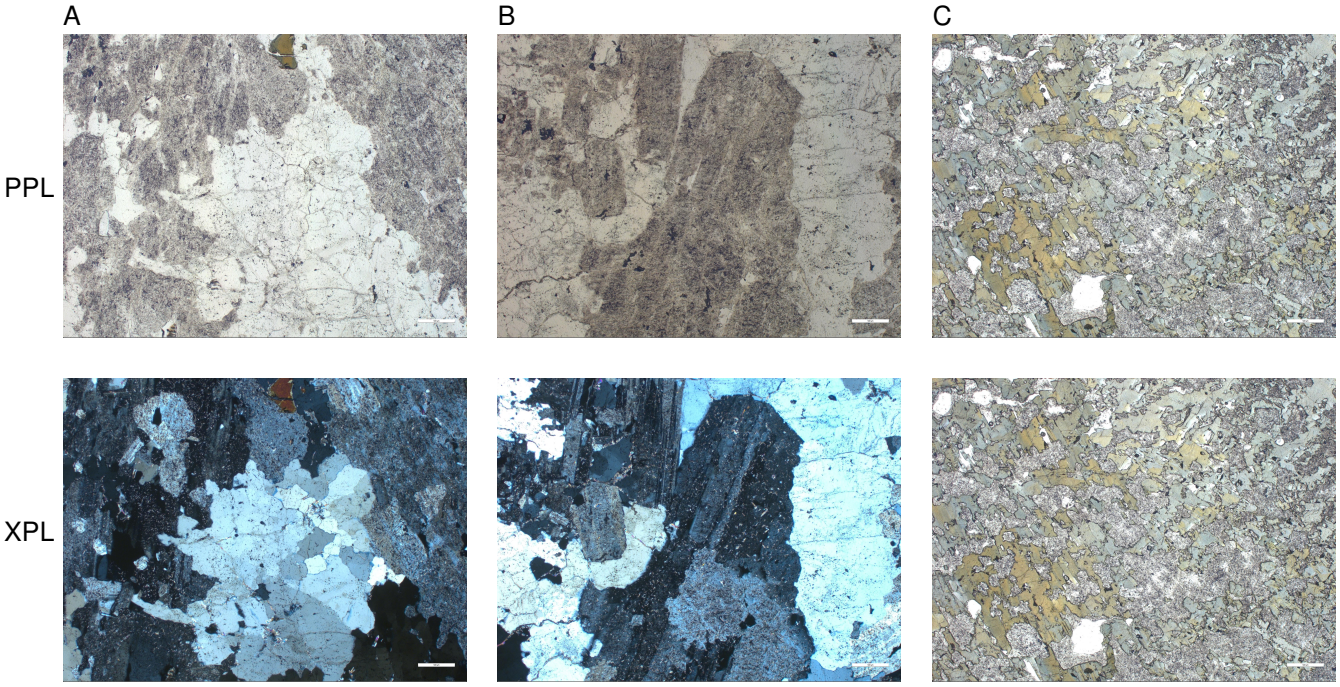
Description / Notes

General
Hydrothermally altered, lots of little pathways often filled with quartz, border of section shows talc-like vein

Quartz	Orthoclase	Plagioclase	Biotite	Muscovite	Other / Accessory Minerals
Anh-subh; boundaries often serrated; f.g. and m.g.	dirty' look in PPL, anh-subh, twinning, some sericitized, altered, perthite common	uncommon, often altered to K-fsp?, anh-subh, no microcline	anh, pale in PPL, pleochroic haloes, partially or fully replaced by msc	anh, rainbow pleochroism in PPL,	topaz, cordierite?, opaques, zircon

Location	Sample ID	Lithology
Fahsel Quarry, Saxony, Germany	FG3a	Greisenized Granite

Microscope	Zeiss Axio Imager.M2
Camera	Axio Cam MRc5
Objective	EC Epiplan-Neoflur Zoom 2.5x/0.075 Pol M27



A) B) C)

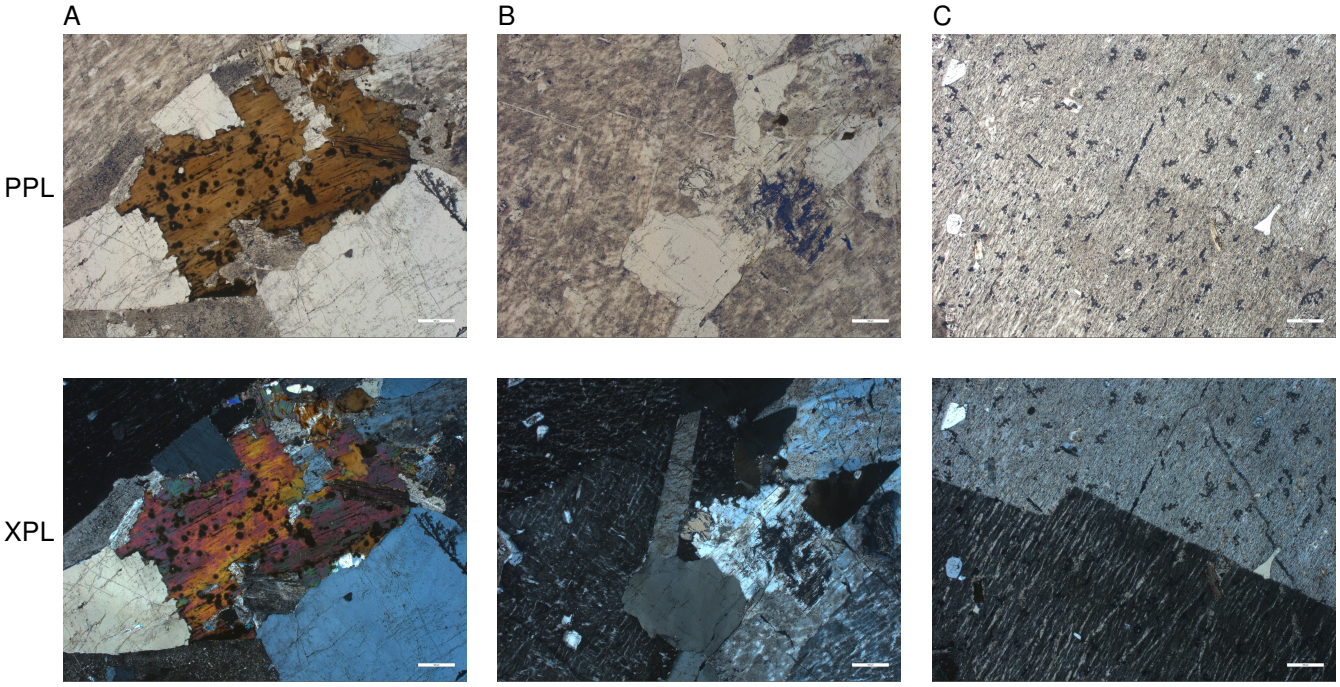
Description / Notes

General
plg replaced by tur (or poikilitic?) only in one half of the section. Very heavily altered.

Quartz	Orthoclase	Plagioclase	Biotite	Muscovite	Other / Accessory Minerals
Anh-subh; boundaries often serrated; c.g. and m.g.	Uncommon, dirty' look in PPL, anh-subh, very sericitized, altered, perthite common	often heavily altered, sericitized or replaced by tur, anh-subh, no microcline	absent	anh, rainbow pleochroism in PPL, often radial aggregates	tur (very common), zrc, apa

Location	Sample ID	Lithology
Fahsel Quarry, Saxony, Germany	FG3b	Greisenized Granite

Microscope	Zeiss Axio Imager.M2
Camera	Axio Cam MRc5
Objective	EC Epiplan-Neoflur Zoom 2.5x/0.075 Pol M27



A) B) C)

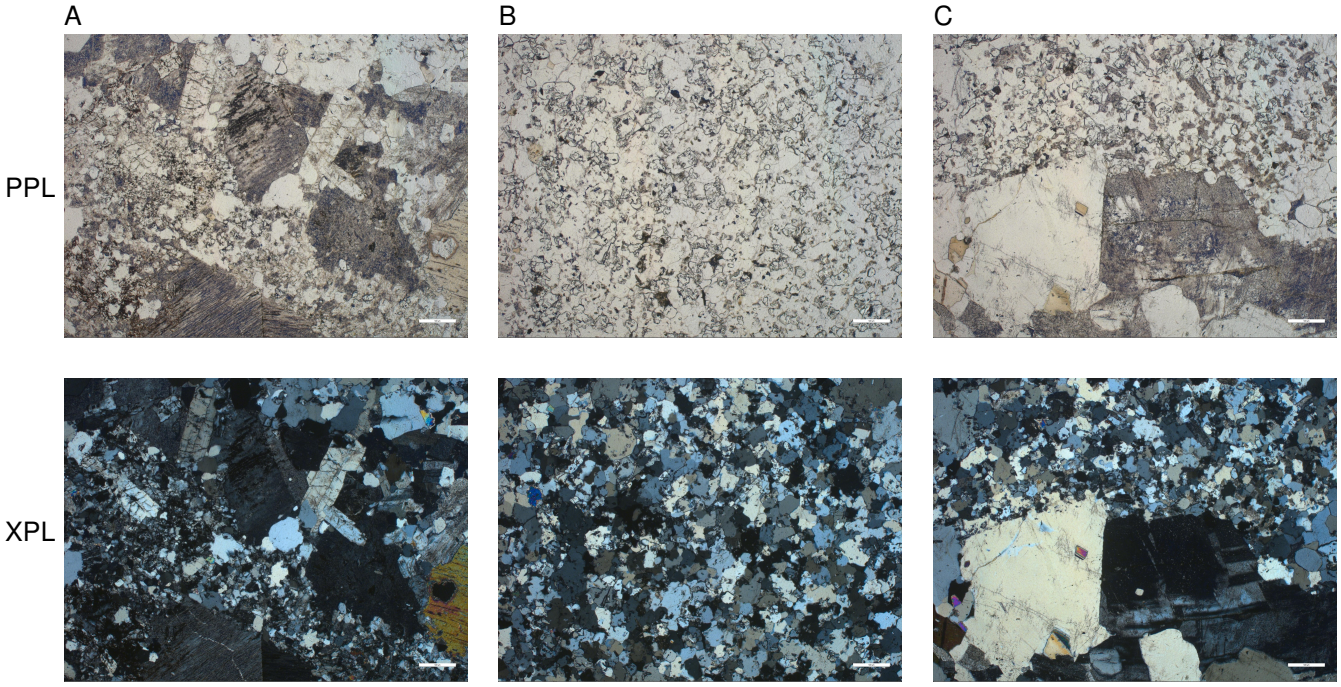
Description / Notes

General
Noticeably less altered than FG3b, mostly feldspars are affected

Quartz	Orthoclase	Plagioclase	Biotite	Muscovite	Other / Accessory Minerals
Anh-subh; boundaries often serrated; c.g. and m.g.	dirty' look in PPL, subh, common twinning, some sericitized, altered, perthite common	Subh-anh, often altered more than K-fsp, perthite, no microcline	anh, pale in PPL, pleochroic haloes, partially or fully replaced by msc	uncommon, sometimes replaces biotite	apa, zrc, crd?,

Location	Sample ID	Lithology
Fahsel Quarry, Saxony, Germany	FG4	Greisenized Granite

Microscope	Zeiss Axio Imager.M2
Camera	Axio Cam MRc5
Objective	EC Epiplan-Neoflur Zoom 2.5x/0.075 Pol M27



A) B) C)

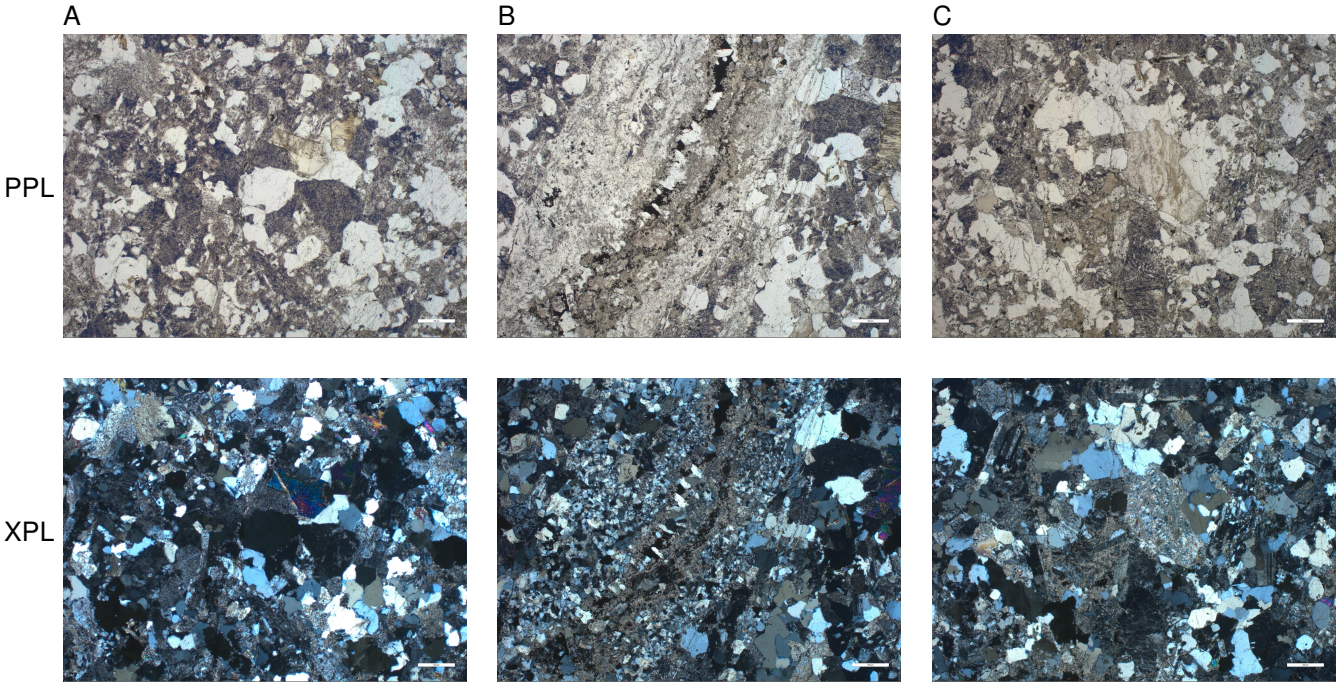
Description / Notes

General
wide vein of fine-grained qz-fsp running through, aplite vein? In some places altered with hematite

Quartz	Orthoclase	Plagioclase	Biotite	Muscovite	Other / Accessory Minerals
Anh; boundaries often serrated; f.g. and c.g.	dirty' look in PPL, subh, common twinning, some sericitized, altered, perthite common	uncommon, anh, alteration to K-fsp, sericite, deformation twinning	Uncommon, anh, pale in PPL, pleochroic haloes,	uncommon, anh, alteration product, sometimes radial aggregates	apa, zrc

Location	Sample ID	Lithology
Fahsel Quarry, Saxony, Germany	FG5	Greisenized Granite

Microscope	Zeiss Axio Imager.M2
Camera	Axio Cam MRc5
Objective	EC Epiplan-Neoflur Zoom 2.5x/0.075 Pol M27



A) B) C)

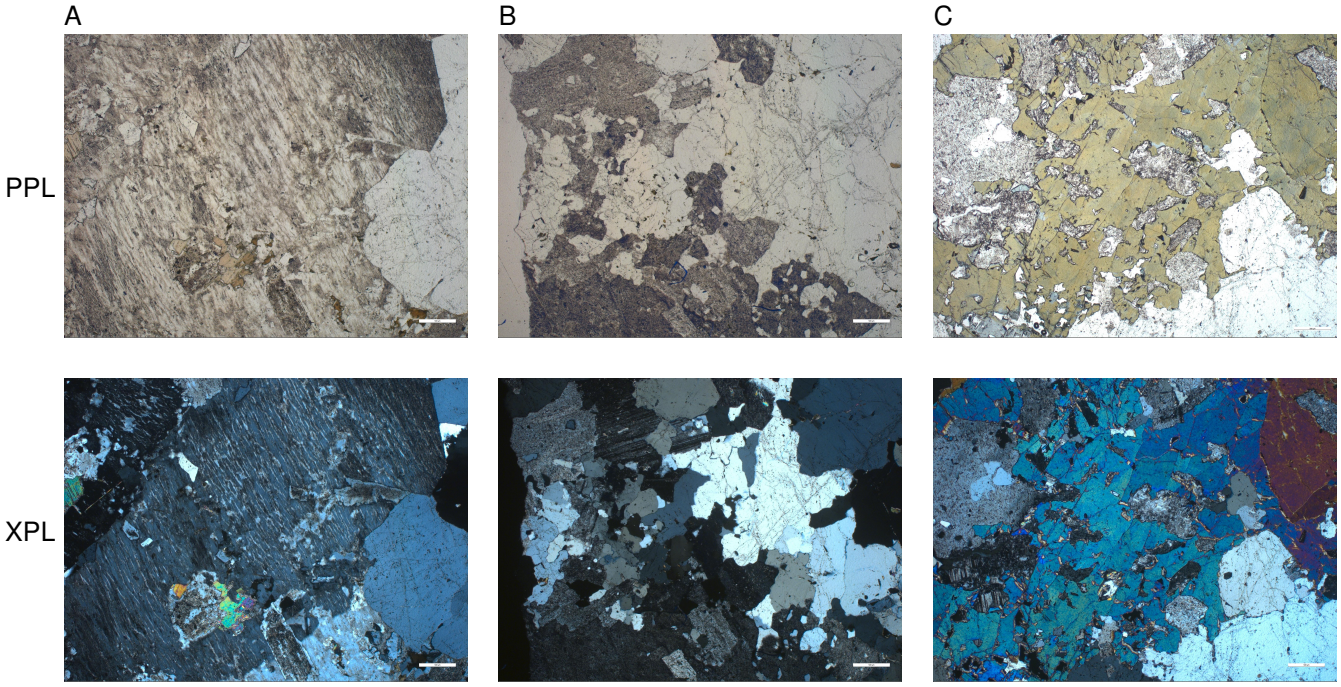
Description / Notes

General
greisen vein running along length, oxides oxidized to hematite in center

Quartz	Orthoclase	Plagioclase	Biotite	Muscovite	Other / Accessory Minerals
Anh-subh; boundaries often serrated; f.g. and m.g., very fine in greisen veins	anh, dirty look in PPL, heavily altered, sericitized, sometimes completely replaced by white mica, perthite absent or very fine	Subh-anh, often altered, perthite absent or very fine	very pale in PPL, most places replaced by msc, pleochroic haloes, anh	anh, rainbow pleochroism in PPL, radial aggregates in greisen veins, tabular otherwise	opaques

Location	Sample ID	Lithology
Fahsel Quarry, Saxony, Germany	FG7	Greisenized Granite

Microscope	Zeiss Axio Imager.M2
Camera	Axio Cam MRc5
Objective	EC Epiplan-Neoflur Zoom 2.5x/0.075 Pol M27



A) B) C)

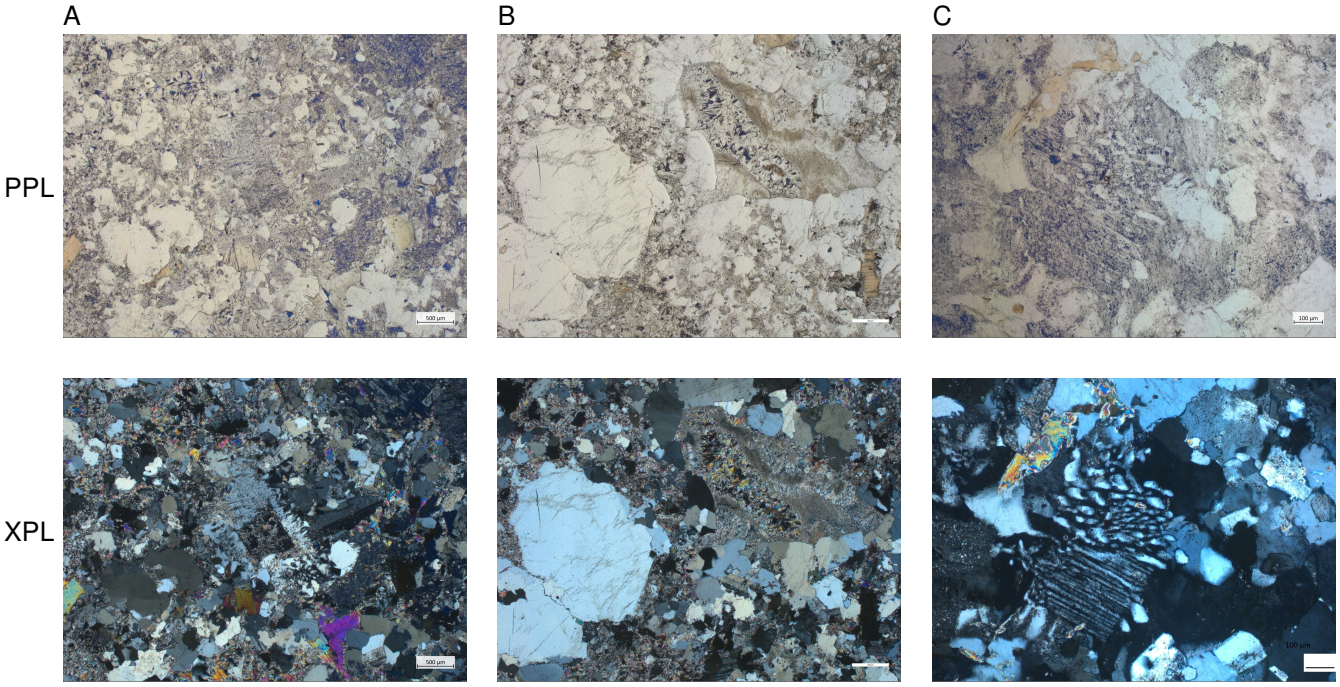
Description / Notes

General
Qz-fsp intergrowths, c.g. tur-qz assemblage at one end.

Quartz	Orthoclase	Plagioclase	Biotite	Muscovite	Other / Accessory Minerals
Anh-subh; boundaries often serrated; c.g. and m.g.,	anh, dirty look in PPL, altered, perthite common, embayments, some zoned	Subh-anh, often altered, perthite, embayments	anh, pleochroic radiation haloes, absent near tur	absent except for few crystals near tur	tur (very common), opq, zrc,

Location	Sample ID	Lithology
Fahsel Quarry, Saxony, Germany	FG8	Greisenized Granite

Microscope	Zeiss Axio Imager.M2
Camera	Axio Cam MRc5
Objective	EC Epiplan-Neoflur Zoom 2.5x/0.075 Pol M27



A) B) C)

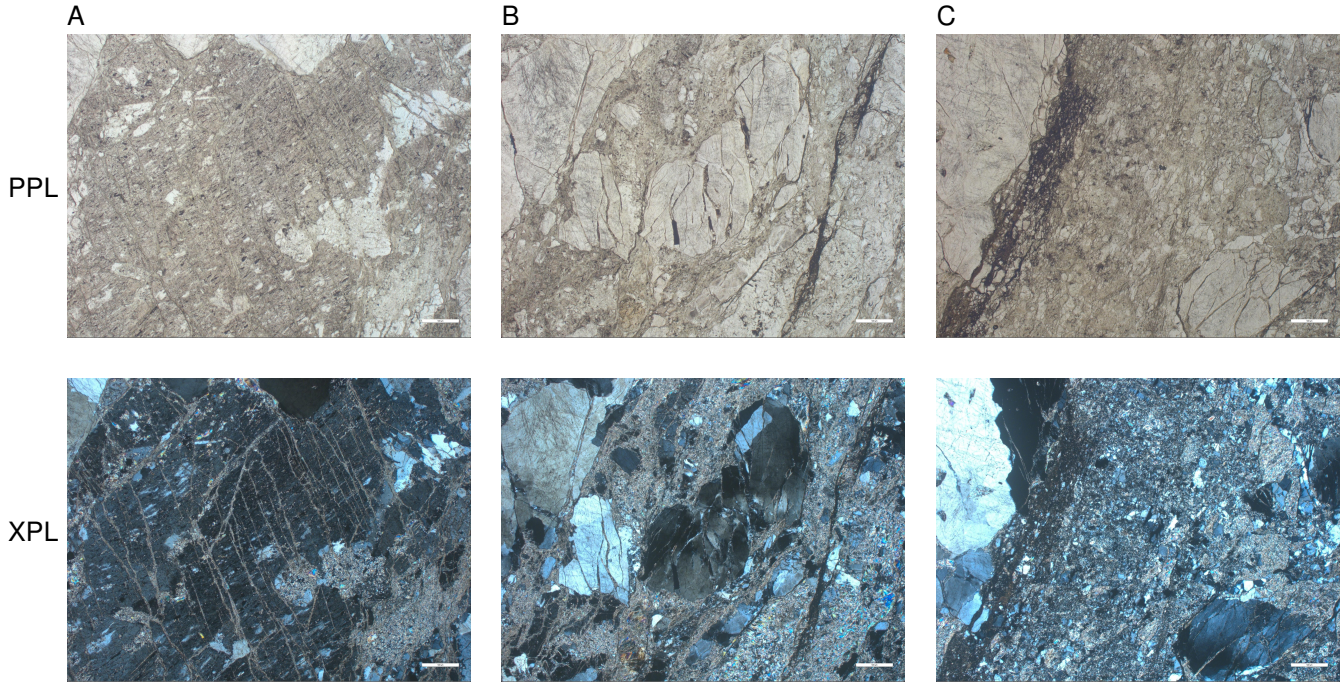
Description / Notes

General
greisen vein along side of section, qz-fsp intergrowths

Quartz	Orthoclase	Plagioclase	Biotite	Muscovite	Other / Accessory Minerals
Anh-subh; boundaries often serrated; c.g. and m.g.	dirty' look in PPL, anh-subh, very sericitized, altered, perthite common, m.g. f.g., replaced by msc in vein	Subh-anh, often altered, perthite, m.g. f.g, no microcline, replaced by msc in vein	anh, pale in PPL, pleochroic haloes, partially replaced by msc	anh, replaces fsp in greisen vein, replaces some biotites partly	crd, zrc, opq.

Location	Sample ID	Lithology
Fahsel Quarry, Saxony, Germany	FG10	Greisenized Granite

Microscope	Zeiss Axio Imager.M2
Camera	Axio Cam MRc5
Objective	EC Epiplan-Neoflur Zoom 2.5x/0.075 Pol M27



A) B) C)

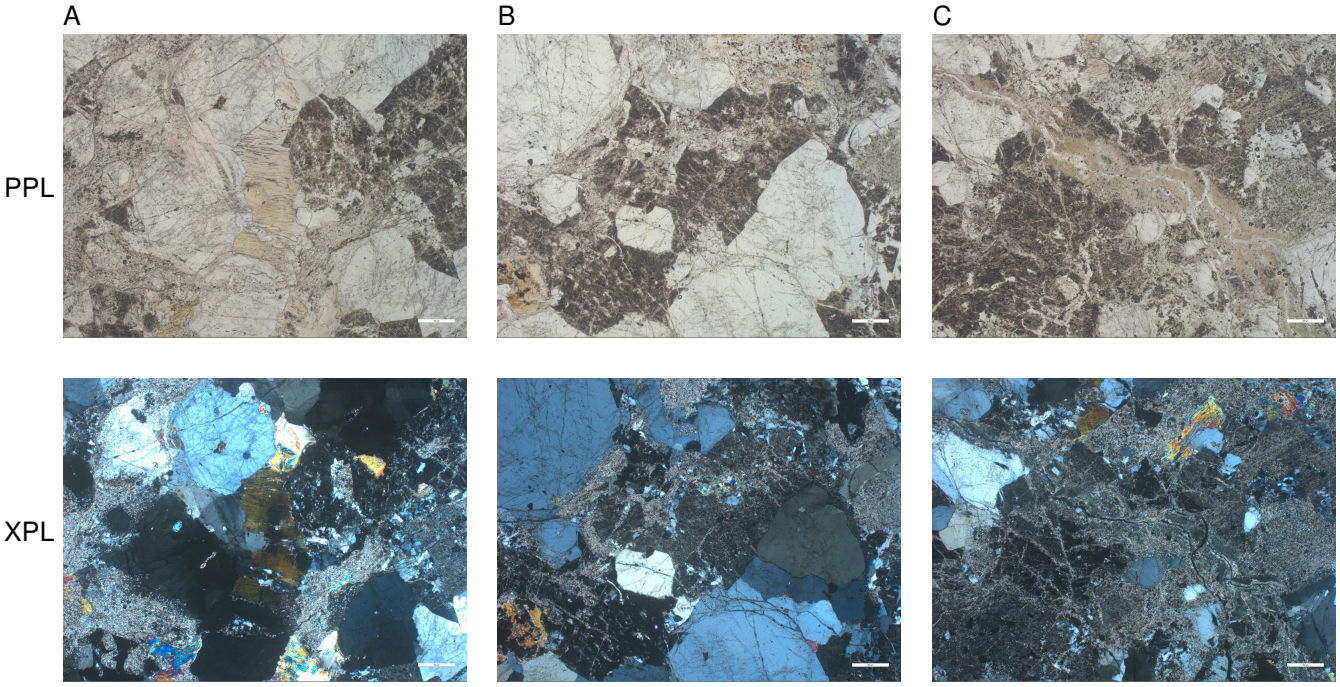
Description / Notes

General
heavily fractured

Quartz	Orthoclase	Plagioclase	Biotite	Muscovite	Other / Accessory Minerals
Anh-subh; boundaries often serrated; c.g. and m.g., heavily fractured	anh, perthite, m.g. c.g., almost completely replaced by mica starting from fractures	absent, likely replaced fully by mica	absent	anh, replaces fsp and present in veins	opq

Location	Sample ID	Lithology
Fahsel Quarry, Saxony, Germany	FG11	Greisenized Granite

Microscope	Zeiss Axio Imager.M2
Camera	Axio Cam MRc5
Objective	EC Epiplan-Neoflur Zoom 2.5x/0.075 Pol M27



A) B) C)

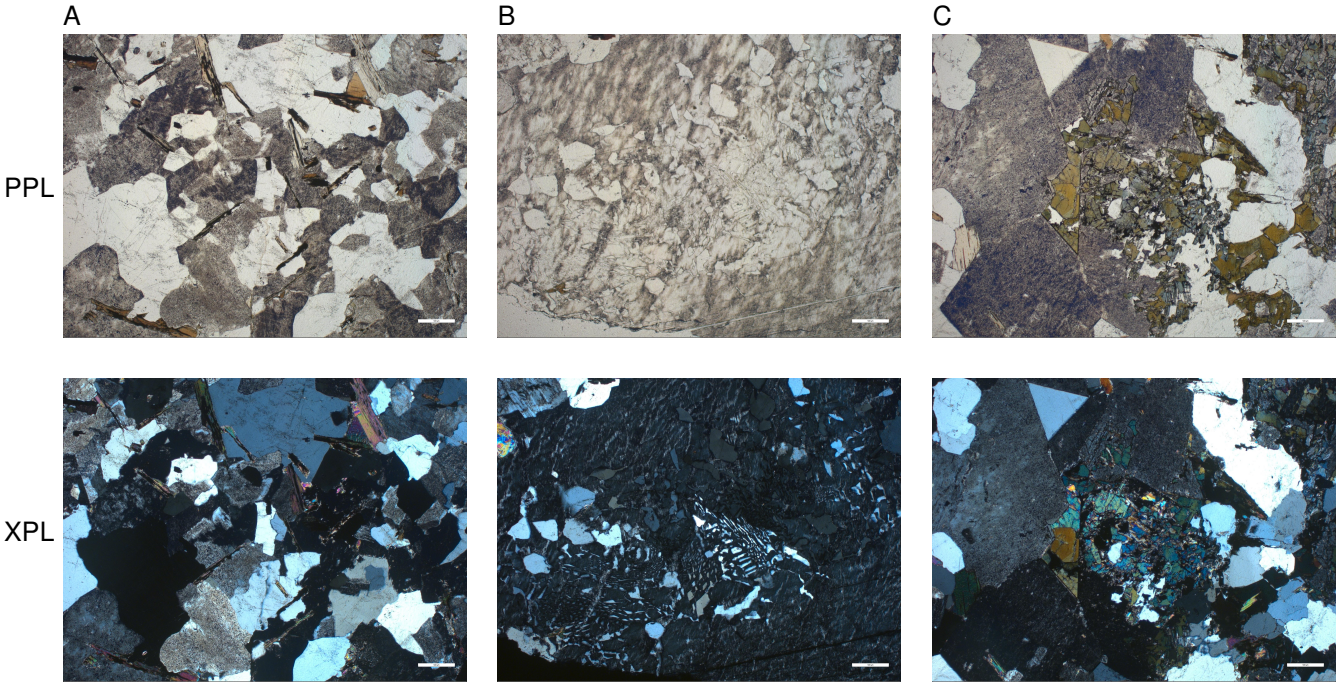
Description / Notes

General
None

Quartz	Orthoclase	Plagioclase	Biotite	Muscovite	Other / Accessory Minerals
None	None	None	None	None	None

Location	Sample ID	Lithology
Fahsel Quarry, Saxony, Germany	FG13a	Greisenized Granite

Microscope	Zeiss Axio Imager.M2
Camera	Axio Cam MRc5
Objective	EC Epiplan-Neoflur Zoom 2.5x/0.075 Pol M27



A) B) C)

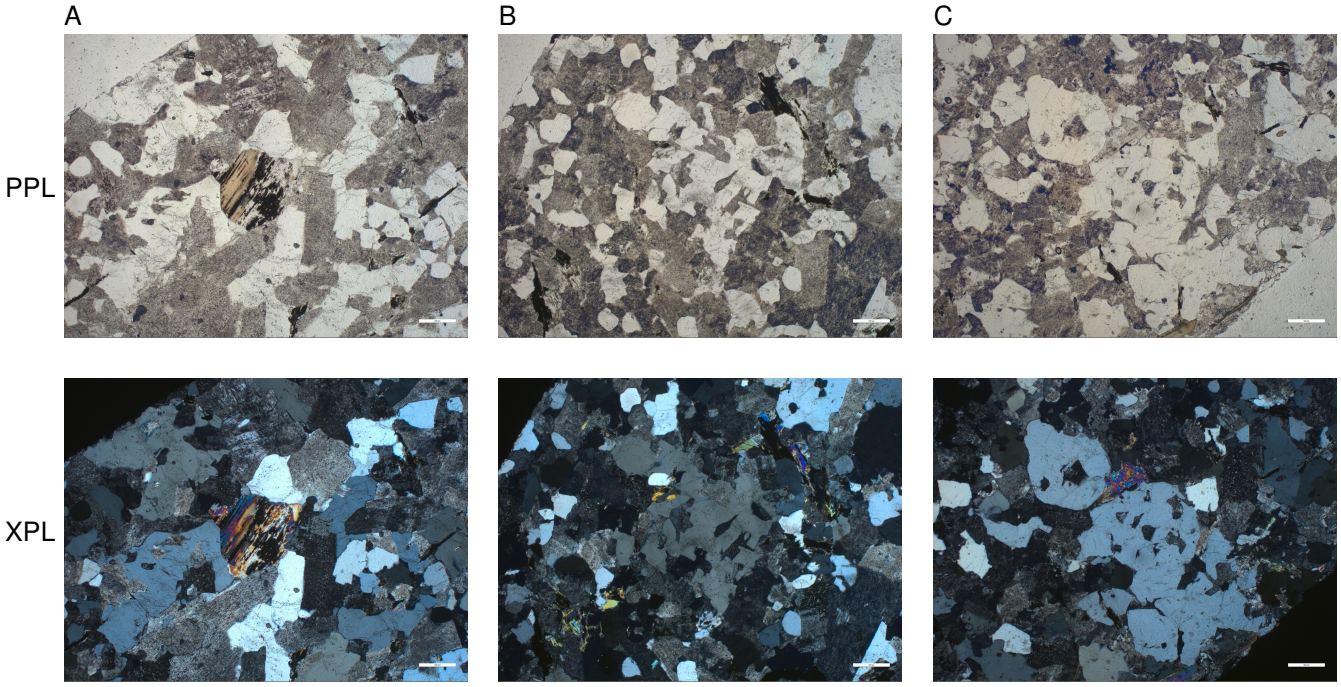
Description / Notes

General
Medium-grained on one side and coarse grained on the other side.

Quartz	Orthoclase	Plagioclase	Biotite	Muscovite	Other / Accessory Minerals
Anh-subh; boundaries often serrated; c.g. and m.g.	dirty' look in PPL, anh-subh, twinning, some sericitized, altered, perthite common, myrmekitic texture in some	subh. Twinning, often sericitized, no microcline,	Subh., forms thin crystals, pleochroic radiation haloes, commonly altered to oxides or msc	replaces bt and fsp, anh., not common	tur, opq,

Location	Sample ID	Lithology
Fahsel Quarry, Saxony, Germany	FG13b	Greisenized Granite

Microscope	Zeiss Axio Imager.M2
Camera	Axio Cam MRc5
Objective	EC Epiplan-Neoflur Zoom 2.5x/0.075 Pol M27



A) B) C)

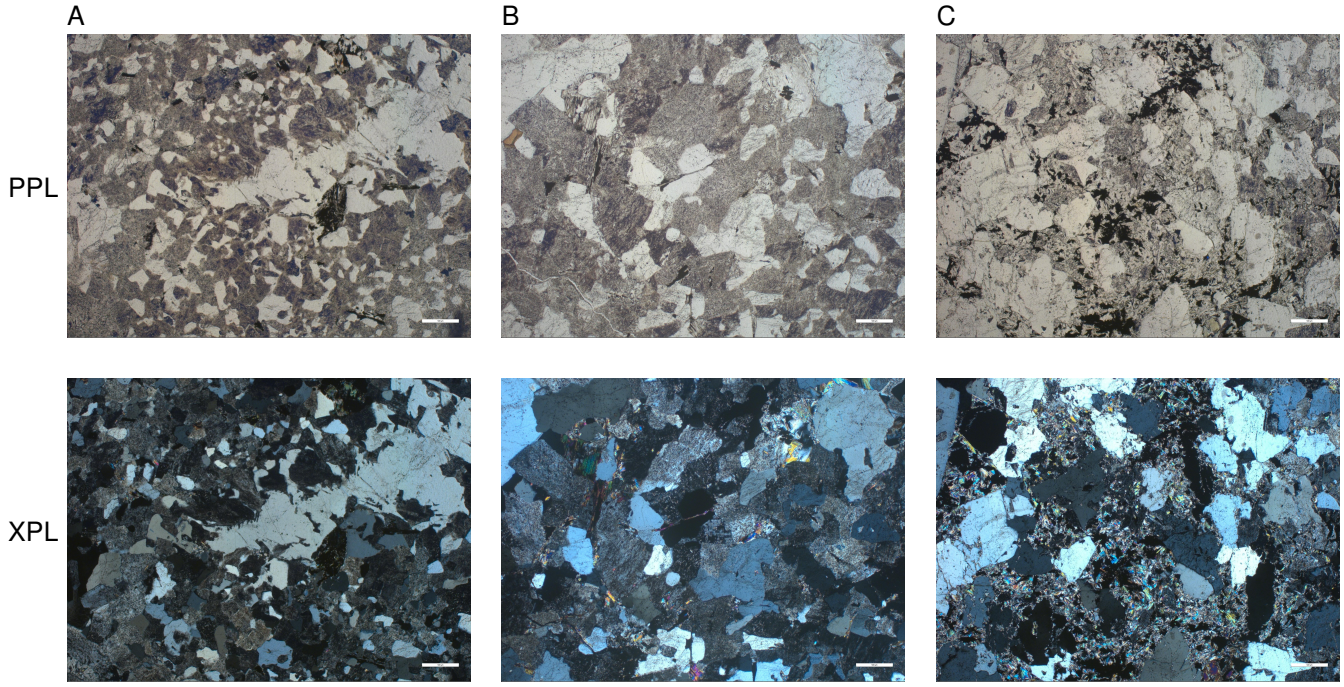
Description / Notes

General
very interesting, looks heavily recrystallized, everything anhedral

Quartz	Orthoclase	Plagioclase	Biotite	Muscovite	Other / Accessory Minerals
Anh., heavily serrated boundaries, m.g.	very dirty looking, very altered. Perthite	Anh., twinning, very sericitized and altered, twinning, no microcline	Anh., mostly fully replaced by opaques	Anh., uncommon, replaces some fsp	opq,

Location	Sample ID	Lithology
Fahsel Quarry, Saxony, Germany	FG13c	Greisenized Granite

Microscope	Zeiss Axio Imager.M2
Camera	Axio Cam MRc5
Objective	EC Epiplan-Neoflur Zoom 2.5x/0.075 Pol M27



A) B) C)

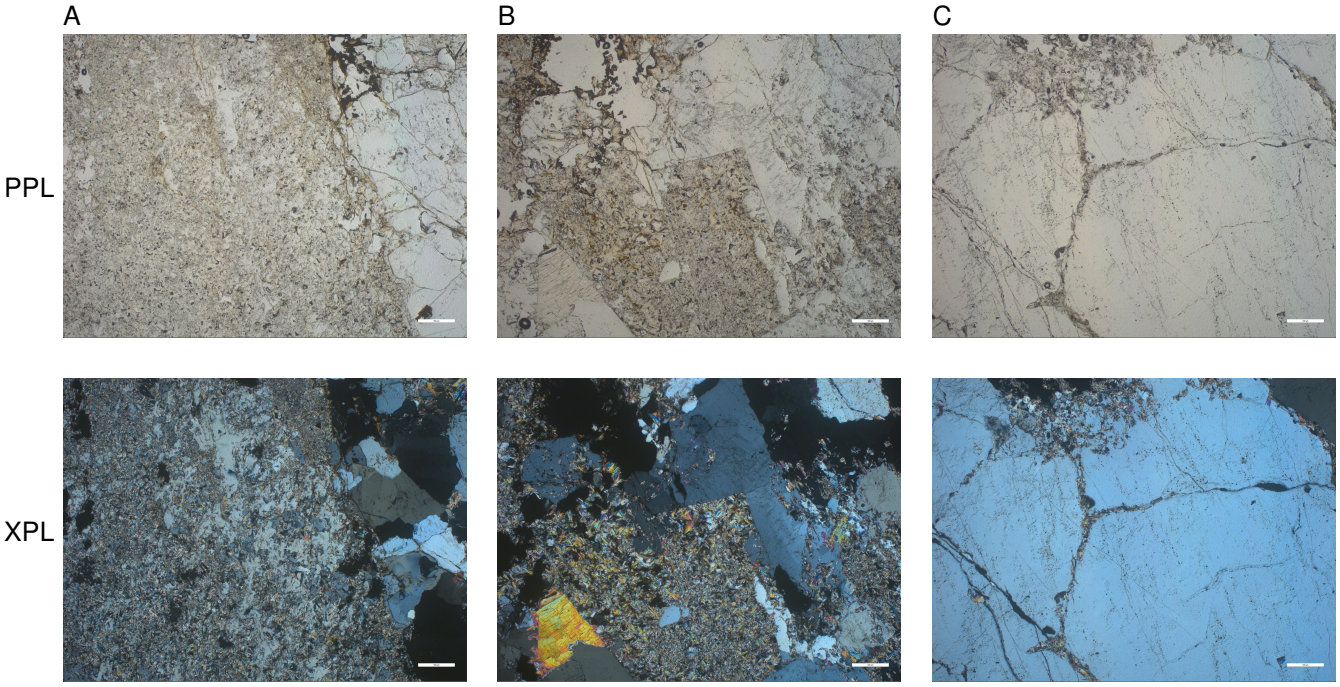
Description / Notes

General
one corned greisenized,

Quartz	Orthoclase	Plagioclase	Biotite	Muscovite	Other / Accessory Minerals
Anh., heavily serrated boundaries, m.g.	very dirty looking, very altered. Perthite	Anh., twinning, very sericitized and altered, twinning, no microcline	Anh., mostly fully replaced by opaques	Anh., uncommon, replaces some fsp, common in greisenized area	opq,

Location	Sample ID	Lithology
Schönheide, Saxony, Germany	SH1	Greisen

Microscope	Zeiss Axio Imager.M2
Camera	Axio Cam MRc5
Objective	EC Epiplan-Neoflur Zoom 2.5x/0.075 Pol M27



A) B) C)

Description / Notes

General
Qz-msc greisen, feldspars completely destroyed

Quartz	Orthoclase	Plagioclase	Biotite	Muscovite	Other / Accessory Minerals
Anh., heavily serrated boundaries, m.g.	absent	absent	absent	common, replaces feldspars together with qz, sub-anh., partially chloritized in places	zrc